DIGITAL MAP AND GNSS FUSION TO ENHANCE LOCALIZATION FOR INTELLIGENT VEHICLE APPLICATIONS

by

Ali Ufuk Peker

B.S., Computer Engineering, Boğaziçi University, 1991

M.S., Computer Engineering, Boğaziçi University, 1993

Submitted to the Institute for Graduate Studies in
Science and Engineering in partial fulfillment of
the requirements for the degree of
Doctor of Philosophy

Graduate Program in Computer Engineering

Boğaziçi University

2017

DIGITAL MAP AND GNSS FUSION TO ENHANCE LOCALIZATION FOR INTELLIGENT VEHICLE APPLICATIONS

APPROVED BY:

Prof. H. Levent Akın .....
(Thesis Supervisor)

Prof. Oğuz Tosun .....
(Thesis Co-supervisor)

Prof. Tankut Acarman .....

Prof. B. Tevfik Akgün .....

Prof. Fatih Alagöz .....

Assist. Prof. Emre Uğur .....

DATE OF APPROVAL: 05.01.2017

ACKNOWLEDGEMENTS

I would like to express my special appreciation and thanks to my supervisor Prof. H. Levent Akın for his outstanding ideas, support, and for his participation in my thesis committee.

I would like to express my sincere gratitude to my co-supervisor Prof. Oğuz Tosun for his invaluable guidance, and patience throughout this study. I greatly appreciate his contribution to my undergraduate and graduate education. It was a formative experience for me to work with him.

I am grateful to Prof. Tankut Acarman for his exceptional support, participation in my thesis committee, and for his valuable comments. I would like to thank Assist. Prof. Emre Ugur for his participation in my thesis committee and jury.

I would like to thank Prof. Fatih Alagöz and Prof. B. Tevfik Akgün for their participation in my thesis jury.

I would like to thank Prof. Ümit Özgüner for his contributions and help.

I would like to present my thanks to my friends Kerem Par, Ali İhsan Danışman, Mustafa Erdem, Atalay Taşkoparan, Murat Duman, and Neville Wells for their continuous encouragement and support.

Finally, I would like to thank my wife Çiğdem, my daughter Selin İlke, my sister Hülya, my niece İdil, my mother Yüksel, and my father Sezai for their love, encouragement, patience, and support.

Part of this research was supported by European Union project GLOVE under Seventh Framework Programme (FP7).

ABSTRACT

DIGITAL MAP AND GNSS FUSION TO ENHANCE LOCALIZATION FOR INTELLIGENT VEHICLE APPLICATIONS

This thesis aims to enhance vehicle localization through the fusion of digital maps and vehicular communication. A particle filter based algorithm for fusing global navigation satellite system (GNSS) receiver, odometer, and digital maps is proposed and implemented. Implementation deployed on an embedded system and tested in the field. Field tests were carried out different in parts of İstanbul to measure the performance of the algorithm in different satellite visibility conditions. Results show that algorithm selects the correct road segment on the digital map with 96% success rate. The proposed algorithm was further enhanced with the addition of mutual positioning on vehicular ad-hoc networks (VANETs). The measurement-based statistical model of relative distance as a function of Time-of-Arrival(TOA) is experimentally obtained. The mutual positioning procedure is investigated in terms of positioning accuracy and network performance through realistic simulation studies with a different number of collaborative vehicles, and the proposed mutual positioning procedure is experimentally evaluated by a fleet of five IEEE 802.11p radio modem equipped vehicles. It is shown that collaboration in a VANET improves the availability of position measurement and its accuracy up to 40% in comparison with the stand-alone GNSS receiver. Local integrity heat map concept is introduced as a new local integrity methodology. Local integrity heat map is implemented and tested with extensive field tests. Algorithm is successful in detecting urban canyons and can be used as an augmentation for GNSS. It is concluded that our fusion framework with the use of digital maps and inter-vehicle communications can be efficiently used for ADAS applications and our local integrity method can further enhance fusion and localization.

ÖZET

AKILLI ARAÇ UYGULAMALARINDA DAHA İYİ KONUMLANDIRMA İÇİN SAYISAL HARİTA VE GNSS FÜZYONU

Bu tez araç konumlandırmayı harita ve araçlar arası haberleşme kullanarak geliştirmeyi hedeflemektedir. Global uydu navigasyon sistemi (GNSS) alıcısı, odometre ve sayısal haritaların parçacık filitresi temelli bir algoritma ile birleştirilmesi önerilmiş ve uygulanmıştır. Algoritmanın değişik uydu görünebilirlik durumlarındaki davranışını test etmek için İstanbul'un değişik noktalarında saha testleri gerçekleştirilmiştir. Sonuçlar algoritmanın %96 başarı ile harita üzerinde doğru yol parçasını seçebildiğini göstermektedir. Önerilen algoritma araçlararası haberleşme ağları (VANET) üzerinde karşılıklı konumlama eklentisi ile daha da geliştirilmiştir. Göreceli mesafenin varış zamanının ölçümü temelli istatiksel bir fonksiyonu deneysel olarak elde edilmiştir. Karşılıklı konumlandırma prosedürü konumlama hassasiyeti ve ağ performansı açısından değişik sayıda işbirlikçi araç içeren gerçekçi simülasyon çalışmaları ile incelenmiş ve IEEE 802.11p radyo modemle donatılmış beş araçlık bir filo ile deneysel olarak değerlendirilmiştir. VANET'lerde işbirliğinin konum ölçümünün yararlanırlığını geliştirdiği gibi tekil bir GNSS alıcısına göre %40 oranında hassasiyetini de artırdığı ispat edilmiştir. Yerel bütünlük sıcaklık haritası kavramı yeni bir yerel bütünlük metodu olarak önerilmiştir. Algoritma şehir kanyonlarının tespit edilmesinde ve GNSS'e bir destek olarak başarılıdır. Sayısal haritalar ve araçlar arası haberleşme kullanan füzyon yapımızın ileri sürücü destek sistemleri uygulamalarında verimli olarak kullanılabileceği ve yerel bütünlük metodumuz ile füzyonun ve konumlandırmanın daha da geliştirilebileceği sonucuna varılmıştır.

TABLE OF CONTENTS

LIST OF FIGURES

LIST OF TABLES

LIST OF SYMBOLS

A	Linear motion system matrice A
B	Linear motion system matrice B
c	Speed of light
c_t	Clock bias
d_b	Distannce to the building b
d_e	Positioning error
e_t	Error vector
f_t	Fault at time t
h_b	Hight of the building b
$h(\cdot)$	A Known nonlinear dynamic measurement function
k_t	A normalizing constant
m_t	Map information at time t
n	Number of satellites
N	Number of particles
N_{eff}	Number of effective particles
n_t	GNSS measurement time t
$p(X_0)$	Probability distribution at X_0 state time index $t = 0$
$p(X_t\|X_t - 1)$	Probability distribution at time t
$p(x_t\|Z_{t-1})$	Prediction for the probability of the vehicle's position
$p(Z_t = z_t\|X_t)$	Probability of receiving measurement z_t n at time t
$r(k)$	Radius of the vehicle k
s_t	Vanet based position at time t
t	Time
T_s	Sampling interval
u_t	Angular speed of ego vehicle time t
v_i	Unkown offset to due errors and noise
$v(i)$	Unknown measurement error of i^{th} collaborative vehicle position
w	Wheel speed rad/seconds

x	x position of the observer
X_i	X ECEF position of satellite i
x_t	Two dimensional location vector at time t
x_t^i	State of particle i at a given time t
x_{true}	True x position
$x(i)$	i^th collaborative vehicle's x position
$\hat{x}$	Estimated x position
$\hat{x}_t$	Minimum mean square estimate
y	y position of the observer
Y_i	Y ECEF position of satellite i
y_{true}	True y position
$y(i)$	i^{th} collaborative vehicle's y position
$\hat{y}$	Estimated y position
Z_i	Z ECEF position of satellite i
Z_i	z position of the observer
z_t	Measurement at time t
α	Angle of visibility on right, a random angle
β	Angle of visibility on left
γ	Line of sigth prevention
σ_x^2	Variance of measurement error in horizantal direction
σ_y^2	Variance of measurement error in lateral direction

LIST OF ACRONYMS/ABBREVIATIONS

2D	Two Dimensional
2DRMS	Twice the Distance Root Mean Square
3D	Three Dimensional
A-GPS	Assisted GPS
ACC	Adaptive Cruise Control
ADAS	Advanced Driver Assistance Systems
AFL	Adaptive Front Lighting
ASN.1	Abstract Syntax Notation One
BDS	BeiDou Navigation Satellite System
BLS	Batch Least Squares
BSD	Blind Spot Detection
C/A	Course Acquisition
C2C-CC	Car to Car - Communication Consortium
CAM	Cooperative Awareness Message
CAMP	Crash Avoidance Metrics Partnership
CAN	Controller Area Network
CBT	Channel Busy Time
CEP	Circular Error Probable
CMS	Camera Monitor Systems
CS	Commercial Service
CSMA/CA	Carrier Sense Multiple Access with Collision Avoidance
DENM	Decentralized Environmental Notification Message
DGPS	Differential GPS
DR	Dead Reckoning
DSRC	Dedicated Short Range Communication
EBA	Emergency Brake Assist
ECEF	Earth-Centered Earth-Fixed
EDAS	EGNOS Data Access Service

EGNOS	The European Geostationary Navigation Overlay Service
EMS	EGNOS Message Server
ESS	Estimated Particle Size
ETSI	European Telecommunications Standard Institute
FOC	Full Operational Capability
FOW	Form of Way
FP7	Frame Programme Seven
FRC	Functional Road Class
FTP	File Transfer Protocol
GLONASS	Globalnaya Navigatsionnaya Sputnikovaya Sistema
GNSS	Global Navigation Satellite System
GPS	Global Positioning System
HDOP	Horizontal Dilution of Precision
ID	Identification
IEEE	Institute of Electrical and Electronics Engineers
IMU	Inertial Measurement Unit
INS	Inertial Navigation System
ITS	Intelligent Transport Systems
LCA	Lane Change Assist
LDM	Local Dynamic Map
LDW	Lane Departure Warning
LIDAR	Light Detection and Ranging
LKS	Lane Keep Support
LOS	Line of Sight
LTO	Long Term Orbit
MAC	Media Access Control
MEO	Medium Earth Orbit
MSA	Mobile Station Assisted
MSB	Mobile Station Based
NHTSA	US National Highway Traffic Safety Administration
NLOS	Non-line of Sight

NV	Night Vision
OBU	On Board Unit
OFDM	Orthogonal Frequency-Division Multiplexing
OS	Open Service
OSI	Open System Interconnection
OVF	Open View Factor
P2P	Peer to Peer
PA	Park Assist
PC	Personal Computer
PLCP	Physical Layer Convergence Protocol
PNT	Position Navigation Timing
PPDU	PLCP Protocol Data Unit
PRN	Pseudorandom Noise
PRS	Public Regulated Service
RCW	Rear Collision Warning
RIMS	Ranging and Integrity Monitoring Stations
RSSI	Received Signal Strength Indicator
RTCM	The Radio Technical Commission for Maritime Services
RTK	Real Time Kinematic
RTS/CTS	Request to Send / Clear to Send
SAR	Search and Rescue
SBAS	Satellite-Based Augmentation System
SIR	Sampling Importance Resampling
SPS	Standard Positioning Service
STNW	Street Network
SVD	Singular Value Decomposition
SVF	Sky View Factor
TOA	Time of Arrival
TSR	Traffic Sign Recognition
TTFF	Time to First Fix
US	United States

USDOT	US Department of Transportation
UTC	Coordinated Universal Time
UTM	The Universal Transverse Mercator
V2I	Vehicle to Infrastructure
V2P	Vehicle to Pedestrian
V2V	Vehicle to Vehicle
VANET	Vehicular Adhoc Network
VSCC	Vehicle Safety Communications Consortium
WAVE	Wireless Access in Vehicular Environments

1. INTRODUCTION

It is well-known that one of the trends in automotive evolution is towards vehicles with autonomous capabilities. Automotive companies have started providing advanced driver assistance systems (ADAS) to increase safety and comfort of the driving experience.

Driver-centric technologies improve driver's awareness by simply warning the driver or taking actions like emergency braking. Most of the global navigation satellite system (GNSS) receivers, cameras, and other vehicular sensors support such applications. Vehicle-centric technologies like anti-lock braking systems (ABS), lane departure warning (LDW) or electronic stability control (ESP) enhance the control of the vehicle. Both driver and vehicle-centric technologies use sensory information for a single vehicle. The introduction of mobile communication infrastructure allows for the sharing of information available in the car with other cars to enhance situational awareness. Communication provides enhanced and more accurate information directly from the ego vehicle to a network of vehicles.

For ADAS and autonomous driving different sensors are used to determine the state of the vehicle and surrounding environment or outside world. External environment sensing involves collecting information about the driving environment. Most important external environment information includes lanes and lane boundaries, nearby vehicles, pedestrians, traffic signs, traffic lights and unexpected traffic participants. Since the quality of sensing of these surrounding environment information is affected by weather, road and light conditions, digital maps can be used to augment information coming from classical sensors. H. Janssen *et al.* [1] presented a good example for augmentation of camera sensor with map fusion for a better traffic sign detection. In the context of speed sign detection [2, 3], map fusion is particularly useful for adverse weather and lighting conditions. Depending on the weather condition one of the sensors may become more feasible and preferred by employing a fusion technique like Dempster-Shafer fusion (see [4]). There are a lot of important attributes available on

the digital map like road directions, turn restrictions and road types which can further improve the contribution of the digital map data [5].

As described in the survey papers [6–8] on ADAS technologies or ADAS equipped vehicles (intelligent vehicles), cameras, radar, and LIDAR are most commonly used sensors for sensing the external environment. In addition to that, because of different type of obstacles and adverse weather conditions, thermopile (temperature) and infrared sensors are also integrated into intelligent vehicle systems. In Figure 1.1, conventional sensors and their related ADAS technologies are summarized [9]. As it may be seen from the figure either the range or the sensing area is limited for conventional sensors.

Sensor Type / Application	Vision	Infrared / Thermal	Long Range Radar 76..81MHz	Short / Mid Range Radar 24..26 / 76..81 GHz	Lidar
Adaptive Front Lighting (AFL), Traffic Sign Recognition (TSR)	X				
Night vision (NV)	x	X			
Adaptive Cruise Control (ACC)	x		X	X	x
Lane Departure Warning (LDW)	X				
Low-Speed ACC, Emergency Brake Assist (EBA), Lane Keep Support (LKS)	x			X	X
Pedestrian detection	X	x		X	
Blind Spot Detection (BSD), Rear Collision Warning (RCW), Lane Change Assist (LCA)	x			X	x
Park Assist (PA)	X			X	x
Camera monitor systems (CMS)	X				

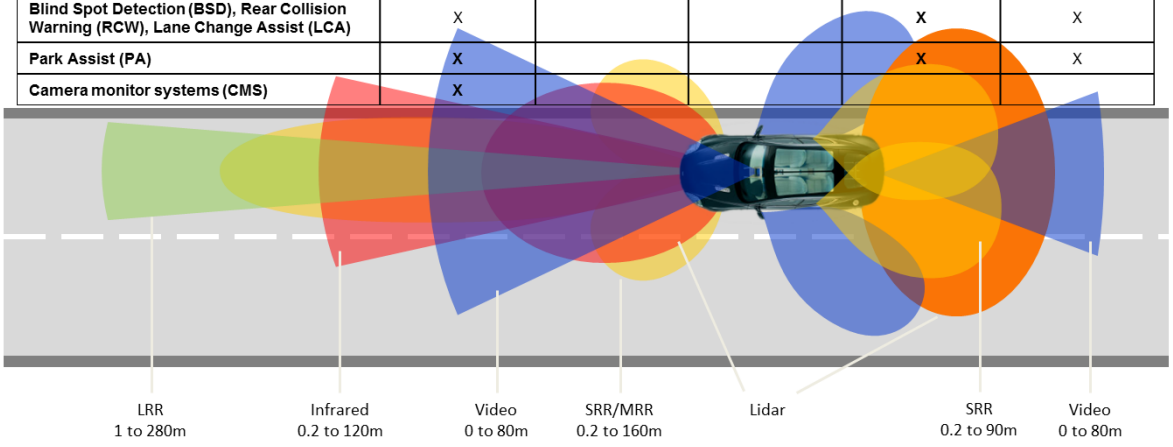

Figure 1.1. Sensors and ADAS Applications (Courtesy of Texas Instruments).

The relative positions of the objects detected by the sensors are also important for the ADAS decisions. Most of the time ADAS decisions are highly dependant on the accuracy of positioning. Positioning can be handled in a local frame by placing

ego vehicle in the center of the local map. Additionally, to be able to retrieve more information positioning can be done in the global coordinates which will also require selecting the correct location on the available digital map, namely map-matching. For example, for the system to decide on an emergency break to prevent a frontal collision avoiding the crash depends on the distance and relative position of the vehicle and whether it is in the same lane as the suddenly braking car.

Global Navigation Satellite System (GNSS) is the infrastructure that allows users with a compatible device to determine their position, velocity and local time in the global frame by processing signals from satellites in space. A variety of satellite positioning systems, including global constellations and Satellite-Based Augmentation Systems (SBAS), provides GNSS signals. While GNSS is the most important technology to provide the position information for an intelligent vehicle system, accuracy and availability are still not enough for fully autonomous driving. Problems like urban canyons and tunnels prevent GNSS from becoming the sole provider of location information in the intelligent vehicle domain.

In many cases, it is logical to fuse different subsystems and sensors with different characteristics to ensure quality required by safety critical applications. Sensor fusion is also attractive to get a better localization accuracy. However, deploying more sensors is not always cost effective and may create maintenance problems. That is why, the core idea of this thesis is to integrate the existing facilities in a car such as digital maps, GNSS, vehicle to vehicle (V2V) communication and odometer to enhance and assure accuracy and availability of the positioning platform. Our approach is innovative in the sense that it uses digital maps and V2V communication as an additional sensor yet it is in an excellent price/performance point since we are mostly utilizing existing off-the-shelf technologies. We propose a generic Bayesian fusion platform where additional sensors can be fused if needed in the near future.

The integrity of the GNSS as a sensor is a critical and a complicated problem. Integrity is defined as the measure of trust for the correctness of the GNSS measurement. To be able to fuse sensors safely, the error characteristic of a given sensor should be

known. We have thoroughly investigated the integrity concept and proposed a method to enhance the fusion of the GNSS with other vehicular sensors.

To be able to propose an innovative but practically applicable method, we reviewed current state of the art for our underlying subsystems. We surveyed current GNSS technologies, available digital maps, and communication technologies. In GNSS domain there are four different global constellations available. Currently, American global positioning system (GPS) and Russian globalnaya navigatsionnaya sputnikovaya sistema (GLONASS) provides global coverage. Europe's Galileo and China's BeiDou Satellite Navigation System (BDS) are partially available. Digital maps reached nearly to global coverage with the demand coming from car navigation systems. Digital maps include a lot of important attributes, such as road types, directions, and speed limitations which can be utilized for an improved localization. Lately, there are attempts to enrich existing digital maps, such as lane geometry, to cover needs coming from ADAS applications.

We also checked other sensor fusion attempts to get better positioning and map-matching. In the literature, we have seen that maps are rarely used to enhance positioning even though map matching is worked extensively. Since the vehicular communication technologies are relatively new to the market, their use for localization has not been exploited yet. Existing attempts does not cover real field tests and do not utilize map fusion [10].

In the first part of our research, we focused on map-fusion and map-matching. We created a Bayesian framework for localization and map-matching using digital maps. We proposed four different versions of a particle filter based map matching and localization algorithm, and we proved that we could enhance positioning and map-matching quality significantly. We tested our proposed algorithms in the field with different road types. We used a vehicle equipped with simple tracking black box integrated with the odometer. We implemented the proposed algorithms on a low cost, readily available embedded system. We also prepared demonstration and simulation environments.

While working on GNSS fusion with digital maps, we realized that local conditions could affect the quality of fusion due to unknown error range of the GNSS receiver. We have attempted to define a novel integrity method to overcome this problem, namely local integrity heat map. The availability of such a heat map can enhance the accuracy of the positioning system through better error modeling and also can provide an integrity feature to define the level of reliability of the GNSS sensor. This type of approach can be used in developing a high integrity enhanced receiver suitable for autonomous driving. A high integrity receiver can output the expected error range. Different thresholds depending on the reported error can be defined to select autonomous, semi-autonomous or manual control of the vehicle.

In the third part of our research, we have focused on vehicular communication and its use for better positioning. We used the idea of dissemination of position information from different channels to overcome local problems like tunnel passages, high buildings. We upgraded existing Bayesian framework by employing additional localization through multilateration of the vehicle to vehicle (V2V) messages.

The resulting system and algorithms are unique in many aspects. We used digital maps and V2V communication as an additional sensor. We also carried real world road tests where in the literature only limited amount of work is available supported with real life testing.

Figure 1.2 provides an overview of our architecture. The application library and the software components, marked with yellow, are implemented on the on-board-unit (OBU) of a vehicle. Most of the sensors can be integrated through a network connection. In our implementation, we utilized a serial hardware interface. Digital map is optimized to lower storage requirements. We also implemented the particle filtering algorithm to fuse all the information coming from sensors. In the Figure, gray items are other possible sensors which can be integrated into the system. Implemented software Bayesian fusion framework is available for easy integration of possible other sensors like an inertial navigation system (INS) as shown in the picture.

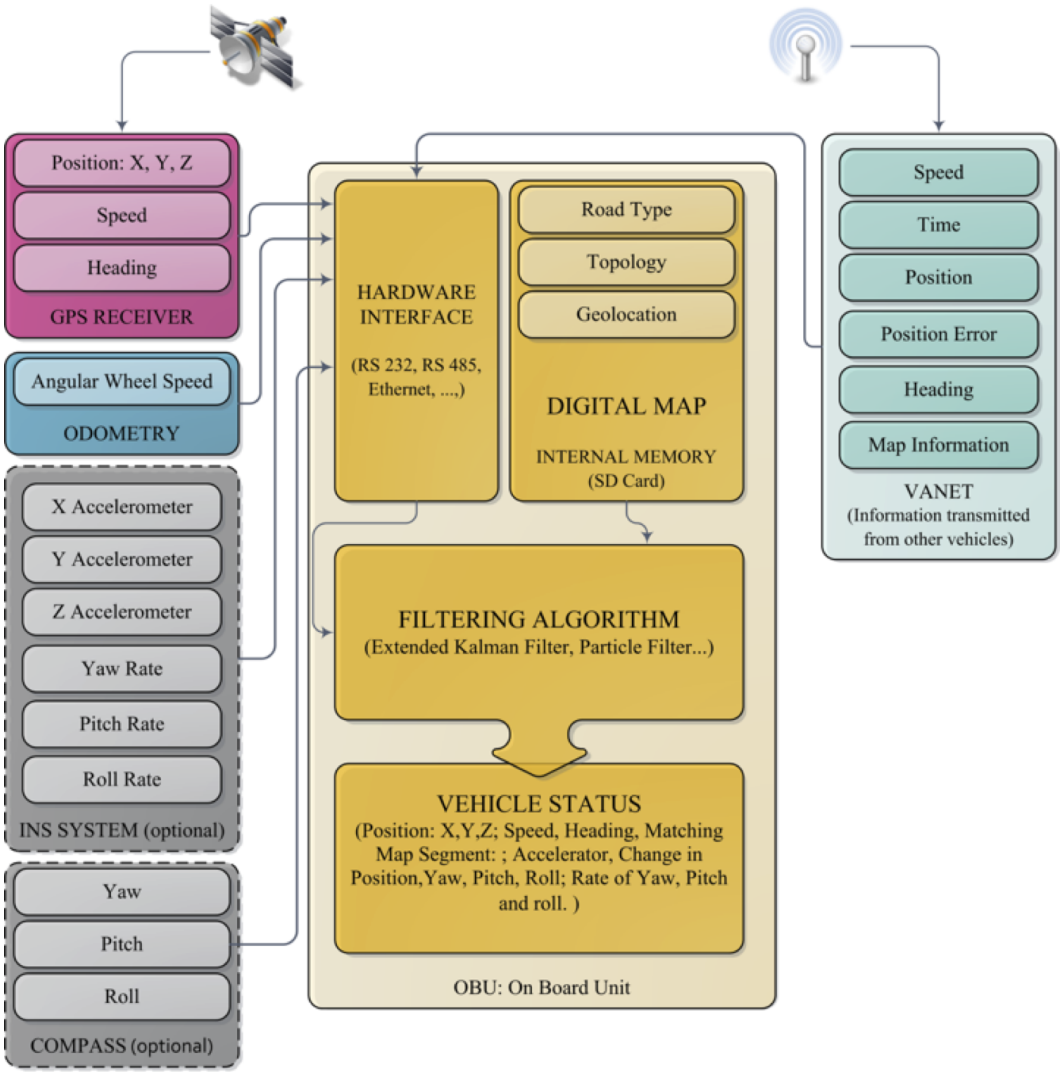

Figure 1.2. Architecture Sensor Fusion for Localization.

1.1. Contributions

Main contributions of the thesis are as in the following:

- A particle filter vehicle localization and map matching algorithm are proposed which utilizes digital map topology. Four different implementations are developed for the proposed algorithm and tested in real world conditions. The reason behind the four different implementations is to make valid proof of the improvement

provided by map fusion. The first algorithm does not use the map information to create a base for the minimum performance of GNSS and odometer based positioning system in a Bayesian framework. Other three algorithms differ in the digital map usage. It is shown that introduction of digital maps improves the location accuracy and map matching performance when map topology and attributes are utilized. More accurate localization is provided with better cost/performance as it employs inexpensive widely available components.

- When compared to existing algorithms in the literature, proposed system outperforms previous algorithms in all urban, suburban scenarios with a similar sensor setup. It reaches the same performance as the algorithms which utilizes expensive sensors or not widely available technologies.
- Local integrity heat map concept is defined and is validated with real world road tests. It is shown effective in detecting urban canyons and can be used as a local correction factor.
- Local integrity heat map concept is compared with other available local integrity models. The proposed method is cost effective and can be used in practical applications.
- A vehicular ad-hoc network (VANET) assisted cooperative vehicle mutual positioning algorithm is proposed. It is shown that previously proposed performance of the particle filter algorithm can be enhanced with the addition of relative positioning measurements.
- VANET based localization is a demanding task in a real field test with moving vehicles. Modeling the time lost at the physical layer of the communication medium was a real challenge and accomplished successfully.
- The algorithm improves location accuracy and even more importantly keeps localization available in the absence of data from GNSS. Performance is proved through simulation as well as the real world tests.
- It is shown that physical implementation of VANET localization differs from simulation drastically due to timing problems. There are a few real world tests in the literature for similar works. Many problematic timing issues have to be solved in real world implementation of VANET localization algorithm, but the

performance of the algorithm successfully demonstrated.

- A Bayesian fusion framework for localization and map matching where additional sensors can easily be integrated is developed. The framework is used for both initial map fusion algorithm and also VANET fusion algorithms.
- The work covered in the thesis is disseminated through nine different publications.
- Implemented algorithms have been used in two European Union and one locally funded research and development projects. Results are successfully demonstrated in public demos.
- A patent application is filed for the heat map concept.

1.2. Outline of the Thesis

Rest of the thesis is organized as follows: Chapter 2 provides detailed information about localization technologies and ADAS. Satellite-based positioning systems are discussed in detail. Fundamentals of VANETs are described. Finally, description of digital maps used in our work is given. In Chapter 3 the proposed particle filter algorithm for map matching and localization is described. Bayesian fusion framework with particle filter implementation is described. Results of the field tests are included. Chapter 4 makes the definition of local integrity concept and gives details about our proposed local integrity heat map concept. Chapter 5 describes VANET assisted cooperative vehicle mutual positioning. Implementation of cooperative positioning through V2V communications are given together with the integration of this information into the Bayesian fusion framework. Simulation results with real field tests are presented. Chapter 6 includes the conclusions.

2. LOCALIZATION TECHNOLOGIES AND ADAS APPLICATIONS

2.1. Introduction

In this chapter, we will provide state of the art in GNSS, VANET and digital map technologies primarily focusing on the aspects utilized by the algorithms developed in this thesis.

Global Satellite Navigation Systems have been developing for many years to provide a more accurate fix and possibly a faster initial positioning. Assistance information has been shown to enhance initial positioning in customer level devices as well. This information can be transmitted in different ways. Satellites, stations, and even vehicles can be used in data dissemination. The most typical GNSS system is GPS. Galileo is a civilian technology from Europe. Glonass is from Russia and BeiDou Navigation system (BDS) also known as COMPASS is a Chinese satellite navigation system. We will explain these technologies in detail especially mainly on GPS and Galileo.

In addition to global localization techniques digital maps and mobile communications are becoming a core technology for better sensing the vehicle environment and improving localization of the ego-vehicle and surrounding vehicles. Digital maps can be considered, and treated, as an additional sensor. When compared with the sensors like camera, lidar, radar they provide longer range information about the vehicle's environment. To be able to use the information in digital maps the correct segment on the digital map should be selected and this is called map matching. The correctness of the map matching is crucial to get the best out of the digital map data.

There are many available forms of the digital map data. Vector and raster maps are the basic two categories. Raster based data are tile based aerial or satellite photos. Raster data require a significant amount of storage and but are simpler to process.

Vector maps are graphs with geolocation information. The vector data mostly consist of lines, curves, polygons and points. Vector data can be stored in different file structures and database models and can be compressed into smaller sizes. Processing the vector data requires mainly graph algorithms and is much more complex than the raster data.

As digital maps are becoming one of the core components of the autonomous driving more detailed maps are needed. In the last years highly detailed maps which include attributes like lane information, detailed 3D buildings, pavements, processed lidar data and road signs have been developed for autonomous driving.

Along with the digital maps, mobile communication is becoming another sensor for the vehicles. The importance of communication and digital maps as a sensor is due to their ability for providing longer range sensing and more trustable information. For example, they are only available sensors which can provide information about locations which are occluded by buildings.

There are many connected car applications utilizing cellular technologies. But safety applications require, a dedicated, responsive and more local communication. Wireless inter-vehicle communication enables information dissemination between vehicles, to improve safety, efficiency, and even to enhance infotainment aspects. Safety applications, like collision avoidance or hazardous road warnings, use location information to estimate collision probabilities between vehicles or mark the location of the current event are examples of use-cases where inter-vehicle communication becomes necessary. Continuous dissemination of location information between vehicles provides a better understanding of the environmental changes and unexpected behaviors. Due to the high mobility and dynamic structure of VANETs, routing mechanisms need periodically updated location information.

2.2. Global Satellite Navigation Systems

2.2.1. Global Positioning System

Global Positioning System (GPS) is the most widely used GNSS in the world. The goal is to provide location and time information to the receivers. Although the initial design is for military usage, civilian usage is in increasing demand. It is freely accessible to anyone using a GPS receiver. The GPS constellation contains 24 satellites but four satellites in line of sight are sufficient to position the user. Positioning depends on the accurate timing information of the signals received. Satellites transmit their location information along with the message generation time. The receiver uses the timestamp and the speed of light to compute the distance from the satellites. The computed distances are used together with satellite positions to reveal the receiver's position. The position found is shown on an underlying digital map stored in the receiver device. Additional features derived from the location information lead location-based applications in the navigation market. Accurate timing information is also used in traffic signaling and base station synchronization. When the number of visible satellites is less than four, the GPS receiver may use other techniques such as dead reckoning, additional information from the vehicle computer, etc. to compensate missing information.

GPS is a fundamental component of a present day vehicle. GPS can be used to find absolute position and velocity. With access to a precise map, a vehicle can determine ego-location with respect to its destination and on the road network. This information is needed, for example, to compute optimal routes or driving directions. With a vehicle-to-vehicle wireless communication system, it can also be used to compute relative position and relative speed information.

The information available from a GPS is:

- Absolute position in a geodetic coordinate system, for example, latitude, longitude, altitude, X-Y-Z earth centered earth fixed, or The Universal Transverse

Mercator (UTM)

- Velocity and course over ground information(Horizontal Speed, orientation to the true north).
- Precise time and pulse per second
- Raw information that can be used for precise post-processing applications

Various levels of accuracy in GPS measurements can be obtained, depending on the types and number of GPS signals received and analyzed, the algorithms, and the availability of externally supplied correction data, including differential correction and real time kinematic correction data. Satellite visibility and geometric configuration is also a significant factor in GPS measurement accuracy, especially in areas with tree foliage coverage or buildings that can occlude signals or create multipath reflections.

Generally speaking, in areas with an unobstructed view of the entire sky and an acceptable orbital configuration of visible satellites, a standard inexpensive or embedded GPS receiver can achieve position accuracies on the order of 5-15 meters. This accuracy is sufficient for providing navigation and routing instructions for a human driver, but it is insufficient for resolving which lane a vehicle is currently occupying.

Correction signals are available from free and public services to achieve the next level of GPS position accuracy. Nationwide Differential GPS (NDGPS) correction signals broadcast in the long wave band and satellite-based augmentation systems (SBAS) such as the Wide Area Augmentation System (WAAS) provided by the US Federal Aviation Administration or the European Geostationary Navigation Overlay Service (EGNOS), [11].

A satellite-based augmentation system (SBAS) capable GPS receiver, using one of these basic differential correction data services broadcast over a large area of the planet, can achieve position accuracies on the order of 1-2 meters. This is a sufficient accuracy level for some safety applications, and can sometimes resolve lane identity. Locally computed differential corrections or commercial SBAS systems can achieve sub-meter accuracies. The sub-meter accuracy provided by SBAS significantly improves

the performance of data collection systems and safety systems, and in some cases, it is sufficient for longitudinal vehicle automation.

The more sophisticated commercial correction services such as EGNOS can achieve position accuracies of 10 cm or better. High precision locally computed real-time kinematic correction systems can produce position accuracies of 1-2 cm. Measurements at this precision are sufficient for full vehicle automation. Of course, both the correction data and the GPS receiver hardware needed to achieve these levels of accuracy are quite expensive.

The time information from the GPS is particularly useful in inter-vehicle communications since it allows the precise synchronization of clocks across multiple vehicles and infrastructure systems.

2.2.1.1. Fundamentals of GPS. As seen in the Figure 2.1 [12] the GPS constellation consists of 24 satellites arranged in 6 orbital planes at an altitude of 12,500 miles (20,200 km). Each satellite completes 2 orbits each sidereal day.

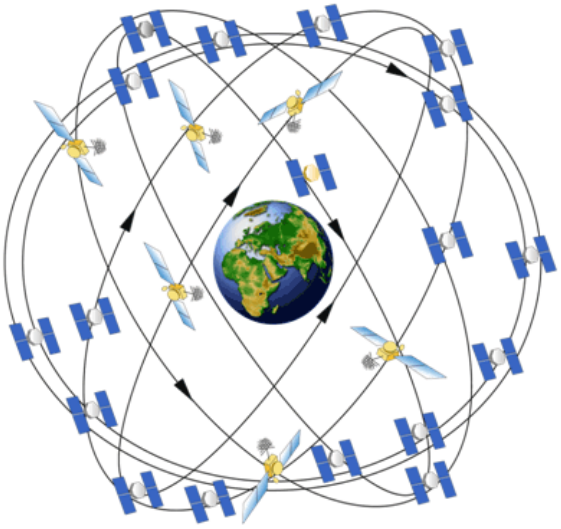

Figure 2.1. GPS Satellite Constellation.

Each satellite broadcasts at least the following signals and information:

- L1 Frequency: 1575.42 MHz (19 cm) at 25.6 W
- L2 Frequency: 1227.60 MHz (24 cm)
- Course Acquisition (C/A) Code (on L1) : 1.023 megabits/sec PRN (pseudorandom noise), 1023 bits long (repeats every 1 ms, 300 km)
- Precise (P,Y) Code (on L1, L2, 90° out of phase)
- Navigation Message : 50 Hz data, 12 minute message time
- Sub frame Data : Coordinated universal time (UTC) and clock corrections, Almanac, Precise ephemeris data (30 sec), Ionospheric propagation data

Newer GPS satellites support signals transmitted on additional frequencies, for example on the L5 (1176.45 MHz) band.

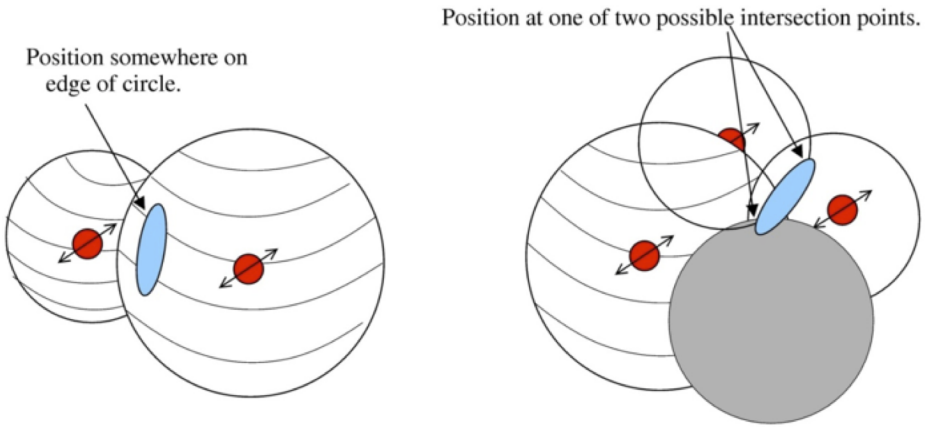

Figure 2.2. Position Information Found from the Intersection of Multiple Spheres (Triangulation).

GPS technology is, fundamentally, based on triangulation and the fact that, in terms of RF signal propagation, distance traveled is directly related to the elapsed time (in a vacuum 3.3 ns is approximately equivalent to 1 meter). Consider that any object that is known to be a distance D from a given point must lie on the surface of a sphere of radius D centered on that point. Two non-coincident points with known distances

from the object define two spheres, and the object must lie on the intersection of those spheres, which is a circle except in exceptional degenerate cases. Three points reduce the possible location of the object to two points, one of which is, in the case of the GPS system, unfeasibly far from the surface of the earth. Thus, to compute the position of an object we need its distance to at least three known points. This is illustrated in Figure 2.2.

Satellites transmit navigation messages. Navigation message includes almanac and ephemeris. Almanac data, which has two formats (YUMA and SAM), contains information about time and status of the satellite constellation. Almanac lifetime is in one week periods. Ephemeris contains the orbital information of each satellite which is used to calculate the position of the satellite in orbit. Ephemeris lifetime is two hours. Ephemeris contains the positions in orbits which can shift as the time passes due to gravity of the sun and moon.

The orbital location of a GPS satellite can be computed precisely using the almanac and ephemeris data transmitted by the satellites themselves coupled with a mathematical model of orbital dynamics. Indeed one of the primary functions of the GPS ground control system is to track the satellites and regularly update the almanac and ephemeris information. What remains is to determine the distance, or range, from each of at least three satellites to the antenna of the GPS receiver.

As mentioned earlier, the distance traveled is a direct function of the elapsed time between the transmission of a signal and its reception. GPS satellites carry atomic clocks of very high precision, and the GPS ground control system ensures that the clocks of all satellites are synchronized to within a few nanoseconds. The data transmitted by each GPS satellite also contain information about when transmissions are made. All GPS satellites transmit on the same frequencies, so each satellite transmits its data stream by modulating its binary sequence with pseudorandom noise (PRN) code. On the L1 channel, the PRN codes are 1023 bits long and thus repeat every millisecond. Since the GPS receiver knows the PRN sequence of each satellite, it can produce its copy of that sequence synchronized to its internal clock and use correlation to determine

the time offset of the received and internally generated signals for each visible satellite. (See Figure 2.3.)

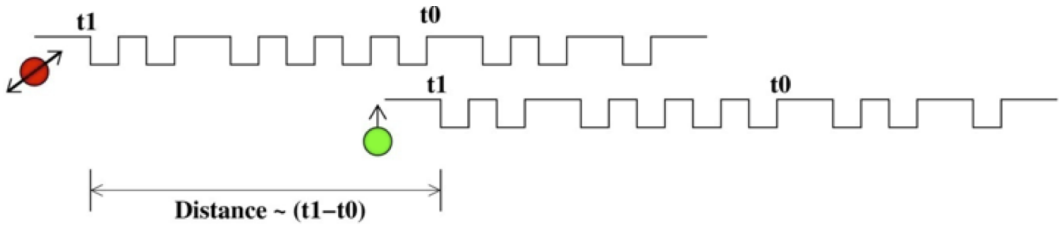

Figure 2.3. Pseudo Range from Temporal Correlation.

However, GPS receivers typically use nothing more than a crystal controlled clock with considerable drift over time relative to the GPS satellites. So it is necessary to align the receiver clock with the satellite clocks. Clock drift introduces the fourth unknown into the problem, and therefore a full GPS position fix requires four satellites at the minimum. Since the clock bias, the difference between the receiver's clock and the satellite clock is unknown, the distance or range measured by the PRN correlation process is called a pseudo range. Expressed mathematically in Earth-Centered Earth-Fixed (ECEF) coordinates, the measured pseudo range for each visible satellite is given by Equation 2.1

$$P_i = \sqrt{(X_i - x)^2 + (Y_i - y)^2 + (Z_i - z)^2} + c_t + v_i \tag{2.1}$$

where (X_i,Y_i,Z_i) is the ECEF position of the satellite, (x,y,z) is the ECEF position of the observer,c_t is the clock bias (c is speed of light), v_i is an unknown offset to due errors and noise, $i = 1 \ldots, n$ where n is the number of visible satellites

With $n \geq 4$ satellites, this forms a system of possibly over determined nonlinear equations that can be solved for the four unknowns using a variety of numerical techniques to obtain the (x, y, z) position coordinates and the clock bias c_t at the antenna of the GPS receiver. As an example, one possible solution technique involves linearizing the pseudo range equations an estimate of (x, y, z) using a Taylor's series approxima-

tion and solving using an SVD/Pseudo inverse approach or a Newton-Raphson iterative approach.

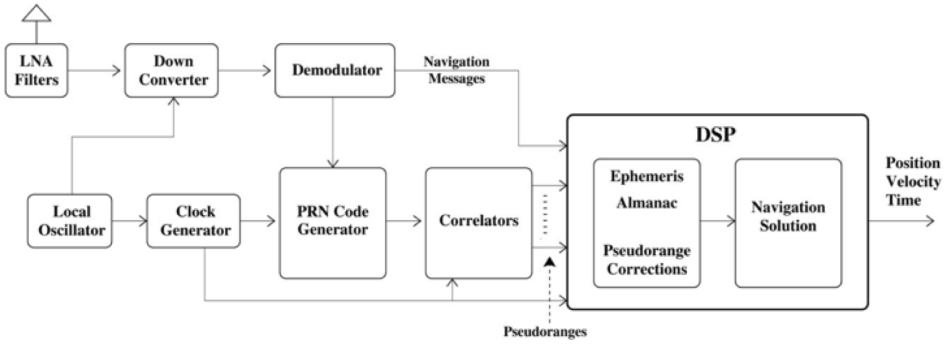

Figure 2.4. Generalized Block Diagram of GPS Receiver.

2.2.1.2. GPS Error Sources. Considering the above, it is clear that errors in the final position solution can arise from errors in any of the fundamental measurements: including satellite position, clocks, and timekeeping, and the pseudo range distance measurements. A basic error budget (1-sigma values) for a standard GPS receiver would be

- Broadcast Ephemeris (satellite position and orbit data): 2.5 meters
- Satellite Clocks: 1.5 meters
- Ionosphere Delays: 5.0 meters
- Troposphere Delays: 0.7 meters
- Receiver Noise and Numerical Computations: 0.7 meters
- Multipath and Diffraction: 1.5 meters

It is worth mentioning that many of these errors can be considered as slowly time varying (autocorrelated) signals or almost as bias terms, so is it common to see GPS position errors slowly wander within a region surrounding the exact position. Given the actual position and the cloud of GPS measurements of the receiver, two different accuracy measures are used in the industry:

- *CEP (Circular Error Probable):* The radius of the circle that is expected to contain x percent of the measurements (a typical percentage could be 50)
- *2DRMS (Twice the Distance Root Mean Square):* The radius of the circle that is expected to contain 95 percent of the measurements

GPS manufacturers tend to report the expected performance of a given receiver using one of these two methods [13].

2.2.2. Galileo

Galileo is the global navigation system of Europe which provides fully autonomous satellite-based positioning, navigation and timing capability for global high-performance services. Galileo is designed to deliver real-time positioning with high precision (meter accuracy) for a publicly available system. Galileo presents dual frequencies as standard. It is interoperable with GPS and Glonass, the US and Russian global satellite navigation systems respectively. By offering dual frequencies as standard, Galileo is set to deliver real-time positioning accuracy down to the meter range. On 21 October 2011, the first two of four operational satellites designed to validate the Galileo concept in both space and on Earth are launched. Two more followed on 12 October 2012. In-Orbit Validation (IOV) phase has been followed by new Full Operational Capability (FOC) satellite launches. Soyuz has so far launched four pairs of FOC satellites from French Guiana, on 22 August 2014, 27 March 2015, 11 September 2015 and 17 December 2015. The fully deployed Galileo system will consist of 24 operational satellites plus six in-orbit spares, positioned in three circular Medium Earth Orbit (MEO) planes at 23,222 km altitude above the Earth, and at an inclination of the orbital planes of 56 degrees to the equator [14].

The Galileo system will be an independent, global, European-controlled, satellite-based navigation system and will provide a number of guaranteed services to users equipped with Galileo-compatible receivers.

The Commercial Service (CS) is one of the future satellite-based services planned for the Galileo global navigation satellite system, in addition to the Open Service (OS), the Search And Rescue service (SAR) and the Public Regulated Service (PRS).

The Galileo CS offers attractive opportunities for possible future road services, including added-value data and enabling authentication-based services. In addition to the CS, the signal authentication has also been proposed and considered for possible future evolutions of the Galileo OS signal.

Galileo is partially available at the moment. Commercial GNSS receiver can fuse the information available from Galileo and GPS. In this thesis, we have also used such hardware. The integration is at the chip level as the Galileo service becomes fully available, quality of information from the GNSS receiver should increase.

The Galileo Commercial Service will allow for the development of applications for commercial or professional use owing to improved performance and data with greater added value than that obtained through the OS. In fact, the CS will use the OS signals plus two encrypted signals (ranging codes and data) on the E6 band. It will potentially ensure centimeter level accuracy, improved reliability, and signal authentication to enabled receivers. Typical value-added services could include service guarantees, precise timing services, the provision of enhanced ionosphere delay models, local differential correction signals for extreme precision position determination and other services based on the broadcast of system information data.

The objective of the CS is to provide added value data to the final users of this service, sending information/data through encrypted signals: therefore a cryptographic key will be needed by the users to access them. These added value data will be generated by future Service Providers external to the Galileo system. These Service Providers will pay the European Commission (EC) for the right to transmit their data through the Galileo signals, and they will, on return, charge the final CS users for the reception of their encrypted data. Figure 2.5 presents the CS key players and their role.

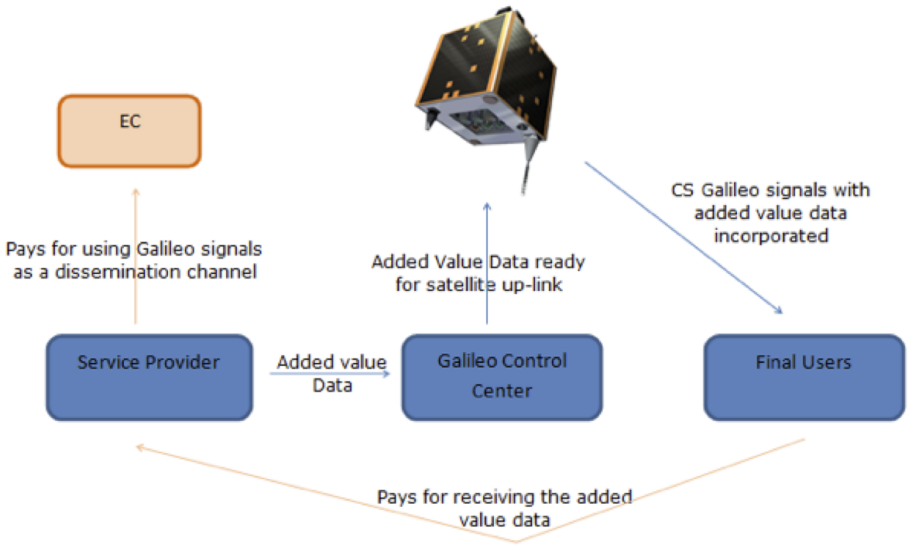

Figure 2.5. Actors Involved in the Galileo Commercial Service.

As far as a possible investigation on the potential role of the Galileo CS in this thesis is concerned, it is also necessary to point out that a complete technical specification document related to the CS signals (also known as Signal in Space Interface Control Document) is still not publicly available. The Galileo CS cannot be considered as a current state of the art, due to the lack of complete information as well as CS signals. As a consequence, the support to the Galileo CS cannot be considered in our developments

2.2.3. GLONASS

GLONASS is the Russian counterpart to GPS. It consists of a constellation of satellites in medium Earth orbit (MEO), a ground control segment, and user equipment. The system was formally declared operational in 1993. In 1995 it was brought to a fully operational constellation (24 GLONASS satellites of the first generation). Reduction in space industry funding led to degradation of the GLONASS constellation. In 2002 the GLONASS constellation consisted of 7 satellites that were insufficient for navigation support of the Russian territory even with limited availability. GLONASS was behind

GPS in terms of accuracy.

A modernization program started in 2002. As a result GLONASS system was preserved and modernized and became operational consisting of GLONASS-K satellites. Ground control segment was upgraded that together with the orbital constellation ensures the accuracy characteristics at a level commensurate with those of GPS The State Standard of time and frequency facilities and the Earth rotation parameters definition facilities were modernized. GNSS augmentation prototypes, a great amount of patterns of core receiving and measuring modules, positioning, navigation and timing (PNT) equipment for civil and specific use and related systems were designed. Currently, system is in use with 24 satellites [15].

2.2.4. BeiDou Navigation Satellite System

BeiDou Navigation Satellite System (BDS) is China's global navigation satellite system which has been developed independently. BDS is composed of three parts: the space section, the ground section, and the user section. The space section contains five geostationary orbit satellites and 30 non-geostationary orbit satellites. The ground section consists of the main control station, the injection stations and the monitoring stations. The user section includes terminals of BeiDou system [16]. It became operational in China in December 2011, with 10 satellites in use and began offering services to customers in the Asia-Pacific region in December 2012. It is planned to start serving global customers upon its completion in 2020.

2.3. Improving GNSS Quality and Availability

Following services are the most common ways to improve GNSS quality or availability:

- *Assisted GPS (A-GPS):* A-GPS is a widely adopted solution typically seen on smartphones nowadays. GPS information is combined with assistance server information to enhance the time to first fix (TTFF) and positioning. A standard

GPS device needs around 30 seconds on average to fix the position because it needs to download the ephemeris and almanac information from the satellites and the bandwidth is low. The A-GPS server provides this information over the terrestrial network to A-GPS receivers to shorten the positioning time. If clock information is also provided, it yields for better positioning as well.

- *The European Geostationary Navigation Overlay Service (EGNOS):* EGNOS uses ground stations to receive GPS data, calculate the corrections and broadcast the fix messages via geostationary satellites. Three geo satellites broadcast corrections and integrity information of the satellite constellation. Beside geo satellites, EGNOS has ground stations for different purposes such as mission control, wide area network and monitoring station
- *EGNOS Data Access Service (EDAS):* EDAS is a ground-based access to EGNOS information. The primary goal is to disseminate EGNOS corrections on terrestrial networks. If the receiver is out of range of EGNOS satellites such as in urban canyons, EDAS can be used.
- *Differential GPS (DGPS):* DGPS is another kind of GNSS augmentation system that use ground-based reference stations that enable the broadcast of differential information (rover) to improve accuracy. In contrast to EGNOS, DGPS do not provide integrity information.

2.3.1. Assisted GPS

Assisted GPS is yet another GPS receiver that uses assistance information from other sources than the satellite to enhance time to first fix (TTFF). A-GPS receiver can fix the position in a warm start case under five seconds. The assistance data includes ephemeris, almanac and time information. The use of this information depends on the operating mode. Assisted GPS has two modes of operation:

- *Mobile Station Based (MSB):* Mobile station can provide ephemeris and almanac which lets the receiver to find satellites quickly. In this case, the network can also provide precise time to the receiver.

- *Mobile Station Assisted (MSA):* In this case, the device receives information needed to acquire GPS signals and sends its received signals with its time information to the GPS assistance server. The server is presumed to have good satellite information and sufficient computing resources. It calculates the position using the received information and sends the position back to the GPS receiver.

During cold start, a conventional GPS receiver needs to download both the almanac and ephemeris data while in warm start the GPS receiver needs to download ephemeris only. Ephemeris itself is 900 bits which take 18 seconds to download theoretically since the bandwidth of GPS communication is 50 bps.

Assistance data (ephemeris and almanac) can be transmitted to a device via GSM network which is called the online method. Since GSM network connection is faster than satellite communication, it yields to faster position fixes. Note that real time information is from the GSM provider's A-GPS server. This is beneficial in places with weak signals or where the satellite visibility is restricted due to the conditions such as urban canyons.

In the case of the offline method, the receiver uses Long Term Orbit (LTO) to predict ephemeris whose quality degrades as time passes. The benefit of the offline method is that it enables the receiver to work without any connection and use the assistance provided [17].

In Figure 2.6 [18] a mobile device with A-GPS receiver can receive information from the server to capture signals and sends its signals to the location server. Note that the communication is based on the cellular network. The location server then computes the client's position using its fresh ephemeris data and sends the position back to the receiver device using the network. This is a typical scenario of today's commonly used positioning systems. This scheme shows an example of the online method of positioning with station assistance. Although the apparent benefit of this scenario is the position computation task is assigned to the server, so the receiver only receives the final fix, it

will not work if the connection is lost. In rural areas or if the cellular coverage is poor, positioning will be influenced as well.

Figure 2.6. A-GPS Communication Schema.

2.3.2. EGNOS/EDAS

The EGNOS represents the Europe's first venture into satellite navigation. EGNOS is an SBAS and provides an augmentation signal to the Global Positioning System (GPS) Standard Positioning Service (SPS). Presently, EGNOS augments GPS using the L1 (1575.42 MHz) Coarse/Acquisition (C/A) civilian signal function by providing correction data and integrity information for improving positioning and navigation services over Europe. EGNOS infrastructure consists of three geostationary satellites over Europe and a network of ground stations. Since it is based on GPS, the EGNOS signal does not require major changes to the receivers. Today, many GPS receivers available on the market are also SBAS-enabled, thus, suitable to process and exploit EGNOS signals.

EGNOS currently offers three types of services [19]:

- *Open Service:* The service is provided free of charge without any guarantee or resulting liability. It is open for use to anyone with an EGNOS-enabled satellite navigation receiver. The Open Service was launched on October 1, 2009.
- *Safety of Life signal:* EGNOS provides a valuable integrity message warning the user of any malfunction of the GPS signal within six seconds. This integrity message is essential when satellite navigation is used for safety critical applications, such as flying aircraft or navigating ships through narrow channels. The EGNOS Safety-of-life Service was certified for civil aviation in 2011.
- *Commercial Service:* EGNOS provides a terrestrial commercial data service called the EGNOS Data Access Service (EDAS). EDAS is the single point of access to the data collected and generated by the EGNOS ground infrastructure (RIMS) mainly distributed over Europe and North Africa. Upon registration, EDAS is accessible to authorized users (e.g. added-value application providers) through the connection to a dedicated internet domain.

It must be noticed that EDAS disseminates EGNOS data in real-time: its services are available from July 30, 2012, and are intended to be delivered and maintained over the long term [20]. Figure 2.7 [19] shows the high level architecture of EDAS.

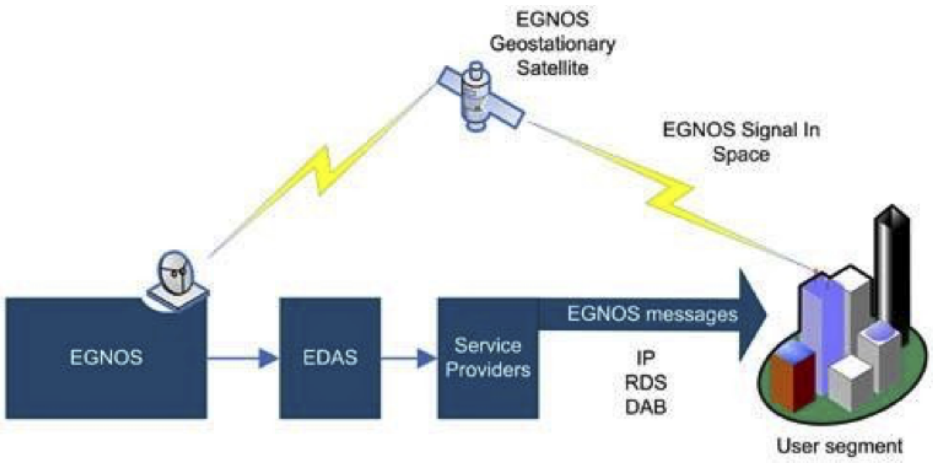

Figure 2.7. EDAS High-Level Architecture.

Table 2.1. EGNOS Message Types, Contents, Refresh and Validity Periods.

Message Type Identifier	Data content	Refresh Period(s)	Validity Period(s)
0	Don't use for safety applications (for SBAS testing)	6	N/A
1	PRN Mask assignments, set up to 51 of 210 bits	120	600
2 to 5, 24	Fast Corrections, UDREI	Variable	Variable
6	Integrity Information	6	18
25	Long term satellite error corrections	120	360
9	GEO navigation message (X, Y, Z, time, etc.)	120	360
7	Fast correction degradation factor	120	360
10	Degradation parameters	120	360
18	Ionospheric grid point masks	300	1200
26	Ionospheric delay corrections	300	600
12	SBAS Network Time/UTC offset parameters	300	86400
17	Almanac Data	300	none

Registered users can access EDAS to form new innovative applications, to integrate into existing services, or to support research programs. These users exploit the different types of the data available from EDAS, which are [20]:

- raw GPS, GLONASS and EGNOS GEO observations and navigation data collected by the entire network of Ranging and Integrity Monitoring Stations (RIMS A, B, C) and Navigation Land Earth Stations (NLES);
- EGNOS augmentation messages broadcast from the EGNOS geostationary satellites, as normally received by EGNOS users. It must be remarked that the raw data can be provided in both ASN.1 and RTCM format. This information is provided by EDAS in real-time with an update rate of one second.

In addition to raw data, EDAS also provides the EGNOS Augmentation Message. The EGNOS augmentation message is formed of a number of distinct message types containing various aspects of the overall augmentation message. The message types provided are summarized in the Table 2.1, where all message type identifiers, data content, refresh and validity periods are reported [21].

As already remarked, EDAS disseminates EGNOS data in real-time. An alternative non-real time source of EGNOS messages via internet is the ESA EGNOS Message Server (EMS), which allows getting the EGNOS messages offline in the form of ASCII files, for post-processing purposes. The EMS service is accessible free-of-charge, using the FTP protocol.

2.4. Vehicular Ad Hoc Networks(VANETs)

VANETs are designed to create a spontaneous data exchange between moving vehicles, and they are one of the key components in intelligent transportation. They are especially good for time-critical and safety related applications. The coverage and applications can be extended with the inclusion of the infrastructure and the pedestrians with the same communication technologies. The range is around 100 and 300 meters which is much better than almost all sensors used for intelligent transport applications. Standards have already defined in Europe, US, and Japan. In US IEEE 1609 WAVE (Wireless Access in Vehicular Environments) protocol stack builds on IEEE 802.11p. In Europe, European Telecommunications Standard Institute (ETSI) builds on a variant of the same radio technology with some adaptations. Vehicle

to Vehicle (V2V), vehicle to infrastructure (V2I), and vehicle to pedestrian (V2P) communication are built on same technology. Messages can be moved further with the use of multi-hops as shown in Figure 2.8.

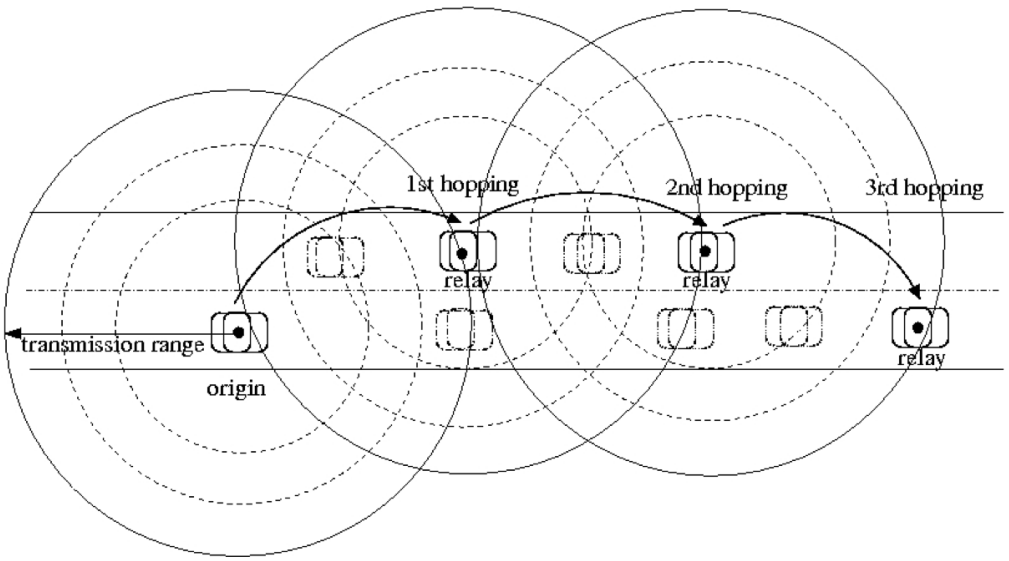

Figure 2.8. Routing with Multi-hop Forwarding.

There are several applications possible like cooperative awareness, road hazard signaling, speed management, toll collection, cooperative navigation, and localization. Since we are focusing on enhancement and use of location information in intelligent transport systems (ITS), we will devote rest of this section on location information in VANETs. In addition to that, it may be easily seen that most of the applications in VANET domain are only possible with a high integrity location information.

2.4.1. Location Information in VANETs

Wireless inter-vehicle communication enables information dissemination between vehicles, to improve safety, efficiency and even to enhance infotainment aspects. Figure 2.9 [22] represents the communication in a typical vehicular communications scenario. For instance, safety applications, like collision avoidance or hazardous road warnings, use location information to estimate collision probabilities between vehicles or mark

the location of the current event. Continuous dissemination of location information between vehicles provides a better understanding of the environmental changes and unexpected behaviors. Due to the high mobility and dynamic structure of VANETs, routing mechanisms need location information which must be updated periodically.

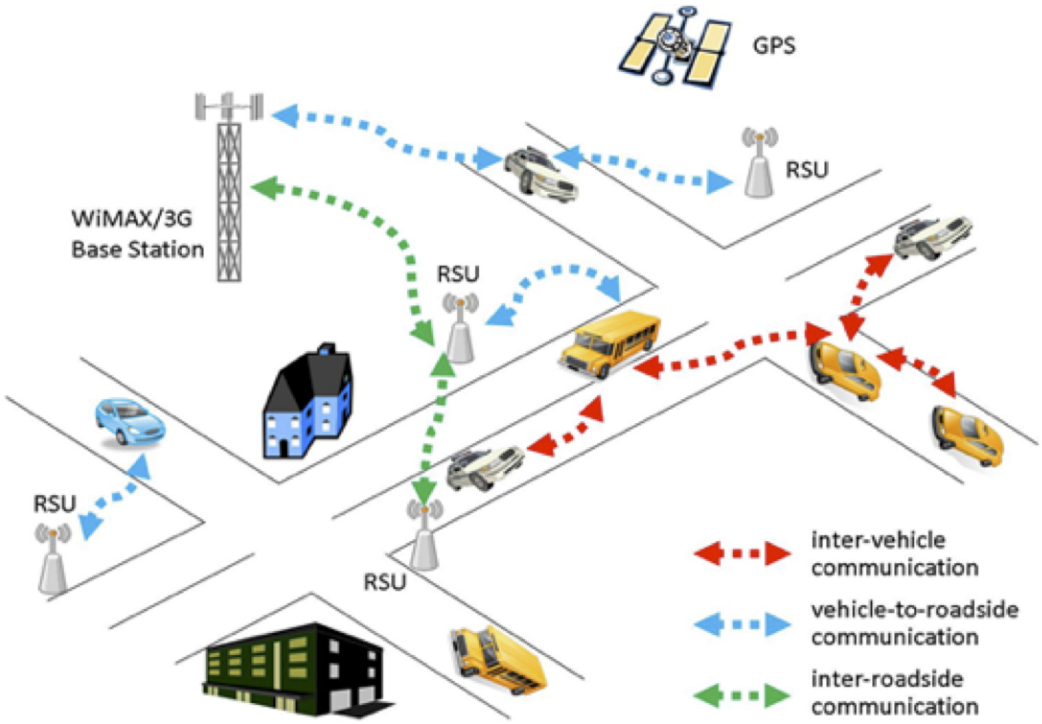

Figure 2.9. A Typical Inter-vehicle Communication Scenario.

From a communications perspective, VANETs are organized by different layers, such as application, facilities, and network layers. The Application Layer is mostly used for safety. Safety applications focus on warning the drivers about the incoming events like sudden brakes, dangerous intersections, control losses, hazardous roads etc. Such applications need at least the location information of the unique event. So the location information dissemination is the basic information, exchanged on the application layer [23].

US National Highway Traffic Safety Administration (NHTSA), the US Department of Transportation (USDOT), and the Vehicle Safety Communications Consortium

(VSCC) of Crash Avoidance Metrics Partnership (CAMP) identify eight applications which provide the greatest benefits concerning safety. Seven of these eight applications need position information dissemination with different frequencies (1 to 50 Hz).To disseminate the required data including location information, a message dispatcher is suggested in [24]. In Europe ETSI TC ITS, i.e. the European standardization group for ITS, currently, specifies the basic applications and their requirements (see ETSI TR 102 638).

The facilities layer is the correspondence of the three open system interconnection (OSI) layers in the OSI model that are between the network and the application layer. The facilities layer has categories such as application support facilities (cooperative awareness message - CAM and decentralized environmental notification message-DENM), information support facilities (local dynamic map - LDM), communication support facilities (addressing mode etc.), common facilities (time and position management, service managements etc.), and domain facilities (DENM management for Road Hazard Warning etc.). These two message sets carry the location information of the source node (ETSI TS 102 637-1, ETSI TS 102 637-2, ETSI TS 102 637-3).

In the case of an application that requires multi-hop, the Network layer needs the position information. Some designs of Network Layer like IEEE 1609.3 does not use multi-hop and with that does not require position information. Car to car - Communication Consortium (C2C-CC) network layer supports multi-hop communication and also geo-networking. ETSI standardized the C2C-CC approach in ETSI TS 102 636-4-X.

Geo-networking provides packet dissemination to a particular destination area or a defined range. Network layer which provides geo-networking requires location information of the source and location information of the destination point if there is one. ETSI TS 102 636-4-1 determines a common network layer header for geo-networking. The position information is represented in source position vector which is the vector from the origin to the destination with additional attributes. A source position vector is described as:

- Geographical position (denoted by POS_LPV)
- Speed (S_LPV)
- Heading (H_LPV)
- Timestamp indicates when the geographical position POS_LPV was generated (TST_LPV)
- Accuracy of the geographical position (POS, LPV)
- Accuracy of the speed (S, LPV)
- Accuracy of the heading (H, LPV)

2.5. Digital Maps

We have utilized a navigable digital map database in vector format in this thesis. There are different database models for digital vector maps. In the following section, we will define attributes and models that we utilize in our development. In this thesis, we developed algorithms where the practical application is possible. Highly detailed maps and local dynamic map concepts are fairly new concepts and only partially available for research and development efforts. We did not utilize high detailed maps in our work due to limited availability. But we will summarize these newer digital map formats to give a complete domain information.

2.5.1. Navigable Map Database

A road contains a type, form of way, maneuvers, speed information and level as shown in Figure 2.10. Road types, namely functional road class (FRC), and form of way (FOW) mainly describe the road, while maneuvers describe the movements on the roads.

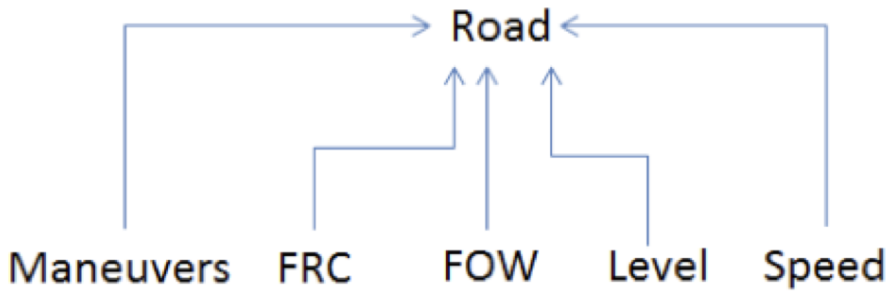

Figure 2.10. Road Model.

These attributes restrict search space for positioning thus yields enhanced accuracy and shorter process time in the real-time implementations of localization and map matching scenarios.

Details of functional road class and form of way are given in Tables 2.2 and 2.3.

Table 2.2. Functional Road Class Codes.

Code	Description
10	Motorway,
20	Major roads of high importance,
30	Other major roads,
40	Secondary roads,
51	Local connecting roads,
52	Local roads of high importance,
60	Residential connecting roads,
70	Residential roads
80	Other roads, usually not suitable for vehicle traffic, e.g. stairs, narrow walkways

Table 2.3. Form of Way Codes.

Code	Description
2	Dual carriage way
3	Single carriage way
4	Round about
5	Major slip road
6	Parallel road
8	Entrance to/exit from a car park
9	Small slip road
11	Poor condition
12	Unpaved
13	Road in a pedestrian zone
15	Service road

Average and legal (maximum) speed information is available on a road segment in the digital map database. Speed attributes are closely related to the road type and street network (STNW) parameter. STWN parameter defines if the road passes through an urban area. Maximum speed information bounds the search space of the vehicle's relative position when current speed of the vehicle is known.

It is possible to classify roads according to FRC and FOW. These classifications then map to speed limit information. The speed information is used in conjunction with FRC in our implementation.

Maneuvers are the list of allowed actions and list of restricted actions for a road to ensure safety and regulations. They are defined for every road that complies. There are four types of maneuvers namely implicit, priority, prohibited and restricted maneuvers.

Restricted maneuvers are the implementation of the traffic rules of directions such as turn sign. Figure 2.11 shows an example restricted maneuver.

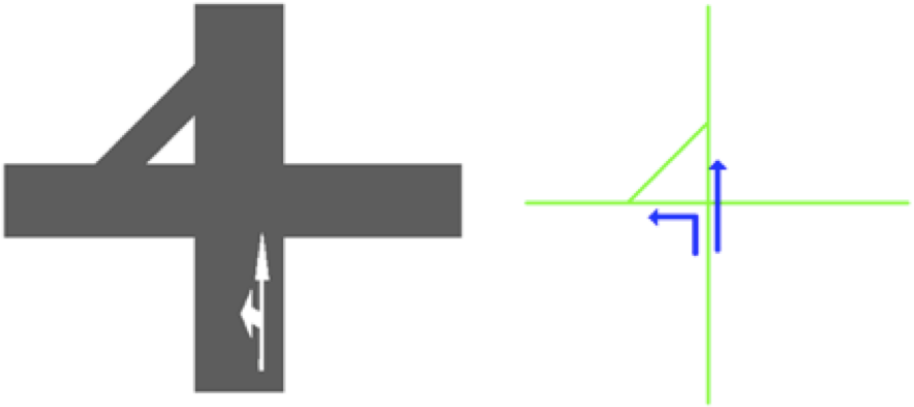

Figure 2.11. An Example of Restricted Maneuver.

Prohibited maneuvers are the implementation of restrictions and prohibited turns such as no U turn signs.

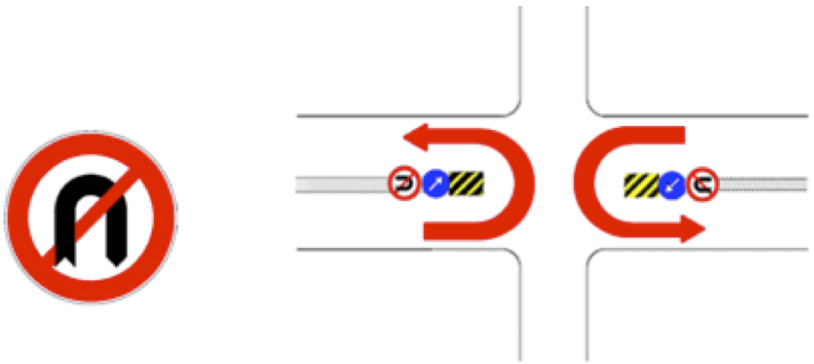

Figure 2.12. Prohibited Maneuver.

Implicit maneuvers are the implementation of turns due to nature of the road or traffic flows although it is not restricted by the traffic signs.

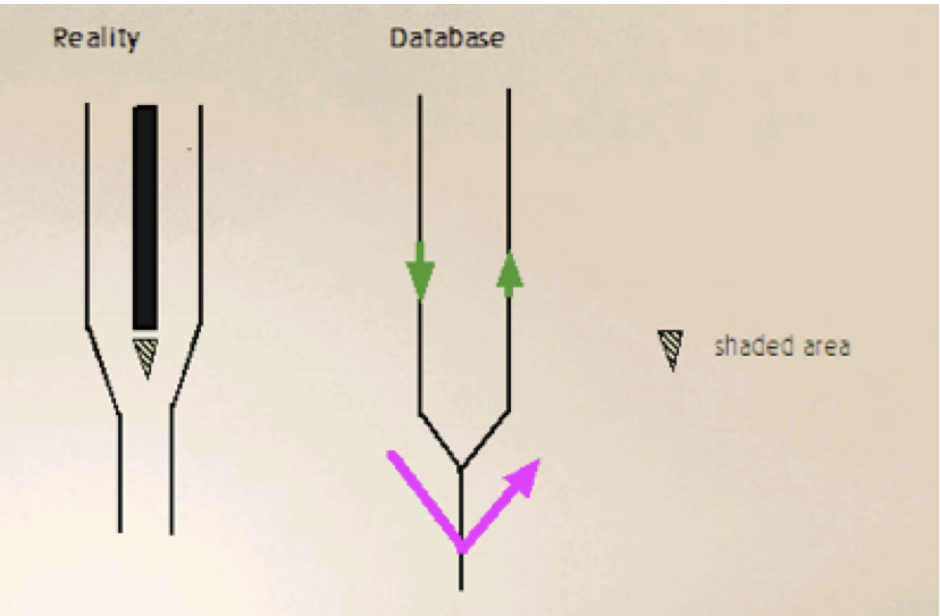

Figure 2.13. Implicit Maneuvers.

Priority maneuvers described when the main road makes a turn while navigation shows straight. As in Figure 2.14, the main road tends to go straight, but because of the traffic sign on the right, it makes a turn.

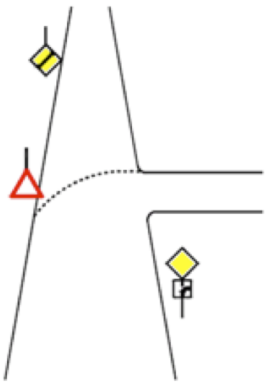

Figure 2.14. Priority Maneuvers.

Another type of maneuver is the bifurcation. Bifurcation is the fork structure ahead of the road that confuses the driver. There are three types of bifurcations namely exit fork, multi-lane fork, and simple fork.

As shown in Figure 2.15 exit fork is described over the roads that exit from the main road.

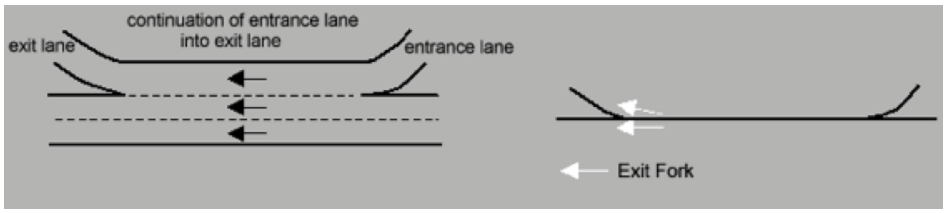

Figure 2.15. Exit Fork.

As shown in Figure 2.16 multi-lane fork is described over the roads that fork the main road lanes.

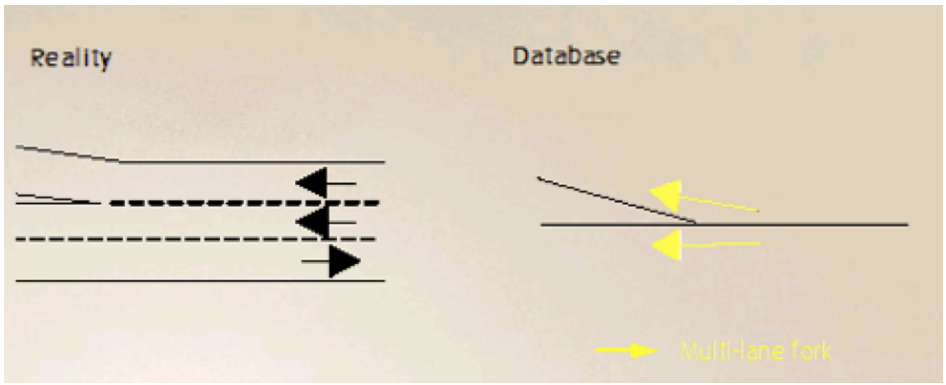

Figure 2.16. Multi-lane Fork.

A simple fork is described if the road forks into two parts without any sign or navigation that confuses the driver. The angle between the parts determines if the fork is a bifurcation or not. (see Figure 2.17)

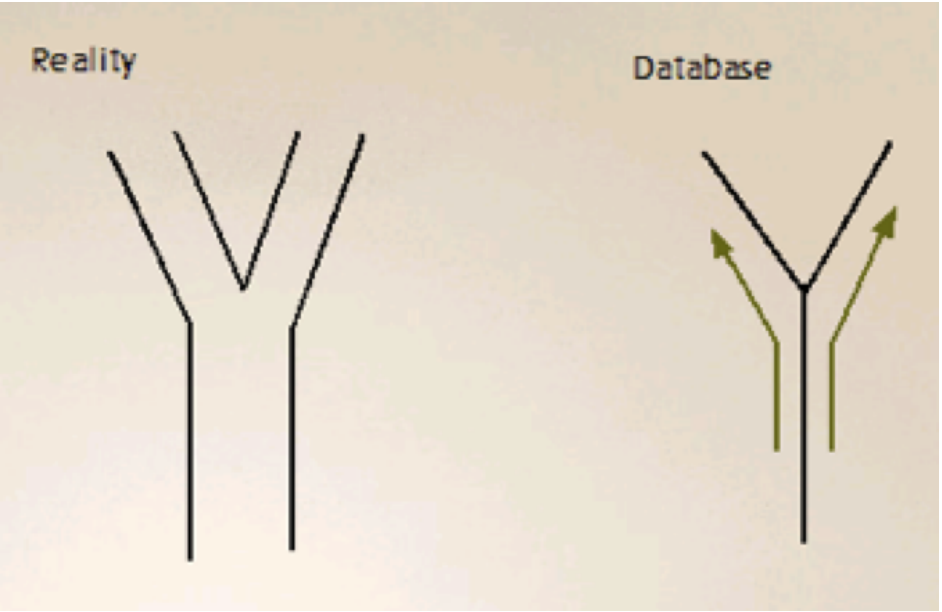

Figure 2.17. Simple Fork.

2.5.2. Detailed Maps for Autonomous Driving

In our work, we use available navigation maps as a sensor for a better localization. As automated driving is coming closer to reality, for reducing the cost of sensors, use of more detailed maps becomes an important concept. For example to make lane level map matching having the lane centerlines can be very useful. Companies like TomTom and Here started to produce examples of such maps.

One of most important features of these maps is detailed lane information. Following features can be available for lanes.

- Lane center lines (lane type, speed restriction, connection type)
- Lane borders (lane border type, color, group)
- Lane groups
- Lane connections
- Height, Width information

Figure 2.18 [25] shows the information captured for detailed lane information. Note that lane borders, center lines are digitized separately.

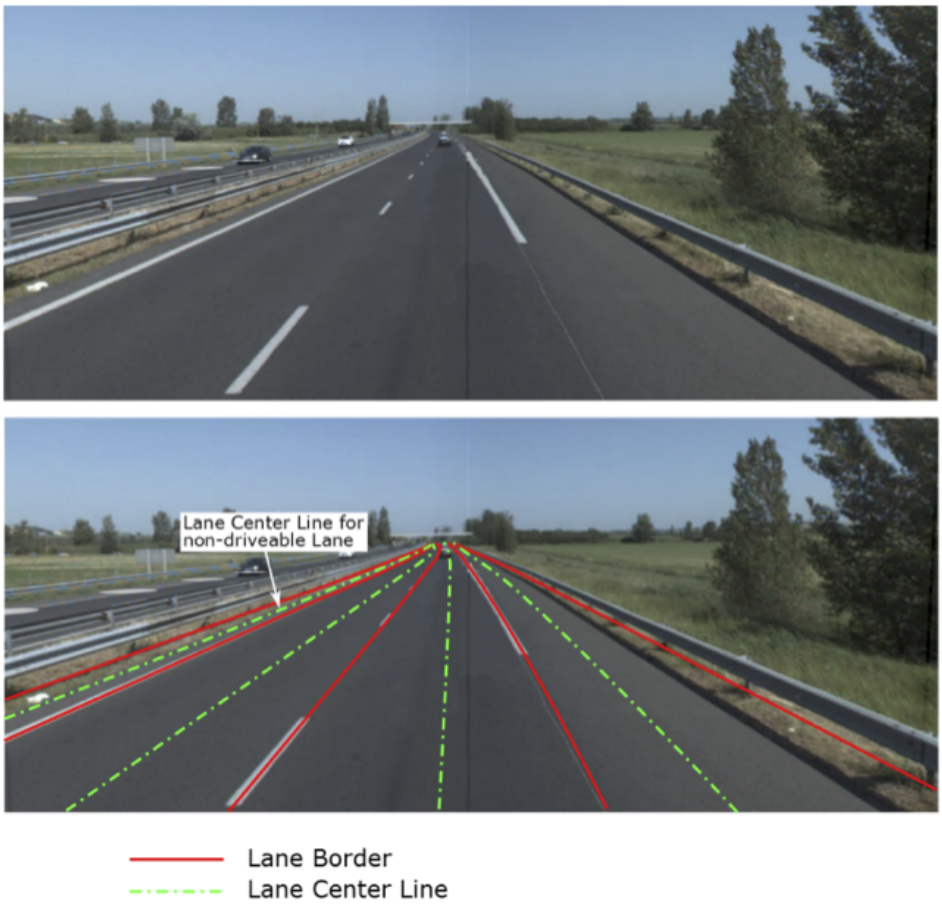

Figure 2.18. Lanes, Lane Borders, Lane Center Lines.

Along with the detailed lane information, detailed maps also carry detailed 3D information. At the current stage 3D building information and building footprints are available in most of the cities. Other than building information, 3D modeling of the road is also available for limited coverage. This information is mostly generated from lidar data and models the view that can be seen from vehicle front side windows. This information can be fused with camera image to enhance the localization or can be very useful for object recognition. Sample data can be seen at Figure 2.19 [25].

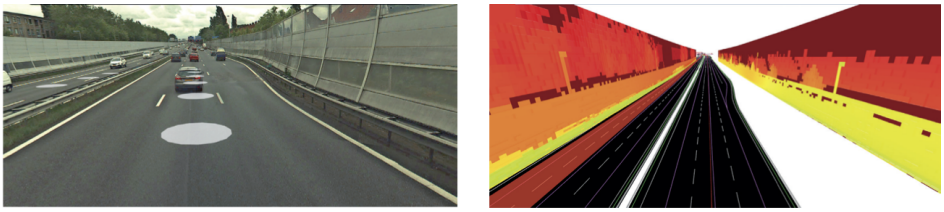

Figure 2.19. 3D Lateral and Longitudinal View of the Roadway.

These features can be easily adapted to the map matching algorithm developed in this thesis. Other than 3D building information rest of the data mentioned in this section is only available for a very limited coverage. Production and update costs are much higher than existing navigable maps. With highly detailed maps, data size becomes much higher, and processing becomes more complex. Even though they can improve localization and object recognition by providing lane level information and front camera view, they are not ready for close to market implementations and price/performance is still questionable.

3. PARTICLE FILTER BASED VEHICLE LOCALIZATION AND MAP MATCHING

For many years digital maps are used mainly for navigation in the automotive sector. In recent years, digital maps are also made available to be integrated to achieve certain functions for autonomous cars and ADAS. There are many attempts to fuse digital map information with other sensors, in some application areas like sign recognition and lane detection [1–4, 26]. It is a common practice to fuse sensors with diverse characteristics to enhance sensing of the outdoor environment. Most of the sensors give information about the nearby environment surrounding the vehicle. Fusing digital maps with other vehicular sensors can contribute to enhanced and longer range sensing of the environment.

In the literature, Bayesian framework is the most frequent method for digital map fusion. In the fusion process accuracy is taken into account as the reliability measure of the digital map. Since a digital map is a static representation of a dynamic world, there may always be differences from the field [27]. In most of the applications with the digital map fusion, it is assumed that the vehicle is correctly matched to a road segment on the digital map. For example, legal speed information is retrieved from the digital map and fused with camera-based traffic sign recognition. But if the vehicle matched to a wrong segment, the information obtained from the map would be totally wrong and misleading. Thus the quality of the digital map is not the only source of error that should be taken into account for digital map fusion. To overcome these problems an enhanced map matching and localization algorithm, which can output a reliability measure is needed.

As explained earlier there are many ADAS applications like collision detection, traffic sign recognition and lane detection that can benefit from map fusion. To be able to fuse the digital map, the vehicle should be matched to a map segment to retrieve relevant information that can be incorporated into the ADAS application.

Our proposed algorithm can be used as the first stage before map fusion in an ADAS application which utilizes digital map fusion. It can generate a correctness measure for the map matching process which can be used as the reliability measure of the digital map in the fusion process. This reliability measure will be utilized by the fusion algorithm like any other conventional sensor.

3.1. Localization and Map Matching

In the ADAS and autonomous vehicles domain, digital maps are integral parts of localization. Many of the recent attempts use digital maps as an additional sensor for localization. Even though map matching is examined as a separate issue in some domains for our target application, it is a better idea to handle map matching and localization at one stage.

Basic map matching techniques are based on geometric analysis (making use of the geometric information of the digital road network, techniques like point to point, point to curve, curve to curve matching) and topological analysis (making use of also the topological features of the roads like connectivity, continuity of the links, road turn, road curvature, etc.). Some advanced map matching algorithms have also been proposed employing more sophisticated techniques like Fuzzy logic, Kalman filter, Dempster-Shafer theory and Bayesian inference [10, 28, 29].

There are many attempts in the literature for enhanced localization. In our application, we are fusing digital maps, odometer, and GNSS receiver. The error sources and characteristics of these sensors are different. Odometer reports distance traveled directly from the wheels and can be retrieved without an extra cost in most of the vehicles. In the literature, additional hardware like an inertial measurement unit (IMU) [30, 31] or a vision system [32] are also integrated to enhance positioning accuracy and availability.

More recently particle filters are proposed for localization and map matching. For example, particle filtering is proposed to fuse IMU and camera to get a better position-

ing in GNSS blackouts [33]. Particle filters can generate more than one estimation with their respective weight. This is very suitable to map matching problem domain, Since there may be more than one street segment possible for a given GNSS measurement. Since our target application is ADAS both localization and map matching is needed and this can be accomplished with particle filter fusion.

In this chapter, we propose an algorithm which uses particle filter together with attributes related to road segments, regions and network topology information in digital maps [34]. Our algorithm is novel in many aspects. Our algorithm utilizes the digital maps in an innovative way. We integrated topological features of the digital maps in likelihood calculation in Particle Filtering algorithm. We have also tested our algorithm in real-world conditions. Many of the algorithms proposed in the literature are not tested in urban areas where GNSS signals reception blocked by high buildings. Some of them depend on highly detailed lane level maps or expensive hardware. As we achieve an acceptable map matching and localization performance, another contribution is the use of inexpensive hardware like a simple GNSS receiver together with odometer which is freely available in most of the vehicles. We proposed a complete system with widely available technologies tested in different areas of the urban area. At the end of this chapter, we have made a comparison of our algorithm with other algorithms in the literature.

Two key information layers of the digital map are used to bias the particles towards more probable areas. The first layer of the digital map is the land use. By checking the land use information, particle location can be determined as, building, green, road segment, parking area, or pavement. It is clear that most likely location for a vehicle moving at a certain speed is a road segment. Type of road segment is also considered. For example, high speeds are more probable in higher class road segments like highways. That is why the probability of being in a particular location is calculated in conjunction with the speed of the vehicle. The second important layer of the digital map is the network topology. As explained in the previous chapter network topology is used for finding possible routes on a digital map by use of attributes like road direction, turn restrictions, nodes and edge connections. By use of network topology of the digital

map reachability of each location for a given particle is calculated.

The proposed algorithm is tested with a real life implementation on a passenger vehicle. Only GNSS receiver and odometer of the vehicle are used as sensors. Hardware which can report odometer pulses and GNSS measurements synchronously is used during the field tests. Four different types of particle filter based localization and map matching algorithms are implemented to be able to compare the contribution of different map features in the same environmental setup. To be able to prove the improvement introduced by the map fusion a simple particle filtering localization algorithm is also tested in the same routes along with the map fused algorithms. Since the performance of the GNSS is highly dependent on the local conditions tests that are not accomplished in the same routes and even in the same time of day may be misleading. Our setup allows testing of all algorithms simultaneously.

The developed algorithm is useful both in urban and suburban roads and does not require an extra sensor. Correct link identification is better than state-of-the-art algorithms with compatible sensors. Algorithms link identification performance is even close to the performance of algorithms which utilizes an IMU which is very expensive. An example tutorial and comparison of some map matching and localization algorithms can be found in [10]. At the end of this chapter, our algorithm is compared with the documented algorithms in the tutorial. We also documented the test environment and sensor setup of each algorithm to be able to present a valid comparison.

3.2. Sensor Fusion

A moving vehicle is considered for localization. The motion model linear in the state dynamics and nonlinear in the measurements is given by,

$$x_t = Ax_{t-1} + Bu_{t-1} + f_{t-1} \tag{3.1}$$

$$z_{t-1} = h(x_{t-1}) + e_{t-1} \tag{3.2}$$

where the state-space consists of a two-dimensional vector $x_t = [x_t, y_t]^T$ at time index t, A and B are assumed to be known linear motion system matrices, $h(\cdot)$ is a known nonlinear dynamic measurement function, [35,36]. The odometer is the input, which is angular wheel speed of the ego vehicle $u_t = w$ [rad/seconds], and faults are denoted by f_t. Measurement vector is constituted by the GNSS receiver denoted by n_t. Considering the map as a sensor does not create a is real measurement. The probability of being in a particular road class and connection to a new road segment are observed, and it is denoted by m_t (see Table 3.1 and algorithm in Figure 3.6). Overall, $z_t = [n_t\ m_t]^T$ is the measurement vector, and e_t denotes the error vector.

3.2.1. Bayesian Filter

Consider a system with state x_t at a given time t. Initial system state can be modeled by its probability distribution $p(X_0)$, where X_0 is the state at time index $t = 0$. Since the system is a Markov process of the first order probability distribution at current time t, current state depends only on the previous state, which can be denoted by $p(X_t|X_t - 1)$. The system can be monitored by sensor measurements z_t, subject to noise. Probability distributions $p(e_{t-1})$, $p(f_{t-1})$ and $p(X_0)$ are assumed to be known but not supposed to be Gaussian [35]. Probability of receiving measurement z_t given the current state of system is given by $p(Z_t = z_t|X_t)$. Computation of the posterior density $p(x_t|Z_t)$ is memoryless, and complete state history is not needed. Under these assumptions, the posterior density is given as follows:

$$p(x_t|Z_t) = \frac{p(z_t|x_t)p(x_t|Z_{t-1})}{p(z_t|Z_{t-1})} \tag{3.3}$$

$p(x_t|Z_{t-1})$ is the the prediction for the probability of the vehicle's position x_t subject to the history of sensor measurements Z_{t-1}. Prediction is calculated by integrating motion model $p(x_t|x_{t-1})$ over posterior $p(x_{t-1}|Z_{t-1})$,

$$p(x_t|Z_{t-1}) = \int p(x_t|x_{t-1})p(x_{t-1}|Z_{t-1})dx_{t-1} \tag{3.4}$$

$p(z_t|Z_{t-1})$ is a normalizing constant denoted by k_t. Inserting Eq.3.4 into Eq.3.3, the update statement of the Bayes filter:

$$p(x_t|Z_t) = \frac{1}{k_t} p(z_t|x_t) \int p(x_t|x_{t-1}) p(x_{t-1}|Z_{t-1}) dx_{t-1} \tag{3.5}$$

Posterior probability is calculated by integrating the motion model and sensor data. Minimum mean square estimate $\hat{x}_t$ is calculated by using posterior probability,

$$\hat{x}_t = \int x_t p(x_t|Z_t) dx_t \tag{3.6}$$

3.2.2. Particle Filter

Analytic calculation of the Bayes filter is not possible. A numerical approximation to Bayes Filter can be implemented by use of Sequential Monte Carlo (SMC) methods which are also known as the particle filter. The sampling importance resampling (SIR) algorithm is one of the most widely used sequential Monte Carlo methods, which allow the system state estimation to be computed on-line, such as tracking algorithms [35].

A SIR filter manages a fixed number of possible system state hypotheses x_t^i, where superscript i denotes the i^{th} individual particle. These individual particles approximately generate the distribution of the system state, $p(X_t)$. The SIR algorithm is computed at each discrete time step.

Posterior probability $p(x_t|Z_t)$ is approximated by a weighted sample set of particle filters. This method converts computationally intense integral calculation into the straightforward summation procedures. Implementation stages described in Figure 3.1

Initialize the individual particles

for $i = 1$ to N **do**

$x_0^i \sim p_{x_0}$

end for

for $t = 1$ to T **do**

for each measurement

Measurement update

Update particle's weight by use of likelihood

for $i = 1$ to N **do**

$w_t^i = w_{t-1}^i p(z_t|x_t^i)$

end for

Normalize weights such that total of weights is equal to zero.

Calculate current state $\hat{x}_t$

$\hat{x}_t \approx \sum_{i=1}^{N} w_t^i x_t^i$ is an approximation of Equation 3.6.

Resampling

$N_{eff} = \frac{1}{\sum_i \left(w_t^i\right)^2}$

if $N_{eff} < N \times Particle\beta$ **then**

Small portion ($Particle\beta$) of particles are contributed to the estimation

Resampling is required

Delete particles with small weight

end if

Transition

According to the motion model, particles are updated.

Based on the updated speed information, denoted by v_{t-1}

Calculate state transition in as an arbitrary movement on $2D$ plane

$x_t = x_{t-1} + T_s v_{t-1} cos(\alpha)$

$y_t = y_{t-1} + T_s v_{t-1} sin(\alpha)$

T_s is the sampling interval

α denotes a uniformly distributed random angle in the interval of $[0,\ 360^o]$

end for

Figure 3.1. Particle Filter Algorithm.

The speed is always a positive value, and its minimum is limited to continue minimally exciting updates in prediction and to continue predicting the probability of the vehicle's position.

Figure 3.2 illustrates the basic flowchart of the location estimation algorithm with the particle filter.

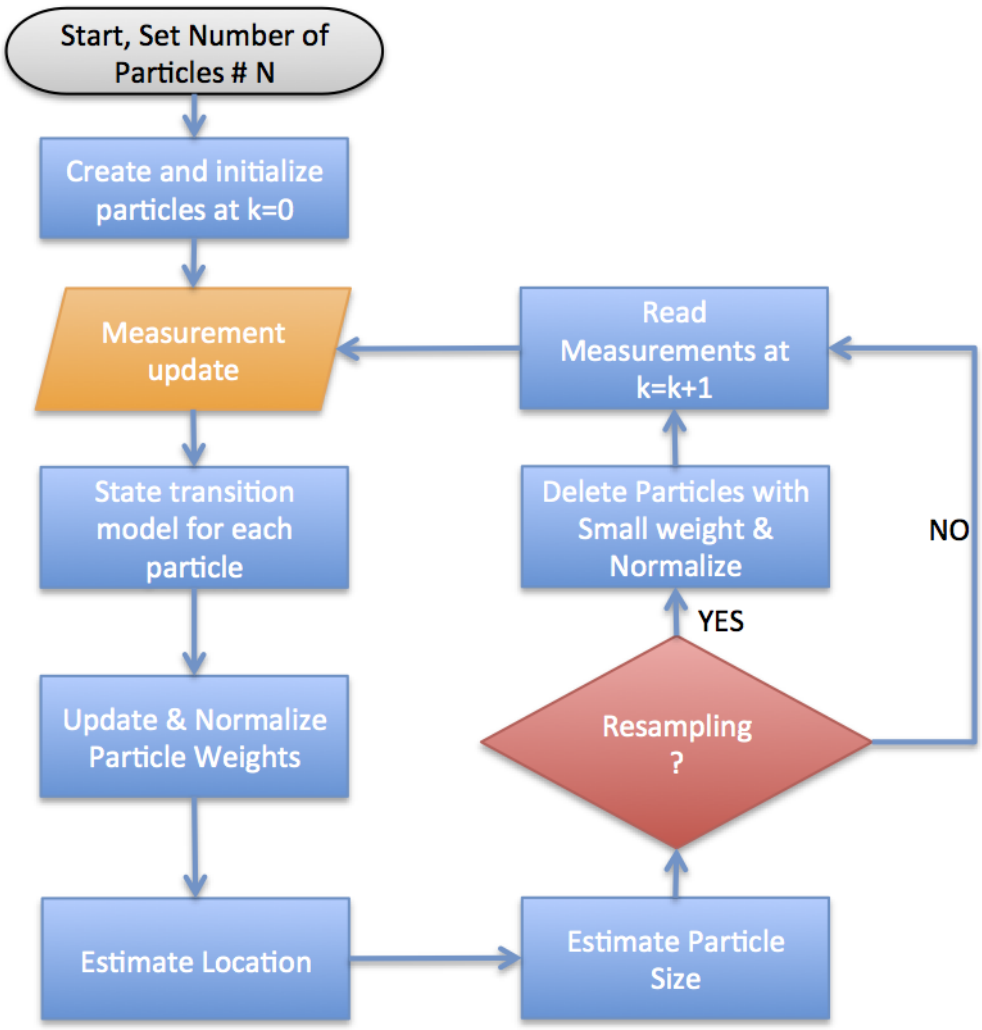

Figure 3.2. Flowchart of Particle Filter Algorithm for Location Estimation.

3.2.3. Weight Update

For each particle, an initial weight is calculated based on the probability derived by the GNSS location data. The probability is determined under the assumption that the deviations of the GNSS are normally distributed, and the standard deviation is changed within the confidence values. The weight of the i^{th} particle for $i = 1, \ldots, N$, and the probabilities at the time instance t is given as follows:

$$w_t^i \alpha P\left(n_t, s_t, m_t | x_t^i\right) = P\left(n_t | x_t^i\right) P\left(m_t | x_t^i\right) \tag{3.7}$$

where n_t and m_t denotes the measurements of GNSS receiver's position and map based prior and posterior localization result, respectively. Weight update of the i^{th} particle based on GNSS measurement is as follows:

$$\left[w_t^i\right]_{xGNSS} = a e^{-1/2\left([x_t]_{GNSS} - \left[x_t^i\right]\right)^2 / \sigma_x^2} \tag{3.8}$$

$$\left[w_t^i\right]_{yGNSS} = b e^{-1/2\left([y_t]_{GNSS} - \left[y_t^i\right]\right)^2 / \sigma_y^2} \tag{3.9}$$

where $a = 1/\left(\sigma_x \sqrt{(2\pi)}\right)$, $b = 1/\left(\sigma_y \sqrt{(2\pi)}\right)$, σ_x^2 and σ_y^2 denotes the variance of measurement error in both of the horizontal and lateral direction, respectively.

We use the Horizontal Dilution of Precision (HDOP) information provided with the GNSS receiver's position solution. To approximate roughly the GNSS signal quality, we convert HDOP into the meter value such as $\sigma_x^2 = \sigma_y^2 = 10 \times HDOP$, [37]. When pseudo-range residual measurements as raw source of information for assessing the GNSS signal quality and the geometrical ranges between the satellites and the receiver (or ephemeris data) is not provided, and only a position solution is available, this practical approach does not violate the position solution improvement of the Particle Filter since while assuming a larger variance due to a multiplicative factor of 10, weight distribution of particles is made within a larger uncertainty interval.

The likelihood derived from the map information needs to be included in the weight calculation. The likelihood function is introduced such that particles tend to the locations whose mean is measured by the sensors or in a simple manner particles tend to prefer the location closer to the measurement. For instance, the weights of the particles in the error range of the GNSS position measurement are higher.

While augmenting the sensor measurements with the map based likelihood function, particles located on the likely and topologically possible road areas will be leveraged. The probabilities derived from the map are multiplied by particle weights. Two different map-based probabilities are considered. The first probability depends on the location of the particle and the speed of the vehicle. The second probability is based on the previous location and the possibility of traveling to the measured location.

Figure 3.3. Zone Probabilities According to Vehicle Speed and Direction.

3.2.3.1. Weight Update with Zone Map. Use of zone maps achieves the basic integration of digital map features. Zones are small grids which store some important attributes of the underlying digital map. The attributes in a zone define the hospitability of a location for a given vehicle speed and direction. Hospitability term is

used to define the probability of a moving object being in a particular area. Similar idea for mobile target tracking domain by use of hospitability maps is suggested by Kanchanavally et. Al [38]. In this work propagation of a mobile target is tried to be estimated depending on the terrain. Hospitability maps capture the effects of such terrains. A hospitability map concept also used in Bayesian framework and provides a likelihood or weight for each point on the terrain's surface for the target to move and maneuver at that location [39].

For particle filter with zone map, first, the zone of a particle is found on the digital map. If the particle speed is non-zero, the particle should be on a road segment. If it is not on road segment, low probability is assigned to the individual particle. If the particle is on a road segment, Table 3.1 is used according to the speed and FRC (functional road class). See Figure 3.3 for a visual explanation. A similar idea is implemented for walking objects without the speed information is used by Min Oh *et al.* [40].

The weight of each particle is updated by matching its position with the road segment, and its speed is used to determine whether being in the specific road class is probable or not. For instance, if the particle's speed is greater than a specified value, the particle should be on a road segment not in other areas such as pavement, parking lot. If it is not on road segment, low probability is assigned to the weight of this particle. Reliability and accuracy of particle's positioning are assured based on speed and map-matched road class, for instance, high-speed driving can only occur with a very low probability on a residential road. The probabilities are assigned as a function of FRC and vehicle's speed and given in Table 3.1. Definition of FRC codes has been previously described in Table 2.2.

Table 3.1. Percentage of Zone Probabilities (%) Subject to Vehicle's Speed.

Speed / FRC	10	20	30	40	51	52	60	70	80
0	11	11	11	11	11	11	14	14	6
20	12	12	12	12	12	12	14	14	0
40	13	13	13	13	13	13	13	9	0
60	14	14	14	14	14	14	10	6	0
90	21	21	20	12	12	12	1	1	0
120	25	23	22	10	10	8	1	1	0
150	30	20	20	10	10	8	1	1	0

Spatial queries are computationally intense operations. For the implementation and testing of algorithms, a simpler way of accessing to underlying map layers is needed. The zone map is a spatial index. It is implemented as a 2D grid. In each cell of the grid, land use (road, building, green, etc.) is stored. If a road crosses the grid cell, index to the road is also available. So that when a particle location is calculated a simple pointer operation finds its respective grid cell.

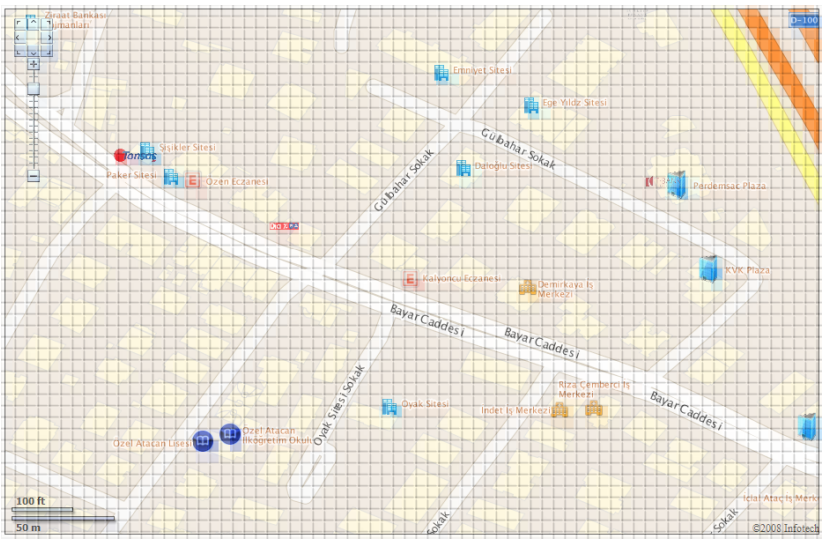

Figure 3.4. Sample Map with Grid Layer.

Grids can be multi level to make the access easier. In this work, we have used one level grid and make the cell size as small as possible to not loose precision. Since the tests are accomplished in Istanbul, Kadıköy sub-district, grid data were small enough to be stored in-memory. If a larger area needed, multilevel indexing can be used to optimize memory requirement for the grid data. A sample grid is shown in Figure 3.4

3.2.3.2. Weight Update with Map Topology. Road network is made of nodes and edges. Edges are made of several vertices. Edges of the network can be bidirectional or unidirectional, i.e., allowing traffic flow in two ways or in one way. When a particle is located on a road segment, some locations on the new road segments can be possibly reachable from this location based on the measured traveling distance provided by the odometer at the next prediction instant. If the new road segment is reachable according to the network topology from the previous network location, then the probability of being in this location is assigned higher then other unreachable road segments.

A local search algorithm updates the weights: If the particle's previous location is matched with the road segment, reachable road segments are searched starting from this point in the forward and backward direction. If the current road segment is unidirectional, the unreachable destination in the backward direction is identified, and weight of the particle located in this inaccessible road zone is assigned low. If the new road segment is reachable from the previous network location, then the probability of being in this new location is assigned a higher value with respect to the other unreachable road segments. Depending on the accuracy of the previous location, medium weight is assigned for the next location estimation reachable for the given traveling distance of the particle calculated by the odometer input. If the new location is reachable from the current road segment, a high probability is assigned (see Figure 3.5).

Figure 3.5. Probability of Routes According to Map Topology.

The algorithm in Figure 3.6 presents updating of map weights based on the prior and posterior localization result. This procedure is inspired by the creation of hospitability map [39] to enforce the particle filter estimation towards more probable areas.

Overall, a different weight is applied to each particle according to the particle location on the map as follows:

$$\left[w_t^i\right]_x = \left[w_t^i\right]_{xGNSS} \left[w_t^i\right]_{map} \left[w_t^i\right]_{route} \tag{3.10}$$

$$\left[w_t^i\right]_y = \left[w_t^i\right]_{yGNSS} \left[w_t^i\right]_{map} \left[w_t^i\right]_{route} \tag{3.11}$$

```
for i = 1 to N do
  for each particle
  Probability of being in a particular road class (Table 3.1)
  if road_id != 0 then
    particle is on the road
    map_weight = map_weight × zone probability
  else
    map_weight = map_weight × SMALL_ZONE_PROB
  end if
  Calculate reachability to the new road segments
  Check if the destination is reachable for the given traveling distance
  if reachable then
    assign HIGH_PROB=0.999
  else
    LOW_PROB=0.001
  end if
  if old_road_id != 0 and road_id != 0 then
    if there is any possible routing from old_road_id to road_id then
      route_weight=HIGH_PROB
    else
      route_weight=LOW_PROB
    end if
  else
    Either the previous particle's location or its current location is not on a road
    segment
    route_weight= MID_PROB
  end if
  total_map_weight= map_weight × route_weight
end for
```

Figure 3.6. Weight Calculation to Estimate Position of the Particles Subject to the Context of the Digital Road Map Data.

3.2.4. Mean Calculation and Map Matching

Following the weight calculation, the mean calculation is accomplished. First, weights are normalized then location information is calculated by use of linear weights. The road segment with the highest weight is the output of map matching. All the information is stored in estimations array. Alternatively, after the location is calculated the closest road segment can be selected. This stage can be combined with other geometric map matching methods to improve the performance even further with a performance tradeoff.

3.2.5. Resampling

When a small number of particles are effective in the estimation a resampling is needed to preserve multi-hypothesis feature of the particle filter. Resampling improves the estimation of future states by concentrating particles into domains of higher posterior probability. However, it reduces the accuracy of the current estimate by increasing the variance of the estimate after resampling. So, resampling must be applied with caution. Resampling only occurs if estimated particle size (ESS) is lower than a certain threshold.When then ESS smaller than this threshold means that only a small portion of particles are active in the estimation. If this is the case, particles with small weights are deleted. Surviving particles are copied according to their respective weights. Resampling is run after mean calculation. Weights are normalized at the mean calculation stage.

3.3. Tests

3.3.1. Test Routes

Three different routes were used during tests. Tests were carried out mostly in urban areas. But the test routes differ in the types of roads included. Both small roads, where sky view is limited, and highways, where urban canyons are less probable, are included. Also, speed limits, network complexity, and road connections differ. Test

Route 1 (see Figure 3.7) includes small streets and secondary roads with a limited line of sight. The second route (see Figure 3.8) consists of highways and small streets. The third route includes main roads without highways (see Figure 3.9).

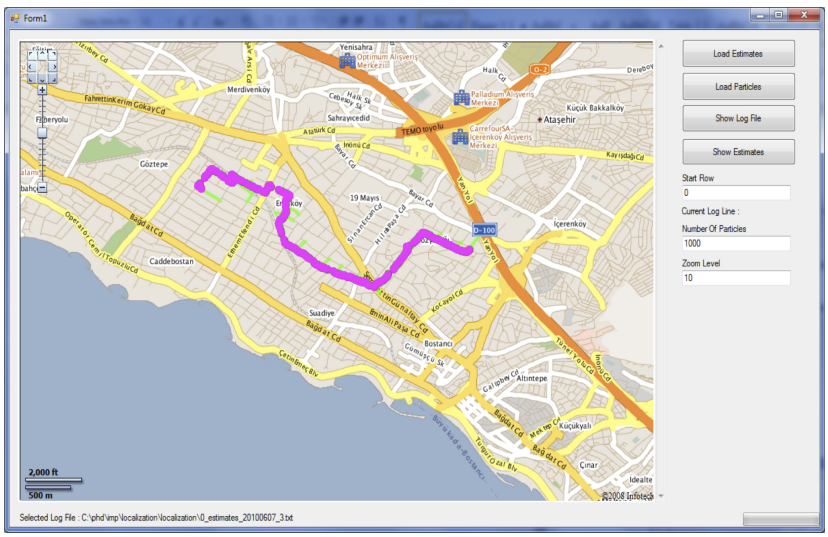

Figure 3.7. Test Route 1.

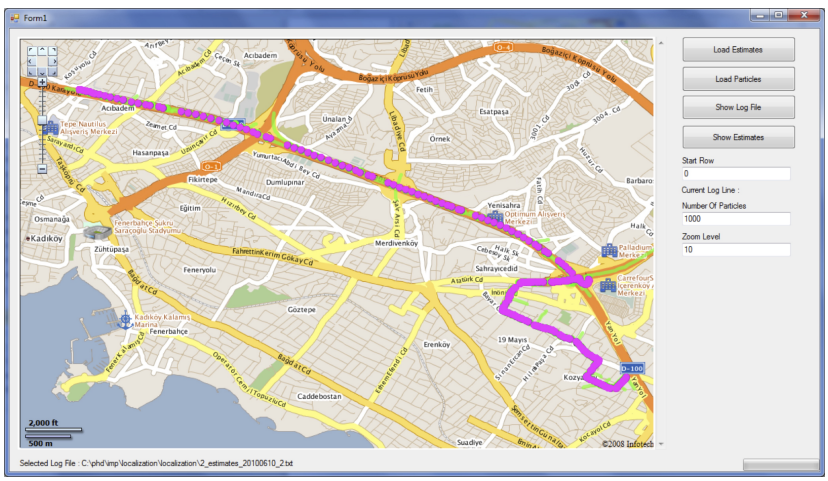

Figure 3.8. Test Route 2.

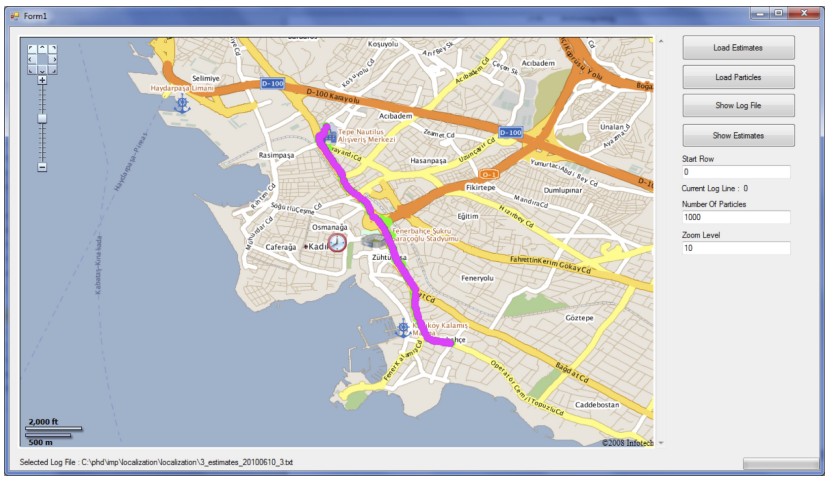

Figure 3.9. Test Route 3.

3.3.2. Comparison of the Implemented Algorithms

To be able to understand localization enhancement of the proposed algorithm four different implementations accomplished. All the algorithms have been tested in three test routes. The following list gives a brief description of implemented algorithms. As stated before all the algorithms tested simultaneously assuring same satellite visibility conditions.

- *Standard particle filter localization and map matching:* Particle filter with odometer readings used in transition model.
- *Particle filter based map matching with map based priors:* Particle filter with use of map location and vehicle speed in weight update stage.
- *Particle filter with map topology and map location:* Both zone maps and map topology used in weight update stage
- *Particle filter with map topology used in transition model:* Instead of using a random distance in transition, map routes in conjunction with odometer readings used in transition model.

As seen in the Figure 3.10, wrong edges can be selected by algorithm one especially in the junctions. Green lines show the location calculated by the algorithm. Purple dots indicate GNSS measurements. Green lines indicate the selected edge by the algorithm.

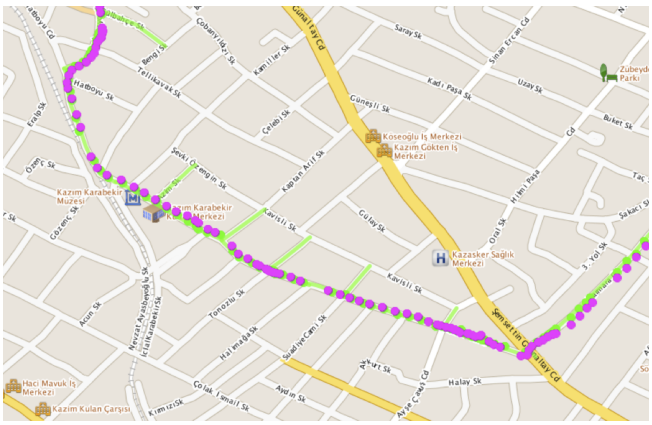

Figure 3.10. Map Matching Mistakes at Junctions - First Algorithm.

When GNSS measurements are not precise enough, our algorithm with map fusion can take corrective action and produce a better localization according to the ground truth. For example, GNSS measurements on less likely areas like building rooftops are avoided. Figure 3.11 shows the corrective action by the second algorithm.

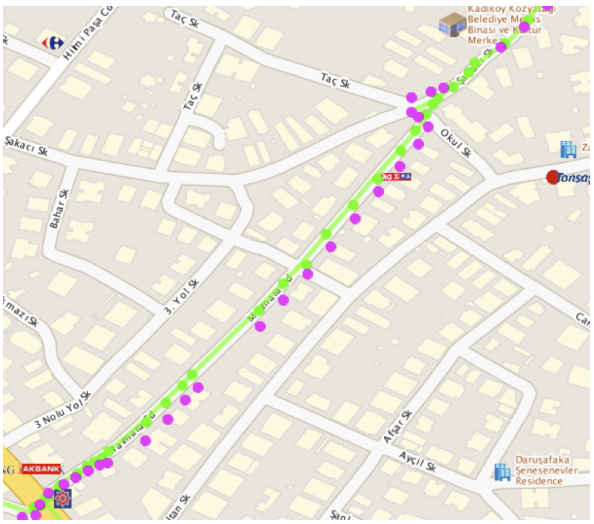

Figure 3.11. Correction with Use of Map Zone Information - Second Algorithm.

One of the desired features of the particle filter is the capability to multiple hypotheses. The behavior of the particles shown in Figure 3.12 illustrates how particle filter can produce multiple hypotheses for edge selection. As it can be seen, there are some number of particles on all possible edges.

When the digital map information is not used, particles are scattered depending on the precision of the GNSS information. When the error increases due to high buildings, particles scatter to a larger area. Figure 3.12 shows the distribution of particles on a narrow road.

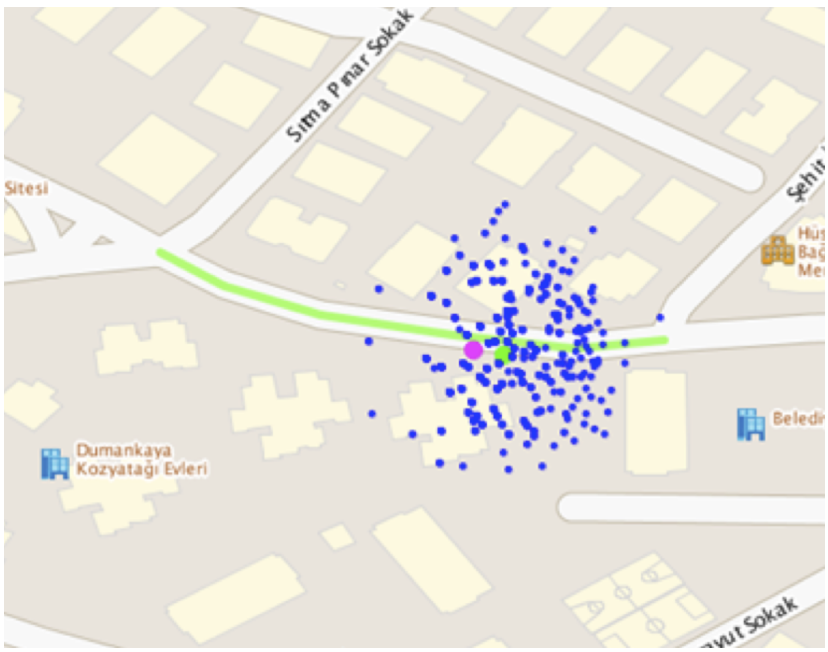

Figure 3.12. Particle Behavior for the First Algorithm.

When the digital map information is utilized, particles are concentrated on the possible edges. It can be seen in Figure 3.13, that the particles are focused on a single edge when there is no other nearby possible edge.

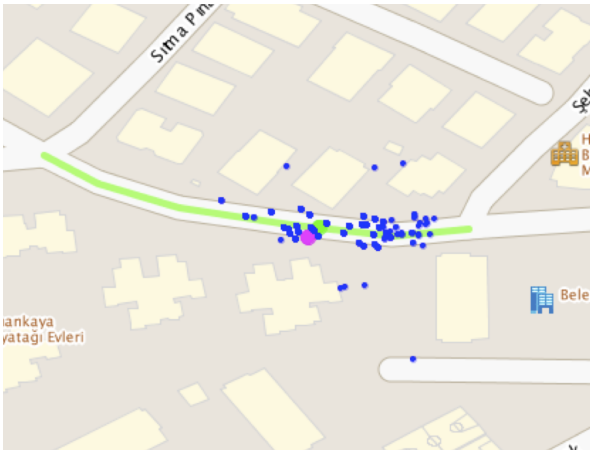

Figure 3.13. Third Algorithm Focuses Particles to a Possible Map Edge.

As seen in Figure 3.14, on junctions particles are distributed among the possible edges. On junctions, more than one hypothesis is generated. As explained earlier multi-hypothesis generation causes a corrective action on the edge selection process. Even if a wrong edge is selected at a junction, it can be corrected quickly along the route. Single hypothesis filters like Kalman Filter can insist on the wrong edge for a longer time. Especially parallel roads can cause this kind of problem for a single hypothesis algorithm [41].

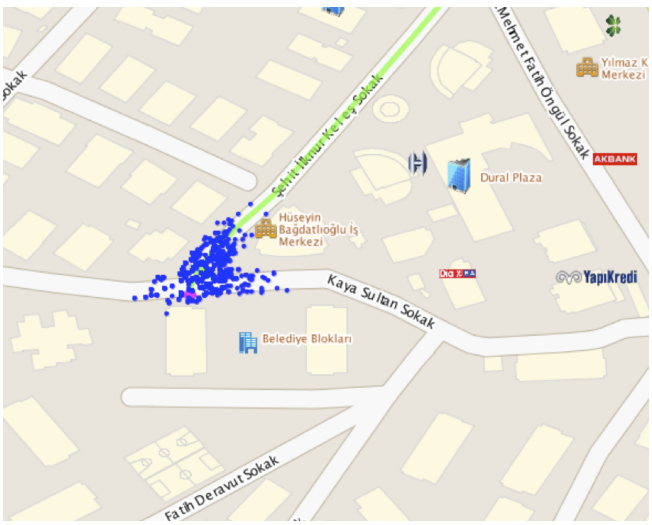

Figure 3.14. Third Algorithm Scatters Particles to Possible Edges.

Even though the multi-hypothesis generation is a nice feature, it can also cause wrong edge selections at the junctions. False edge selection cases are reduced when map topology is utilized. Use of network topology avoids many cases that can happen in complex intersections even if the GNSS precision is diluted. It can be seen from Figure 3.15; routing features of the map database removes most of the edge detection errors.

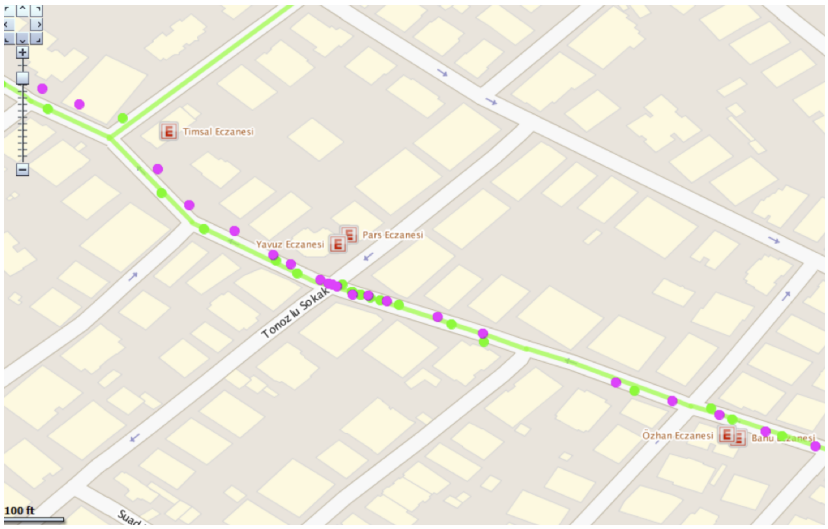

Figure 3.15. Wrong Edge Selection on the Junctions are Avoided by the Third Algorithm.

3.3.3. Test Results

Tests show that the third algorithm improves both location precision and map matching performance. Column number three at the Table 3.2 indicates the number of corrected locations by the algorithm. For example, when a GNSS location is on a rooftop, the algorithm produces a position information closer to the ground truth. Each route tested once. The test procedure is very time consuming because of the ground truth determination problem. In the literature, most of the time a real-time kinematic (RTK) GPS is used to determine the ground truth. RTK GPS requires the base station to be placed in a location with a good reception. Such a setup may not be possible in urban conditions. Also, practical usage of the RTK GPS receiver is

limited when the test routes are long, and speed of the vehicle is high. To overcome this problem we post processed the routes and manually created hundreds of waypoints for each route from photogrammetric maps where the location accuracy is less than 30 cm in the 2D plane. Then we compared these previously known waypoints again manually. Three test routes have 235,250, and 210 test waypoints respectively. For each waypoint, a correct link is selected manually to test the link identification performance of the algorithm. Correct link identification means the percentage of selecting correct link according to the real vehicle location. Corrected locations indicate that location accuracy is under five meter and closer to the ground truth than stand-alone GNSS receiver measurement.

Table 3.2. Test Results.

Route	Algorithm	Corrected Locations	Correct Link Identification	Corrected Locations
1	1	129/235	94%	55%
1	2	205/235	95%	87%
1	3	210/235	96%	89%
1	4	160/235	94%	68%
2	1	142/250	92%	57%
2	2	212/250	96%	85%
2	3	222/250	97%	89%
2	4	160/250	93%	64%
3	1	110/210	94%	52%
3	2	184/210	95%	88%
3	3	190/210	97%	90%
3	4	122/210	94%	58%

Table 3.3. The Performance of Some Existing Map-matching Algorithms.

Authors	Navigation sensors	Test Route	Correct Link Identification (%)	Horizontal Accuracy (m)
Kim *et al.* [42]	GPS	Suburban	?	10.6 (100%)
Kim and Kim [43]	GPS/DR	Urban and suburban	?	15m (100%)
White *et al.* [44]	GPS	Suburban	85.8	?
Pyo *et al.* [45]	GPS/DR	Urban and suburban	88.8	?
Taylor *et al.* [46]	GPS + Height	Suburban	?	11.6 (95%)
Bouju *et al.* [47]	GPS	Suburban	91.7	?
Yang *et al.* [48]	GPS	Suburban	96	?
Quddus *et al.* [49]	GPS/DR Map scale 1:2500	Urban and suburban	88.6	18.1 (95%)
Syed and Cannon [50]	GPS/DR	Urban and suburban	92.8	?
Ochieng *et al.* [51]	GPS/DR Map scale 1:2500	Urban and suburban	98.1	9.1 (95%)
Quddus *et al.* [52]	GPS/DR Map scale 1:2500	Urban and suburban	99.2	5.5 (95%)
Peker *et al.* [34]	GPS Map scale 1:1000	Urban	96.3	5 (or less) (90%)

3.3.4. Comparison of Correct Link Identification Performance

There are many map matching algorithms presented in the literature, but not all of them provide a metric for the success of the algorithm. The performance of a given algorithm is also affected by the type of the test area and inclusion of extra sensors like INS, IMU. Table 3.3 is taken from a survey paper [10]. In this survey along with correct link identification rate and accuracy, details about the test environment and type of sensors employed during tests are also documented.

Kim *et al.* [42] proposes a system which uses GPS, DR and map-matching. A geometric matching is used to determine correct link. Than the vehicles location is projected on the selected link. Extended Kalman Filter (EKF) is used to re-estimate the vehicle position. GPS positions used as the input to the EKF. The biggest problem with this method is if the initial map-matching is not correct filter will even increase the location errors. DGPS with five meter accuracy is used to measure the ground truth.

Kim and Kim [43] proposed a system which uses a GPS receiver, a gyroscope, and a speed meter. They suggest a probability measure for the existence of a car in a particular road by use of distance to the road section and similarity of the vehicle's trajectory to the road segment. An adaptive fuzzy network is used to this refine this measure. Even though the worst case horizontal accuracy is documented, correct link selection performance is not mentioned. This work also uses geometric projection on the road segment after selecting the correct link.

White *et al.* [44] implemented four different algorithms. The first algorithm just selects the nearest edge. The second algorithm uses heading information. In the second algorithm, edges with different headings are ignored. In the third algorithm, topological matching is added on top of the second algorithm. The previous matching is assumed to be correct to be able to check the topology. This algorithm is also further enhanced by the use of matching car trajectory to the map curves. The ground truth in the tests is generated by a manual operation like our work. Algorithm is tested in four different

routes best performance was 85.8 percent but same algorithm achieved between 66 percent and 70 percent in other test routes. As is expected from the methodology employed performance fluctuates depending on the route types that are used in tests.

Pyo *et al.* [45] proposed a map-matching algorithm using the Multiple Hypothesis Technique (MHT). Pseudo-measurements are generated for all links within the validation region as defined using the error ellipse derived from the navigation sensors (GPS/DR). A topological analysis performed to assign probabilities to the hypothesis. Method is similar to a particle filter with a small number of particles. This method depends heavily on the previous location for the topological analysis. It can suffer from the incorrect selection of the previous link. The average correct link selection performance of the five different route tests is 88.8 percent.

Taylor *et al.* [46] implemented a system which tracks all possible edges for a given vehicle. Then eliminates non-possible lines through a road reduction filter(RRF). The system uses height data from the map to intervene position calculation of standard GPS software. Ground truth for comparisons also handled by RTK GPS. The correct link identification ratio is not documented.

Bouju *et al.* [47] implemented three different algorithms for map matching along with a server based spatial data management system. The first algorithm is a simple nearest distance algorithm. The second algorithm shifts the position collected from GPS for a certain amount of distance. As we will describe on the next chapter determination of this shift is a significant problem without a practical solution at the moment. The third algorithm also adds the use of heading information. Algorithms are similar to the ones proposed by White *et al.* and they produce slightly better results. But this is due to usage of pre-known error bias. A pre-kwon error bias can be calculated with the approach that we propose in the next chapter.

Yang *et al.* [48] proposed an algorithm based on Dempster-Shafer's method. The GPS input to the algorithm filtered through a Kalman Filter. The algorithm uses a simple point to curve matching. With 1075 test points in a closed test circuit, the

algorithm reaches 96 percent correct link identification performance. The test area is not an urban area which puts a shade on the documented performance. Even with only GPS measurements 91 percent link identification documented in the paper which is quite high and shows that test circuit has a good GPS reception.

Quddus *et al.* [49] uses topological aspects of the digital map database together with speed and heading information. The system uses an empirical weight assignment for possible edges. GPS receiver, odometer, and a gyroscope are used for measurements. Tests are achieved both in urban and suburban areas. Even though system utilizes a gyroscope as an additional sensor, correct link determination is at 88.6 percent.

Syed and Cannon [50] implemented a fuzzy logic map matching algorithm. The proposed system utilizes GPS and gyro. The success of the algorithm highly depends on the first link identification. Algorithm uses 30 seconds to make the first fix which is not acceptable for ADAS applications.

Ochieng *et al.* [51] proposed an algorithm which constructs an elliptical error region on junctions. When the vehicle travels through a single link, simple matching methods are used. GPS, odometer, and a gyroscope are integrated into the system to support DR. The system highly depends on the correctness of previous map match results.

Quddus *et al.* [52] further improved above mentioned algorithm by adding the speed of the vehicle, connectivity of the road network, quality of the position solution (HDOP), the position of the fix relative to the candidate link. The system is not tested in urban conditions due to problems in the ground truth. The system also uses an additional gyroscope sensor.

Tests show that algorithm 3 improves both location correction and map matching performance. As it may be seen from Table 3.2 correct link identification performance of our best algorithm is between 96%-97% depending on the test route. Even though the test environment changes in our test routes performance of our algorithm does not

fluctuate. When compared with the Table 3.3 performance is higher than algorithms which use only GPS. Algorithm by Yang *et al.* is close but it only covers suburban roads where GPS reception and tall buildings is not a problem, and road network is not complicated. The other two algorithms whose performance seems slightly better are using additional sensors. As a result, our algorithm provides the improved performance without the cost of these additional sensors.

4. LOCAL INTEGRITY HEAT MAP

Expected reliability of a sensor determines its involvement to the estimation during the fusion process. As a result error characteristics of a sensor should be modeled for a successful fusion. In the implementation of fusion of digital maps described in Chapter 3, GNSS is the main sensor, and its error characteristic is generated from horizontal dilution of precision (HDOP). Low HDOP value translates to a better positional precision due to the wider angular separation between satellites. But HDOP value does not translate to an expected error in meters. An empirical conversion from HDOP to meters is used to make the implementation simpler, and a larger variance of the error is assumed not to violate position solution improvement of the particle filter. During the implementation, it was noted that understanding the error bound of the GNSS receiver can improve the resulting position precision.

GNSS signals are affected by atmospheric conditions and urban regions. The real determination of the error in meters depends on local conditions like blockage of GNSS signals especially in urban areas with smaller streets and high buildings. Effect of atmospheric conditions has been studied and modeled [53]. Problems caused by atmospheric conditions can be handled by SBAS as explained in Chapter 2 section 2.3. However, the most significant source of errors is due to multi-path and fading effects caused by the urban buildings obscuring satellite visibility. The areas with low satellite visibility are called urban canyons. GNSS signals scatter, get reflected or slow down because of buildings and this leads to error buildup. There is no known solution to this problem which can be practically implemented.

Classical integrity, like SBAS, targets to detect and correct errors due to satellites or atmospheric conditions [54] but do not handle the local urban canyons problems as it is mainly targeted for use in avionics. However, in vehicle localization, urban canyons cause another major source of error, namely multi-path and fading in which classical integrity has no particular counter-measure. Dealing with urban canyons require local information about the environment. This creates a high demand for the

local integrity techniques. Recent studies discuss local integrity [55]. Even though technique proposed by Margaria et. al can solve the problem resources required for a practical implementation is not seem feasible. The technique requires the collection of pseudorange residuals from GNSS receivers through a mobile network for a sidereal day. The amount of data to be collected for a small region is very high, and practical implementation requires full coverage at least in urban areas. In this chapter, we define a local integrity heat map that determines urban canyon areas and estimates positioning error depending on the region and time of the measurement. Local integrity heat map is implemented as a digital map attribute [56]. Digital map will also be fused as an additional sensor to enhance localization and map matching. Tests accomplished at different urban environments show that local integrity heat map has an important potential for local error estimation and can be used as a local augmentation method.

4.1. Local Integrity

The concept of "Local integrity" of the received GNSS signal can be addressed as the definition of an integrity concept capable of taking into account not only the system but also the environment nearby the receiver. A typical GNSS receiver needs external information (for example from EGNOS/EDAS) for improving the positioning accuracy and for providing integrity information. However the traditional SBAS integrity concept shows several limitations in vehicular applications, especially in urban/suburban scenarios: basically, the classic integrity concept has been tailored to aeronautical applications, with the GNSS antenna in open-sky conditions, then with a limited impact of possible satellite visibility problems and multi-path errors. In open-sky conditions, SBAS aims to detect and compensate possible errors due to satellite faults (e.g. inaccuracies in ephemeris information or onboard clock malfunctioning) or due to the propagation channel (e.g. changes in ionospheric delay). The evaluation of local effects (like multipath and receiver noise) on the pseudo-range measurements (and on the positioning) is required for the analytical models, which usually depend on the satellite elevation only. Conversely, SBAS models typically do not deal with possible time- and space-varying degradations, depending on the local environment and on the

receiver features (e.g. multi-path mitigation capability): this is the main reason why the classic SBAS integrity concept does not fit urban scenarios, where the degraded positioning cannot be easily predicted by analytical models.

The concept of "local integrity" is mainly intended to try to overcome these limitations. When the local conditions are taken into account, additional information about the degradation of the received signals, due to local effects, can be exploited.

Notably, it would also be possible to combine observations taken at the same place over multiple days due to the repeatability of the GNSS satellite/user geometry. In fact, the geometrical conditions (relative position between a GNSS receiver and each satellite) are known to be repeatable, and the periodicity depends on the GNSS satellite orbits.

For example, GPS satellites have an orbital revolution period of 11 hours and 58 minutes. Every sidereal day (23 hours and 56 minutes) a GPS satellite passes over the same place on the Earth. Thus it is seen by a receiver with the same azimuth and elevation (leading to the same GDOP). For a particular position of an urban map, every day the signal from a GPS satellite is expected to be received 4 minutes in advance with respect to the previous day, with the same satellite/user geometry and then with comparable degradations due to multi-path effect (e.g. see [57]). This concept can be extended to GNSS signals other than GPS: for example, it has been verified that the current repeat cycle of the Galileo satellite orbits is approximately ten days.

Conceptually with the use of digital map information and measurements during all orbital revolution periods can produce error patterns for a specific location. Hypothetically for every urban location on Earth, a survey for a full orbital revolution period can give us all the required information about the local environment. But this is not possible practically, considering the amount of field work required. That is why we introduced local integrity heat maps to create the information for a given period from the existing digital maps without field survey. By understanding local conditions better and use of repeatable geometry we can create a database to estimate possible

local errors introduced by the environment better.

Figure 4.1 shows an excellent example of the basic idea. In the figure, a selected area in the map is processed for different times for line-of-sight(LOS) visibility of the satellite constellation. Since the satellite locations are known, and the main obstacles are buildings for ground location LOS visibility for a particular location can be calculated. For example, at location A in the Figure 4.1 number of direct line of sight satellites are six at four in the morning, whereas at seven number of LOS satellites are four. LOS visibility will directly affect positional accuracy at location A. This illustration shows that a prior knowledge about satellite visibility is possible which can be used to define a local integrity measure.

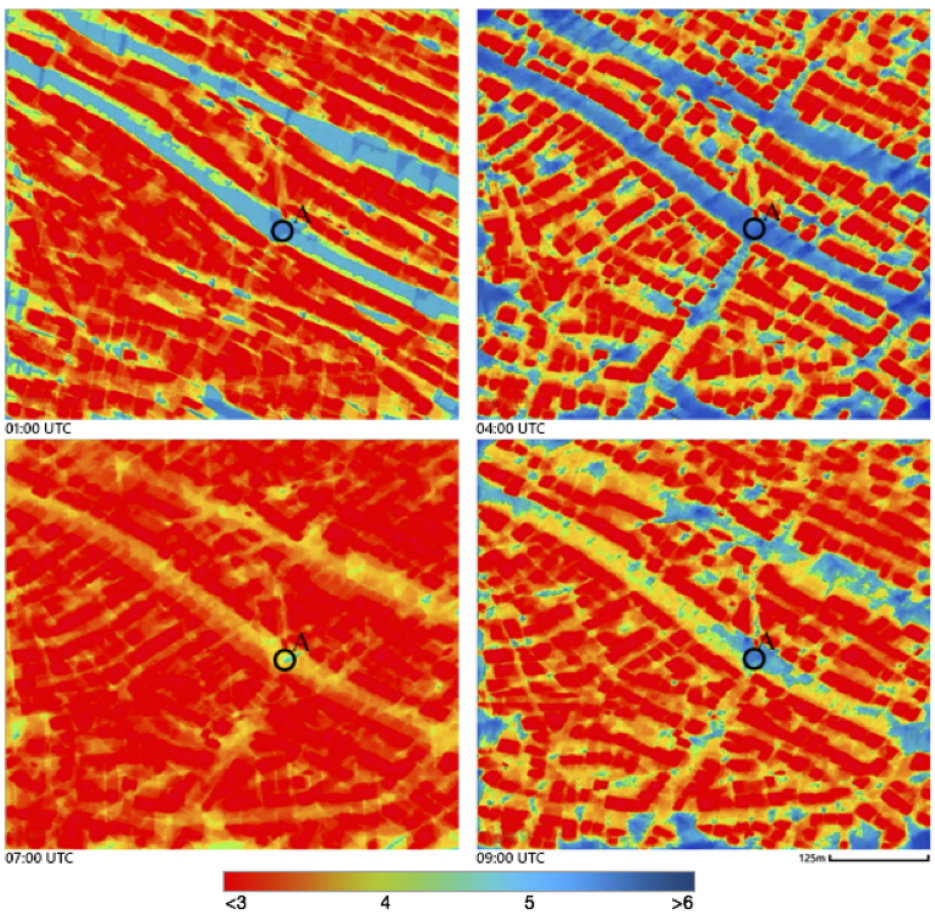

Figure 4.1. Satellite Visibility Heat Maps.

4.2. Related Work

In the literature, there are several countermeasures for solving problems caused by the urban canyons. As explained in previous chapters different sensors are fused to handle GNSS availability problems. The cooperative navigation that we have proposed in this thesis can also handle some difficult cases like tunnel passages. With the cooperative navigation, other cars with a better reception will continue share information through mobile communication in the absence of GNSS signals. However, urban canyon determination is not studied in detail. An urban canyon is an area which has high buildings, tunnels, bridges and other obstacles that cause multi-path effect and fading in GNSS signals. Information about the local environment is needed for urban canyon determination. Urban canyon modeling was first investigated in climate and meteorology literature. Sky View Factor (SVF) is defined to measure radiation emission and climate changes in urban canyons. This is analogous to GNSS signals. In [58] authors described a model for urban canyons to measure radiation emission that is based on the viewable portion of the sky. We tried to determine the portion of the sky which is directly visible to the GNSS receiver's antenna. This indicates that line-of-sight GNSS satellites are in fact correlated to the urban canyon factor. Currently, 3D building information is widely available in commercial digital map databases in most of the metropolitan cities. 3D building data is produced with aerial photogrammetry and has a very high accuracy (under 30 cm). To determine urban canyon, Sky View Factor (SVF) should be calculated. SVF measures the sky view possible from the point of observation, and it is widely used in different forms and formulations in the literature [59–61]. Even further, some methods require extra equipment like fish-eye camera to detect urban canyon geometry [61].

4.3. Methodology

We focused our work on vehicle localization, but the method we defined can be used for stationary positioning as well. To simplify the problem, we will focus on the scenarios where the vehicle is moving and follow the road centerlines. Road centerlines are created at the digital map production by drawing a line which passes through the

middle of the road. We implemented the local integrity heat map as a map layer with possible urban canyon regions. The position error and other necessary information for urban-canyon detection are attributes in the heat map layer. We defined Open View Factor (OVF) as the indicator of urban canyons.

The OVF should be calculated depending on the location of the observer. Since we would like to have a pre-calculated OVF measure for a given location, we will reuse the grid system we introduced in Chapter 3 for fast computation. As we described earlier, the grid system is a representation of the digital map as an independent layer. Heat map and distance errors are calculated according to the road centerline and stored in the grid system.

In our method, local integrity heat map provides the location of possible urban canyons at the grid level. It is based on a grid system that stores all the necessary information to deduce possible positioning errors. Urban canyons are determined by OVF computed for all the grids in the system. In Figure 4.2 urban canyon regions are denoted with polygons on the map.

Figure 4.2. Urban Regions with High Buildings.

Following digital map attributes are used in the creation of local integrity heat map:

- Building footprints and 3D information: Detailed information about buildings is polygon layer in the digital map database. This layer is generally digitized from aerial images. It covers building height and building footprint.
- Number of lanes. Available especially for highways and major roads.
- Road center lines

Figure 4.3 is the corresponding heat map for the Figure 4.2 computed by our method, regions with a higher possibility of an urban canyon are closer to the color red.

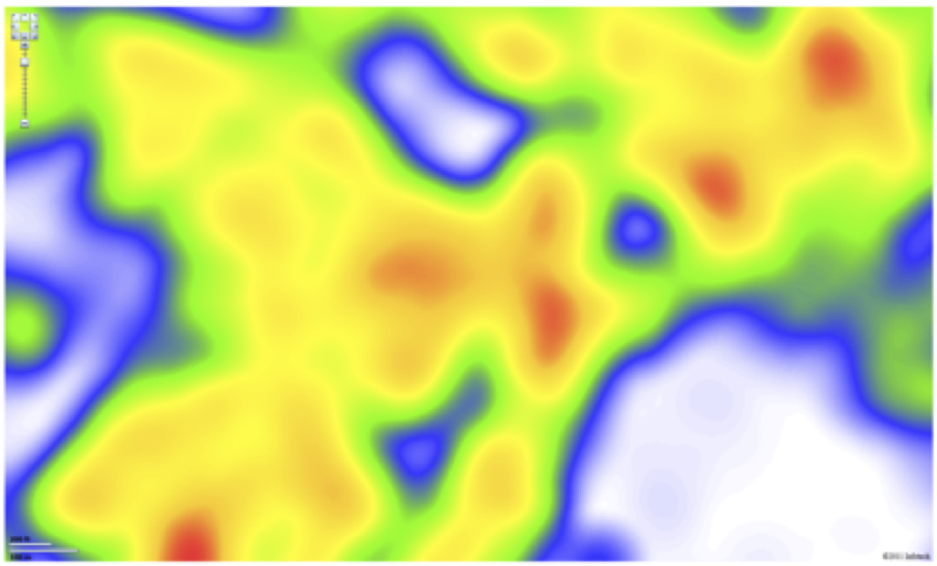

Figure 4.3. Sample Local Integrity Heatmap. Red colors show possible urban canyon locations.

4.3.1. Grid System for Heat Map Calculation

The digital map is conceptually divided into $3 \times 3m$ squares and denoted with red squares as shown in Figure 4.4. We have selected grid size as $3 \times 3m$, since the obstacles

around the observer are not tiny objects, they are buildings which have widths greater than $3m$. It would be a computational intense to compute smaller than $3 \times 3m$. Most of the time the OVF values are the same for a couple of consecutive grids even with the 3×3 grids. A smaller grid size may also be used, but it would increase processing power and storage requirements without adding too much value. Grids can be larger or multilevel depending on the implementation, memory and processing requirements.

Information about the road segment is stored in a grid cell. If a road intersects a grid the corresponding id is stored in the grid attributes. A grid cell also contains angles to its left and right buildings. Any other attributes for positioning error such as the line of sight satellites and measured pseudo-range residuals and possible distance errors (in meters) are stored in the grid cell. The distance error is defined to be the distance from the measurement point to the closest point on the road centerline (i.e. perpendicular distance).

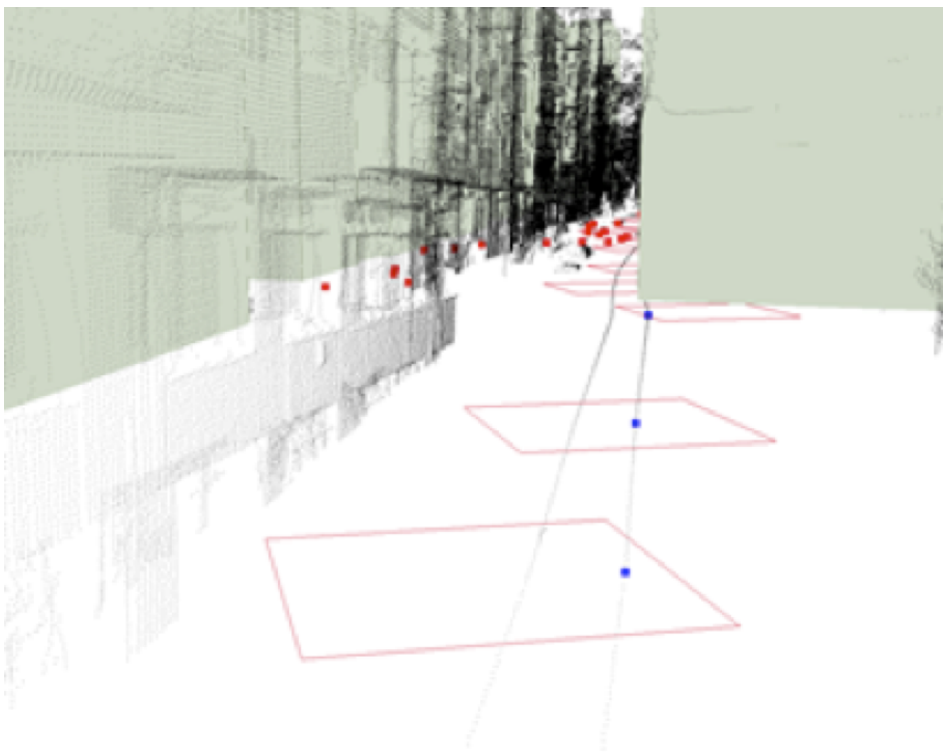

Figure 4.4. Grid Display from Street Level with Lidar Data.

4.3.2. Open View Factor

OVF is used to define possible urban canyon regions precisely. It is the main indicator. As a matter of fact, as the urban canyon gets deeper, GNSS signal noise increases. We derived Open View Factor (OVF), from SVF, to measure how deep and narrow the urban canyon is from the point of measurement. Height to width ratio of the surrounding buildings are used to measure the line of sight prevention from the point of measurement. The line of sight prevention, γ is calculated as in Equation 4.1.

$$\gamma = \arctan\left(\frac{h_b}{d_b}\right) \tag{4.1}$$

where h_b is the height of the building b and d_b is the distance to the building b. γ is computed for the buildings both on the left (γ_l)and right side (γ_r) of the midpoint of the grid on the road centerline. Then we calculate the open angle for the both right and left as in Equation 4.2 and 4.3

$$\alpha = 90 - \gamma_l \tag{4.2}$$

$$\beta = 90 - \gamma_r \tag{4.3}$$

Open View Factor (OVF) depicted in Figure 4.5 is defined as in the Equation 4.4.

$$OVF = \alpha + \beta \tag{4.4}$$

Note that OVF values are based on straightforward calculations. For every grid cell that is visited during a route (of n grids), OVF can be computed with running time in the order of $O(n)$. Since computation requirement is low when the vehicle computer does not have a storage for the digital map OVF can be calculated online. In this case, the digital map information may be retrieved dynamically through a mobile

communication facility.

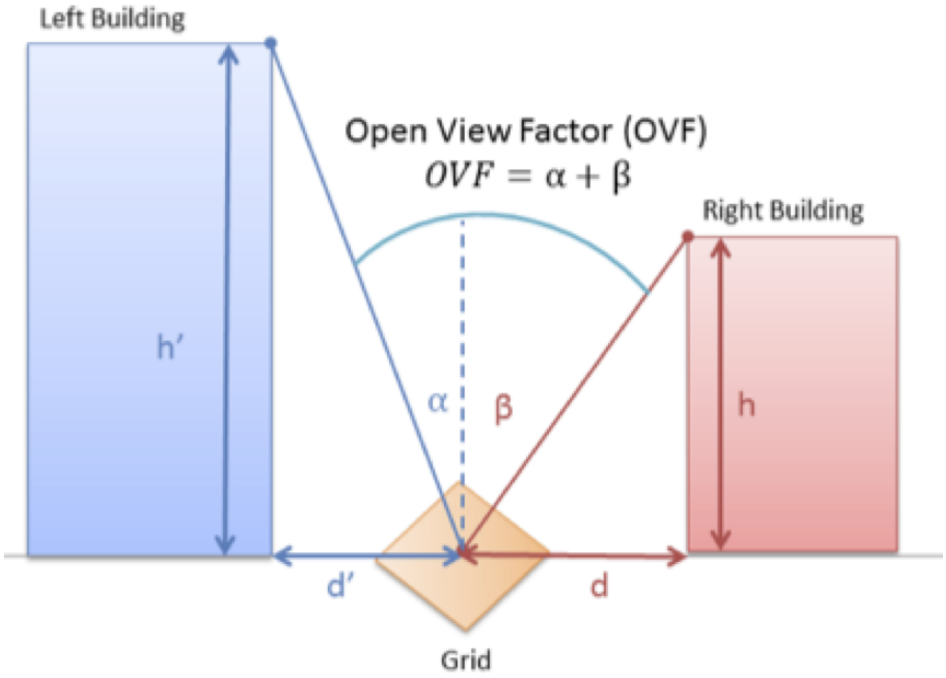

Figure 4.5. Open View Factor Calculation

4.4. Experiments

We carried out two real-world experiments. Firstly, a controlled field experiment was conducted on different streets at Istanbul. In this field test, RTK GNSS device that is capable of position fix under 10cm error and a laser scanner LIDAR is used to validate the map database used in our implementation. The second experiment was accomplished with the GNSS data collected from a vehicle tracking system.

4.4.1. Controlled Field Experiment

We ran several field tests to validate heat map and collected pseudo-range residuals for Local Integrity. To accomplish the field test, we obtained an RTK GPS with its stationary radio modem, LIDAR, and several GPS devices and attached them to

our demo vehicle as shown in Figure 4.6. Field tests were done in Istanbul on specifically selected narrow streets with mid-rise buildings, which are indeed potential urban canyons

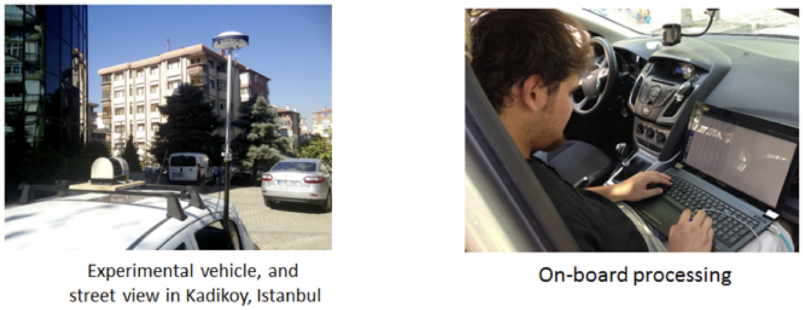

Figure 4.6. Field Test Setup.

Determining ground truth and understanding different GPS receivers is a challenging process. Especially real-time kinematic GPS devices are very expensive and hard to configure. When the environment has high buildings aligning the base station, this is not a simple task and can lead to errors. RTK GPS devices are more suitable for land survey operations of stationary objects. When moving objects like cars considered, a survey with an RTK GPS is not very practical and should be supported by other sensors.

(a) (b) (c)

Figure 4.7. Images of the Equipment Used in the Field Tests: (a) Ashtech RTK GPS (b) Ublox GPS (c) SICK Lidar.

Standard embedded GNSS receivers widely available on vehicle tracking boxes do not provide extra information like pseudo-range residuals. This is why to get the best test data we use more than one GNSS receiver and a LIDAR. Experiment setup contains several positions from different GPS devices such as the one from Vehicle Tracking black box, Ublox GPS [62] and Ashtech RTK GPS [63] shown in Figure 4.7. Moreover, SICK LIDAR [64] makes laser scanning of the environment and measures the actual heights of the buildings around and the distances to those buildings from the point of the observer. Real data are used as validation data for the heat map concept. Pseudo-range residuals collected in the field are used as the primary input to local integrity.

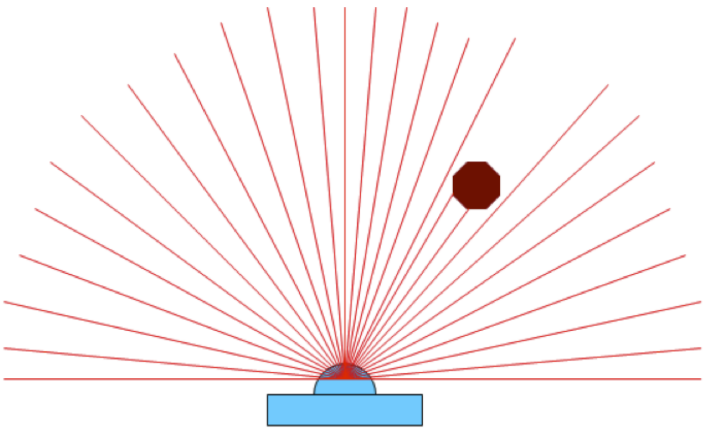

Figure 4.8. Lidar Working Principle.

Ashtech real-time kinematic (RTK) GPS is used for precise positioning. The building footprint data coming from 3D aerial photogrammetry can provide under 30 cm precision. Ublox GPS is used as a mass market GPS that can output pseudo-residuals. SICK LIDAR is used to scan the environment to measure the height and validate the Heat Map model. SICK LIDAR used in the experiment is a single layer outdoor LIDAR which is used for vertical scanning although it is produced for horizontal scanning. The range of the LIDAR used in this experiment is around 100 meters. The range is enough for our test area with narrow streets. LIDAR working principle is shown in Figure 4.8.

Even though building footprints produced from high accurate aerial photos they are a static representation of the real world. Buildings are digitized from rooftops. In the real traffic, there are more obstacles like trees, high vehicles, balconies. These objects are collected by LIDAR. There are also other objects which can cause noise in LIDAR data collection. LIDAR point cloud shows how the digital map data can deviate from the real world.

Figure 4.9. Buildings in 3D, Lidar Point Cloud and GPS Measurements

Grids on the narrow streets and positioning information from Ublox (red) and Ashtech RTK GPS (blue) is shown in Figure 4.9. Note that there are shifts in Ublox positions compared to grids. This is due to urban canyon and precision of the mass

market receiver. Difference between RTK GPS and Ublox locations is an example on how urban canyon affects the positioning.

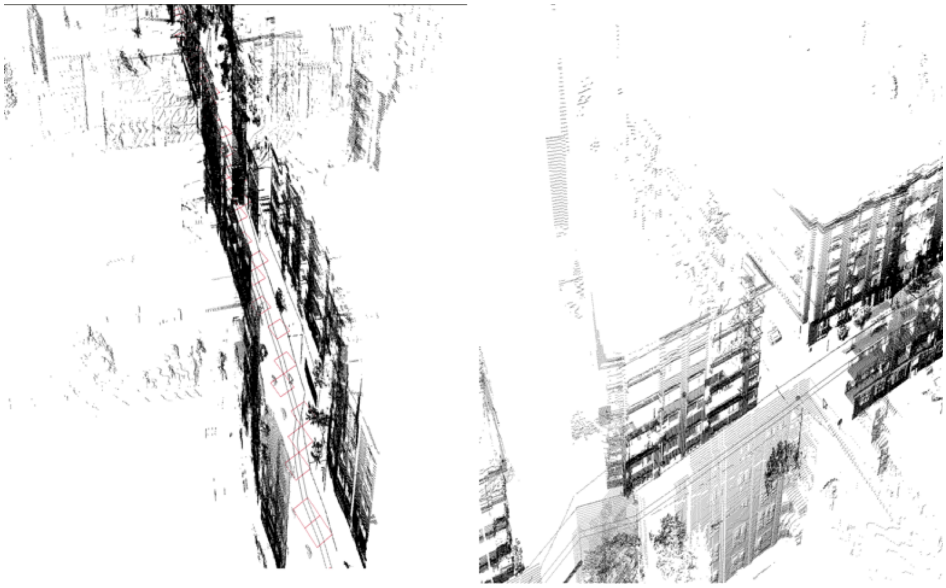

Figure 4.10. LIDAR Scan

Figure 4.10 shows LIDAR scan results with grids drawn on the streets. Note that fine details are present in the LIDAR scans due to high precision of the laser. The challenge is to align the high precision laser scan image on the buildings on the digital map because to align the building correctly positioning should be fine. The reference position is Ublox receiver, therefore, there are shifts due to urban canyon effect of the test field. As the position calculated by Ublox receiver shifts, the laser scan images shifts accordingly.

4.4.2. Real-World Vehicle Tracking Data

This experiment is a real-life dataset collected from the registered vehicles for the last one year on the streets mentioned above from Infomobil vehicle tracking system [65]. The tracking database contains more than 70000 vehicles while most of them are passenger cars and used for commercial purposes therefore the data density is high on working hours. The advantage of such a tracking system is that any method devised

from this data set can be applied to practical usage since data for all of the country can be collected within days.

4.4.3. Experimental Results

Road centerline is validated with RTK GNSS footprints. Our first target for the field test is to check if there is a real urban canyon at the spots determined by the heat map. We checked around ten streets where the color is red from the heat map. The position error was above 20 meters. Since we now the exact location of the buildings from high precision digital maps it is easy to measure position shift within a controlled environment. With the digital map information we can first check if the RTK has been configured correctly by use of previously known locations from the map, then we can use RTK for the ground truth. Without this setup, determining the ground truth in an urban canyon environment is very problematic. Results of the controlled experiment reveal that the digital map database is suitable to be used in OVF calculations.

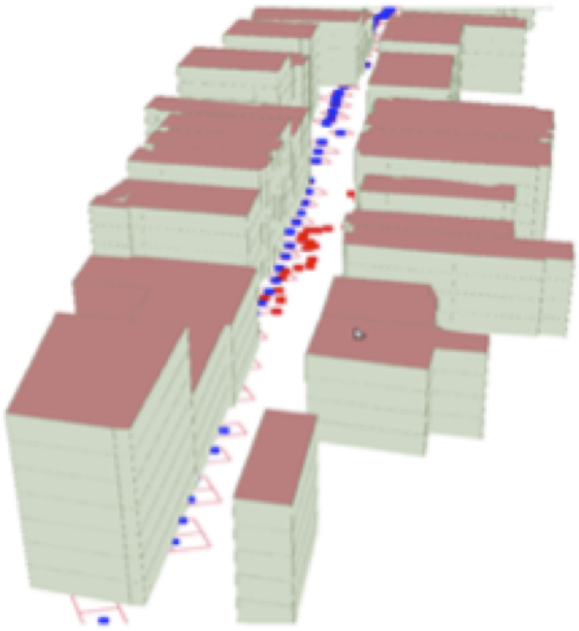

Figure 4.11. Field Test Results with Grid Information.

In Figure 4.11 grids on the narrow streets and positioning information from Ublox (red) and Ashtech RTK GPS (blue) is shown. The Figure shows the positions over grids. Note that there are shifts in Ublox positions compared to the grids. This is due to urban canyon and the precision of the mass market receiver. This figure explains how urban canyon affects the positioning.

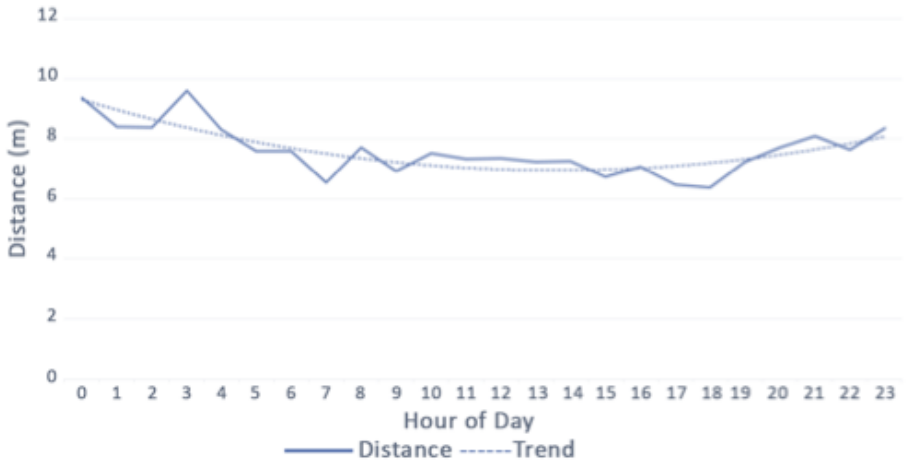

Figure 4.12. Distance Error with Respect to Hours of Day.

Real-world vehicle tracking logs for the last 365 days is collected for the validated roads from the first experiment. OVFs for these roads are calculated and stored in grids. We know that visible satellites used in position fix change during the day. It is because satellites revolve around the Earth twice a day, so the set of satellites observed differs in a day. We examine the distance error with respect to hours of a day, and the results are presented in Figure 4.12. Distance error decreases as time goes to noon then increases again. A second-degree polynomial fitted according to the error distance trend is shown as a dashed curve. It is due to the change in the satellite set used in position fix. The same behavior is expected for all other days.

We examine the relation between OVF and the distance error. The results are presented in Figure 4.13. We observe that as the average OVF increases, the distance error tends to decrease as it is expected. Average OVF value means the average of

OVF values from the grids of the measurements during the hour. Since it is a street and vehicles are passing through, they record position at different times at different positions of the street. In the aggregated analysis, we average the OVF values as we averaged the distance errors. Otherwise, OVF is a fixed value for the grid and depends only on the building structure dataset.

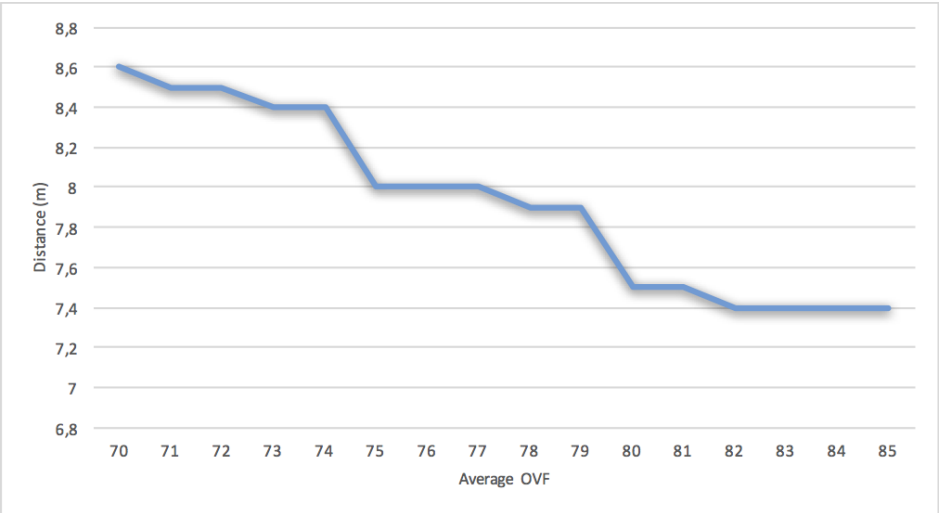

Figure 4.13. Distance Error vs. Average OVF.

We also observed that change in distance error during a 24 hour period due to satellite set changes from side to side depends on the heading and the positions of the satellites used in calculations. Therefore speed and direction of the vehicle in the query are also important. In Figure 4.14, position shifts in different times of a day is presented. Small green dots are the LOS satellites while small dark red points denote non-line of sight satellites. Satellite set in position calculations is shown in a polygon frame. The satellites are for the experiment with calculated positions are shown in green. We observe that the position error shifts towards to the satellite set in calculations. For the satellite set of red light red dots, the satellite set is mostly on the other side of the road. Therefore we are further investigating the position shift according to the satellite set as an on-going study.

Figure 4.14. Position Shifts due to Satellite Set in Computations.

5. VANET-ASSISTED COOPERATIVE VEHICLE MUTUAL POSITIONING

5.1. Introduction

This chapter contributes to the enhancement of reliability and availability of the position information by using sensors provided on a vehicle. We present set of procedures to blend GNSS and V2V communication to improve the performance of the stand-alone on-board GNSS receiver and to assure mutual positioning with a bounded error. Particle filter algorithm is applied to enhance mutual positioning of vehicles, and it fuses the information provided by the GNSS receiver, wireless measurements in vehicular environments, odometer, and digital road map data including reachability and zone probabilities. Measurement-based statistical model of relative distance as a function of Time-of-Arrival is experimentally obtained. Positioning accuracy and network performance is examined through realistic simulation studies with the different number of vehicles included in mutual positioning procedure. The proposed mutual positioning procedure is experimentally evaluated by a fleet of five IEEE 802.11p radio modem equipped vehicles. Collaboration in a VANET improves the availability of position measurement and its accuracy up to 40% in comparison to the stand-alone GNSS receiver. We have disseminated our work in this chapter in [66, 67].

Standard technology for a vehicle's absolute position measurement is the GNSS/GPS receiver. However, stand-alone receiver's performance can be poor due to an obstructed view of the entire sky or due to a poor orbital configuration of visible satellites. Various level of accuracy in GPS measurements can be obtained, depending on the types and number of GPS signals received and analyzed, the algorithms, and the availability of externally supplied correction data (including differential correction and real-time kinematic correction data).

5.2. Related Work

Recently, peer-to-peer (P2P) cooperative positioning and communication have also been shown to improve the stand-alone GNSS receiver performance by sharing information between collaborating users [68, 69].

Several limitations and technical challenges lie along the implementation of hybrid positioning techniques. For instance, low-level raw data are not provided on a standard inexpensive or embedded GPS receiver, and mostly its recorded logs were used [70] or clustering for mutual positioning may not be effective due to closely traveling vehicular nodes and their redundant position information apart from management complexity of clusters [71, 72]. Furthermore, wireless ranging measurements have an unrealistic standard deviation of 5 meters and fusion of range measurements is also not adequately covered, [73, 74]. In [75], GPS pseudorange corrections as the low-level data are broadcasted by vehicular nodes in a close vicinity. Each GPS receiver fuses received corrections to reach a better accuracy. As the number of collaborations increases, the error is simulated to be exponentially decreased. However, this method is applied to the artificially generated GPS data on a map whose segments are 20 cm in length, and the position error is assumed to be 14.06 meter on an open sky, and the V2V communication has a range of 100 meters restricting its usability.

Inexpensive sensors such as a GNSS receiver, odometer, a commercially available road map data used for navigation purposes and the off-shelf IEEE 802.11p modem are used toward modeling and implementation. Beyond the state-of-the-art, a measurement-based statistical model of Time-Of-Arrival (TOA) is developed, and this model is used in the simulation study, and then experimentally validated for a limited number of vehicles on a real road test by using automotive grade embedded devices. The particle filter algorithm and its weight update are based on all possible information related to the absolute position, road infrastructure, vehicle motion and mutual positioning in a Vehicular Ad Hoc Network (VANET) via fast data packet exchange by using IEEE 802.11p physical layer. We implement particle filter by leveraging the particle's occupancy on the road segment and topology of the digital map. The digital

road map is used as a sensor to bias the particles towards a road segment. The Digital map is used as a prior information about the vehicle location in conjunction with the vehicle speed to enhance localization. Vehicle's displacement is calculated by odometer reading, and it is used in transition model along with the map topology.

5.3. Methodology

The cooperative approach that we utilized for vehicle positioning is shown in Figure 5.1. VANET-assisted cooperative mutual positioning is considered to be a sensor with different characteristics whereas GNSS position measurement is another sensor. Particle Filter algorithm is tuned by adding additional functionalities such as map matching and the routing probability of the Ego Vehicle at the intersections. Multilateration range estimation is used to generate vehicle location with position and time information provided by neighbor vehicles. The result of the multilateration process is fused with GNSS and odometer with particle filter. The output of odometer is considered to be the input to the motion model of each particle to estimate the Ego vehicle's position.

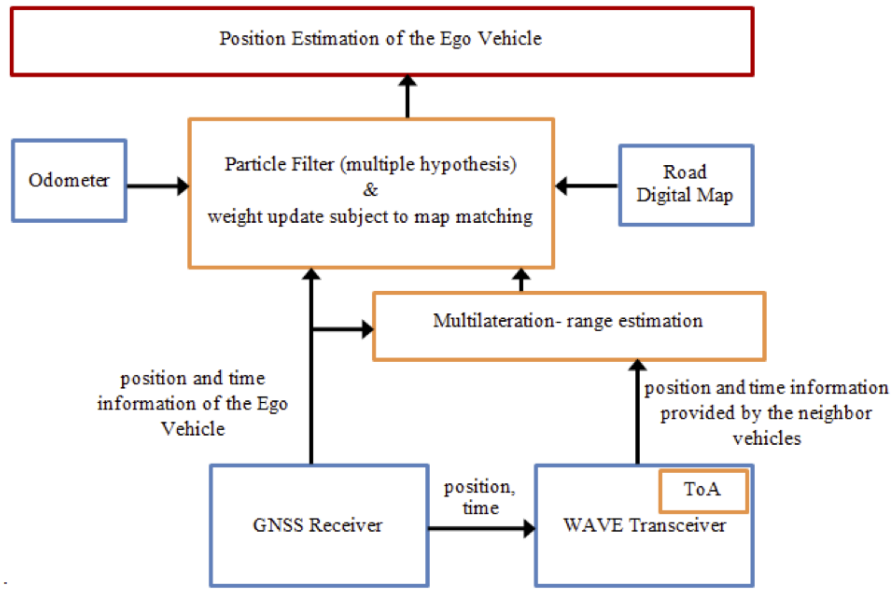

Figure 5.1. System Setup.

This approach introduces several practical issues, such as the presence of suitable on-board equipment enriched with V2V technology and its underlying protocol to exchange TOA packets with neighbors for exploiting mutual positioning techniques with minimally exciting TOA packet collisions. In fact, cars are supposed to exchange information about both position and distance. The GNSS receiver provides a UTC time, as a certified time-reference (which would be particularly useful to timestamp the information at TOA packet reply-request instance). Collaboration by exchange of ranging data between vehicular nodes is done on the basis of reply-request. Small size data packet is sent to each of the neighboring vehicular nodes with a timestamp on it. The receiver vehicular node replies with an adding of another timestamp denoting the internal delay of the node for processing at the physical layer. Each vehicular node in the vicinity is communicated during 100 milliseconds see Figure 5.2 for the basic of flow of the reply-request process.

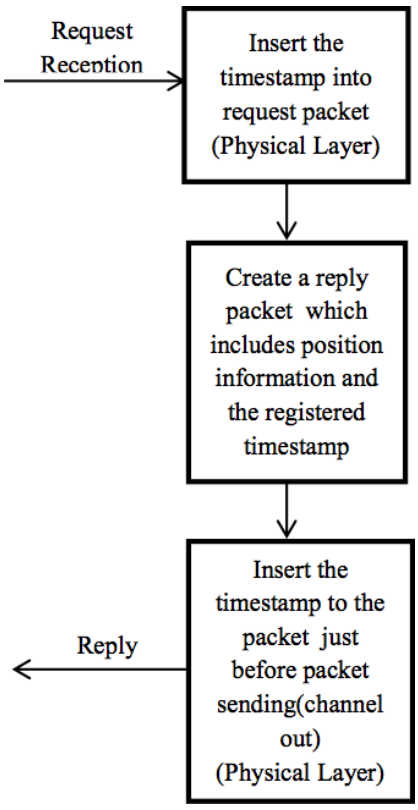

Figure 5.2. Measurement of TOA on the Basis of Reply-request Mode.

Multilateration algorithm is used to estimate the ego vehicle location through communicating with the neighbor vehicles in the radio transmission range and exchanging small size data packets, in which the GNSS position measurement of each vehicle is transmitted with its timestamp. To measure ranging distance with respect to the neighbor vehicles, TOA values of these exchanged packets are calculated. TOA is calculated by counting the quartz oscillators cycles between the instances of sending and receiving the data packet. Figure 5.3 shows the flowchart of the augmented particle filter with TOA measurement integration. To determine the neighbor vehicles location table is used. The ranging request is sent to neighboring vehicles with the time stamp. If the reply is received within five milliseconds, time of flight is calculated with the current time stamp. Distances are calculated and used in location calculation. The result is sent to the particle filter for fusion. If not enough answers are received localization is accomplished without multilateration.

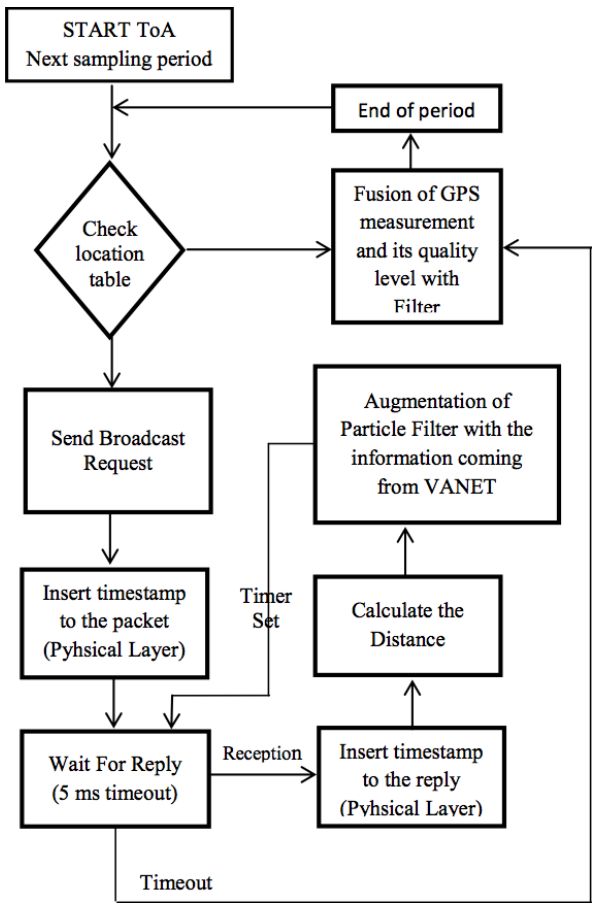

Figure 5.3. Flow Chart of Ranging Measurement.

5.4. Wireless Measurement Modeling by Use of IEEE 802.11p

In this section, we first elaborate Time-Of-Arrival (TOA) measurement and design of protocol by using IEEE 802.11p physical layer properties. Then, the procedure of multilateration is incorporated as a position estimate with TOA-based ranging error statistics.

Throughout this chapter, the ego vehicle has an IEEE 802.11p wireless modem and initiates the TOA protocol and ranging request. TOA measurement is designed as a low-latency protocol that is supported by each vehicular node either for replying to the TOA measurement request or initiating a request to measure the time of flight in collaboration with the set of randomly selected neighbor vehicular nodes in VANET. The presence of the neighbor vehicular nodes must be detected by cooperative awareness messages (CAM) a priori.

TOA measurement is characterized in a peer-to-peer manner, where the ego vehicular node sends a TOA request and its neighbor replies after updating certain fields in the TOA reply data packet. Since VANETs are asynchronous networks and quartz oscillator of OBUs may vary from each other due to drift, TOA is measured for the round-trip time of data packet travel between the ego and neighbor vehicular node and vice versa to avoid clock synchronization requirement.

To model time of flight, the reply packet is sent back to the sender. After TOA data packet is sent to the output queue of the modem in order to be transmitted to the wireless media, quartz oscillator cycle and clock time value are saved into the registers at the instance of sending the TOA measurement data packet. Cycle and time are saved one more time at the instance of receiving the same TOA packet that has been replied back by the corresponding neighbor node. On the side of the corresponding neighbor node, the same procedure of saving quartz oscillator cycle and clock time value are repeated to measure the internal delay of the replying node before transmitting the TOA data packet.

Measurement-based statistical error model of relative distance as a function of TOA is experimentally obtained. Since VANETs are asynchronous networks and quartz oscillator of On-Board Units (OBUs) may vary from each other due to drift [76], TOA is measured for the round-trip time of data packet travel between the ego and neighbor vehicular node and vice versa to avoid clock synchronization requirement.

The off-the-shelf IEEE 802.11p physical layer modem and carrier sense multiple access/collision avoidance (CSMA/CA) media access control is used to access the wireless media channel. 802.11p driver is compiled and a unicast communication of this particular TOA data packet involving timestamps at receiving and sending instant, source and destination media access control (MAC) addresses, packet ID, and received signal strength indicator (RSSI) of the power level received by the antenna of the source and destination vehicular node is achieved for requesting and replying. Also, in the TOA reply packet, the neighbor node writes delay occurred between the reception and sending timestamps of the TOA packet and changes the TOA protocol header to the reply mode. Additional delay can be caused by internal processing time, and it is written in the reserved field of the TOA packet, and it can be subtracted from the overall round-trip time of TOA packet by the sending node after the receipt of TOA reply packet.

Table 5.1. Round-trip time-of-flight Measurement-based Model.

Relative distance	Normal distribution parameters (ns)		Confidence interval (ns)	
	mean	deviation	mean	deviation
0.1	946554	1041	[946417 946692]	[958 1062]
50	946619	1023	[946483 946754]	[984 1058]
70	946764	1028	[946627 946901]	[975 1052]
150	947145	1037	[947009 947280]	[965 1054]

The stationary experiments were conducted in the university campus parking lot. Two 802.11p modems were used. TOA measurement is initiated by the node at the entrance of the parking lot, and the replying node is placed away while incrementing the relative distance about 10 meters after each measurement of flight time. TOA requests are made by the ego vehicular node at each 10 milliseconds for the time duration of 10 seconds. For each slot and its corresponding relative distance, the TOA measurements were collected and analyzed. The measured TOA values for each distance are tested by the function of Chi-square goodness-of-fit test in Matlab [77] and validated as a normal distribution with a mean and variance.

Normal distribution and confidence interval parameters are given in Table 5.1. The standard deviation is about 1000 nanoseconds (ns) for the round-trip of TOA packet flight time, which gives a deviation about 150 meters in one way.

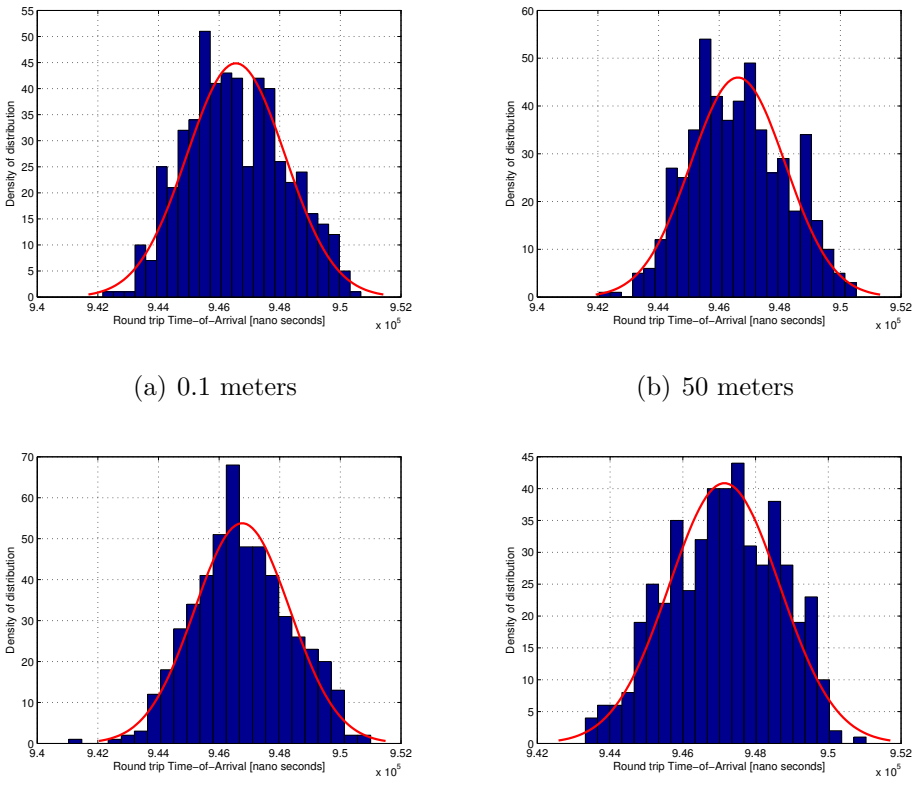

(a) 0.1 meters

(b) 50 meters

(c) 70 meters

(d) 150 meters

Figure 5.4. Round-trip Flight Time Versus Density for 4 Different Stationary Modem's Relative Distance (Δd=[0.1; 50; 70; 150] meters).

The first measurement data are collected when the relative distance between two OBU modem antennas are very nearly located on the top of the ego vehicle, i.e., about 0.1 meters and for some other selected position slots situated at 50, 70 and 150 meters away from the stationary requesting node (i.e., ego vehicle) round-trip TOA versus density is plotted in Figure 5.4. Measurements of round-trip flight time versus the relative distance are plotted in Figure 5.5. The bias for round trip TOA measurements is taken as the mean of normal distribution in Table 5.1. In Figure 5.5, measurements are also compared with the ideal flight time computed by dividing the relative distance to the speed of light in air, $c = 299705103m/s$. The speed of light in the vacuum is $c = 299792458m/s$, in air particles, humidity affects the speed of light.

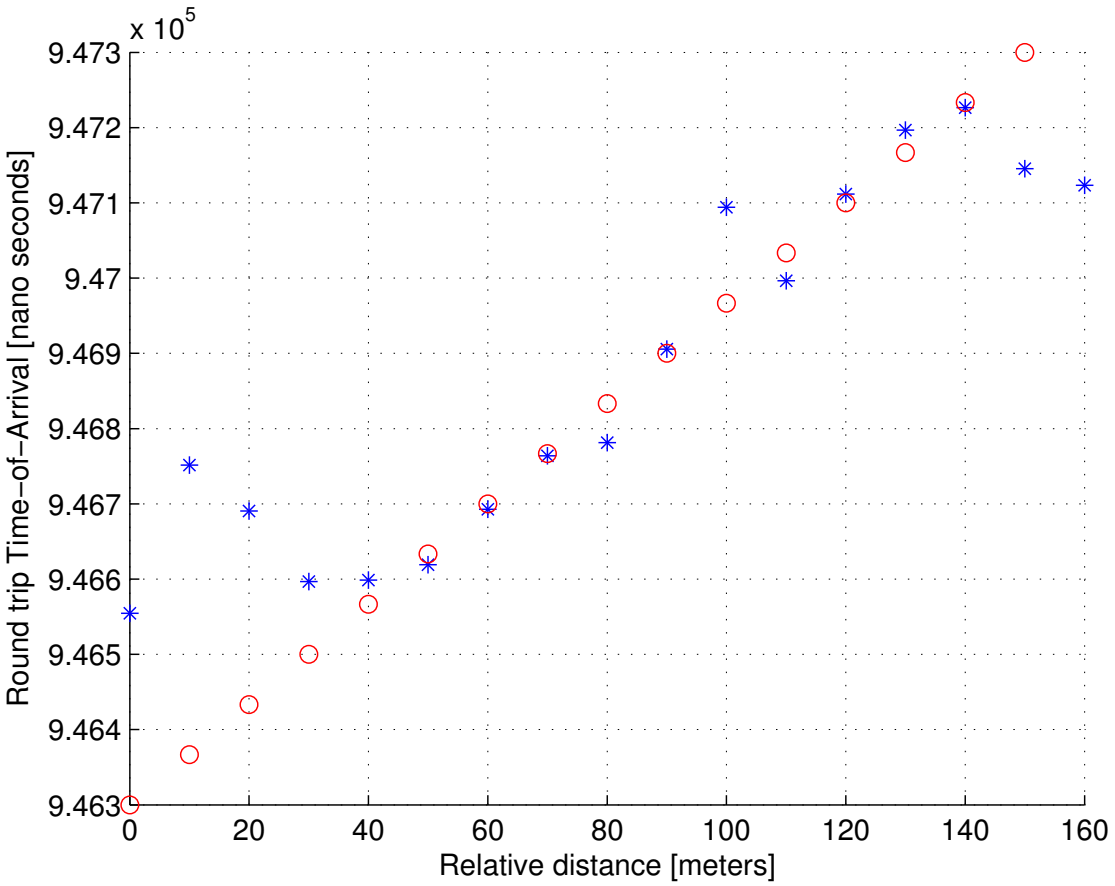

Figure 5.5. Relative Distance Versus Flight Time: Experimental Measurements are Marked by '*' and Compared Versus Flight Time, Marked by 'o'.

To validate the bias value of measurements and to compute time delay caused by 802.11p modems, physical layer properties are revisited. 802.11p is an amendment to the 802.11a Wi-Fi standard. 802.11p contains a similar physical layer convergence procedure (PLCP) to 802.11a/b/g. 802.11p does not require a request to send/ clear to send (RTS/CTS) handshaking and support for packet fragmentation. 802.11p uses orthogonal frequency-division multiplexing (OFDM) with 48 subcarriers and four pilot carriers with a nominal bandwidth of 10 MHz and uses multiple modulation schemes with OFDM to support bit rates from 3 Mbps to 27 Mbps [78].

The first task of the OFDM Physical Layer Convergence Protocol (PLCP) sublayer is to create a frame that can be easily demodulated at the receiver. This frame is called the PLCP [13] protocol data unit (PPDU), a breakdown of which is shown in Figure 5.6. The first task of the PLCP sublayer is to create a frame that can be easily demodulated at the receiver.

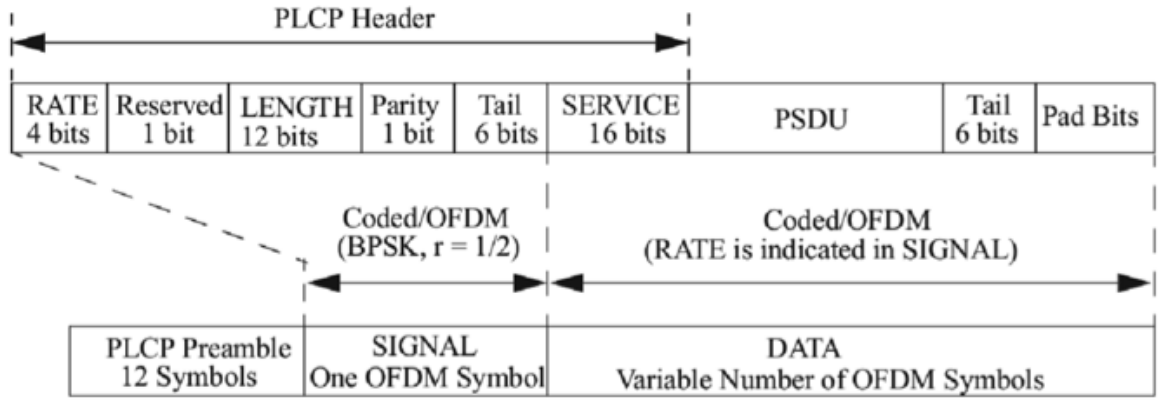

Figure 5.6. PLCP Protocol Data Unit.

A PLCP preamble of fixed length (for 802.11p, this is 32 microseconds), which is used for synchronization at the receiver. The PLCP header of 802.11p contains 4 bits for the rate, 1 reserved bit, 12 bits for length, 1 bit for parity, 6 bits for the tail and 16 bits for service making overall 5 bytes of header. The overall packet size is the sum of 155 Byte TOA packet and 5 Byte PLCP header, whose total is 160 Byte data. During

the experiment, the data rate of 3 Mbps is used, [79]. TOA reply-request time delay is biased at 943333 nanoseconds following the time delay calculation which is given in Table 5.2. This bias value represents the minimum value of the sum of time delays at the physical layer and validated by the several measurements for different distance values as plotted in Figure 5.4 (see, for instance, the minimum TOA i.e., time of flight in the distributions). TOA is added to this bias value. This bias value is evaluated by the experimentally measured round trip time initial delay value, (see for instance minimum value of distributions plotted in Figure 5.5), and the experimental results are supported by the calculation given in Table 5.2. Time-of-flight is added to this bias value, which makes possible the calculation of the relative distance between the two 802.11p modems.

Table 5.2. Time Delay Calculation During the TOA Reply-request.

Item	Delay Cause	Delay (nano seconds)
I	E[Total transmission delay of the TOA data packet]	$2 \times \frac{160 \times 8[bits]}{310^6[\frac{bits}{seconds}]}$=853333
II	E[Preamble processing delay for the requesting node only]	2× 32000 =64000
III	DCF interframe space (DIFS) delay	16000
VI	Short interframe space (SIFS) delay	10000
I + II + III + VI	TOA reply-request (round-trip) time delay	943333

5.5. Sensor Fusion

The same methodology used in Chapter 3 augmented with TOA measurements. To fuse TOA based localization weight update of the particle filter is augmented. Motion model is the same as Chapter 3 as follows,

$$\mathbf{x}_t = A\mathbf{x}_{t-1} + Bu_{t-1} + f_{t-1} \quad (5.1)$$

$$z_{t-1} = h(\mathbf{x}_{t-1}) + e_{t-1} \quad (5.2)$$

This time the measurement vector is constituted by the physical sensors being a GNSS receiver and a V2V radio modem used to measure TOA and to share position information in VANET, denoted by n_t and s_t, respectively. Overall, $z_t = [n_t\ s_t\ m_t]^T$ is the measurement vector, and e_t denotes the error vector.

5.5.1. Particle Filter with TOA

There is a minor change in the transition stage of the particle filter. The ego vehicle's velocity is multiplied by a factor of two to prevent the prediction bias, which may be caused by high error values of TOA measurements. Updated state transition given by equations 5.3 and 5.4.

$$x_t = x_{t-1} + 2T_s v_{t-1} cos(\alpha) \quad (5.3)$$

$$y_t = y_{t-1} + 2T_s v_{t-1} sin(\alpha) \quad (5.4)$$

5.5.2. Weight Update with TOA

For each particle, the initial weight is calculated based on the probability derived by the measurements of GNSS position and TOA-based mutual positioning result. Probability is calculated under the assumption that the deviations of the GNSS and TOA measurements are normally distributed and the standard deviation is changed with respect to the confidence values. The weight of the i^{th} particle for $i = 1, \ldots, N$,

and the probabilities at the time instance t is given as follows:

$$w_t^i \alpha P\left(n_t, s_t, m_t | \mathbf{x}_t^i\right) = P\left(n_t | \mathbf{x}_t^i\right) P\left(s_t | \mathbf{x}_t^i\right) P\left(m_t | \mathbf{x}_t^i\right) \tag{5.5}$$

where n_t, s_t and m_t denotes the measurements of GNSS receiver's position, TOA-based mutual position and map based prior and posterior localization result, respectively.

Weight update based on TOA measurement:

$$\left[w_t^i\right]_{xTOA} = c_{TOA} e^{-1/2\left([x_t]_{TOA} - \left[x_t^i\right]\right)^2 / \sigma_{TOA}^2} \tag{5.6}$$

$$\left[w_t^i\right]_{yTOA} = c_{TOA} e^{-1/2\left([y_t]_{TOA} - \left[y_t^i\right]\right)^2 / \sigma_{TOA}^2} \tag{5.7}$$

where $c_{TOA} = 1/\left(\sigma_{TOA}\sqrt{(2\pi)}\right)$ and σ_{TOA}^2 denotes the variance. A normal distribution in a variate is denoted by each particle coordinate with a mean $\left([x_t]_{GNSS}, [y_t]_{GNSS}\right)$ related to GNSS position measurement and $\left([x_t]_{TOA}, [y_t]_{TOA}\right)$ TOA measurement based mutual positioning, and variance $\left(\sigma_x^2, \sigma_y^2\right)$, σ_{TOA}^2, respectively.

5.6. Simulation and Experimental Study

The augmented particle filtering algorithm and its redefined weight update are tested with simulations. Different characteristics of sensors, buildings with their dimensions on the 3D local urban map are included in simulations. Positioning accuracy improvement and availability are studied considering a different number of aiding vehicular nodes in both of the line-of-sight (LOS) and non-line-of-sight (NLOS) condition. Realistic simulator of urban mobility (SUMO) [80] and V2V network simulator (ns-3) [81] is coupled. Visualization is enhanced to illustrate the map attributes such as possible signal occlusions due to buildings and necessary algorithms are developed with C++ in the ns-3 simulator platform.

SUMO is used to generate the position of the vehicular nodes, and their speeds are varied in a predefined interval of a given minimum and maximum speed value. 3D

digital map of Kadıköy municipality of Istanbul is used for inner city area modeling. The vehicular nodes are artificially generated at the main intersections with a frequency of 1 vehicle per seconds. Network simulator (ns-3) is used to simulate vehicular communication. In order to comply with the European Profile Standard ITS-5G [82], the Wi-Fi implementation in ns-3 is adapted accordingly, IEEE 802.11p physical and MAC layer is implemented. CAMs are broadcasted with a value of 19 dBm on the 10 Mhz channel at 5.9 GHz with a data rate of three Mbit/s. Signal quality is deteriorated with the use of Nakagami distribution model in radio propagation to model the non-line-of-sight propagation in an urban area [83]. NLOS and Nakagami model with the path loss exponent component of three is used, which allows a communication range of 550 meters. The list of the simulation parameters is given in Table 5.3.

Table 5.3. List of Simulation Parameters.

Parameter	Value
Vehicle Velocity	Max 20 m/s
Vehicle Penetration Rate	1 veh/s
Path Loss Exponent	3
Propagation Loss Model	NLOS + Nakagami
Transmit Rate	3 Mbps
Transmit Power	19 dBm
Carrier Sensing Threshold	-99 dBm
Transmit Range	550 m
Reference Distance	1 m
CAM Rate	10 Hz
CAM Size	88 Byte
Simulation Time	100 s
Number of Simulations	10
Simulated urban area size	1 km × 2 km

During the simulation and experimental study, the number of particles is 1000 and $ESS = 0.25$ is used. GNSS position error of each vehicle is subject to a nor-

mal distribution with a variance of 10 meters, which indicates that reliable in-route navigation suggestions can be made based on the GNSS signal quality. For the round-trip of TOA measurement, the standard deviation is about 1000 nanoseconds (ns) and causes positioning error about 300 meters (see, for instance, Table 5.1). Therefore, the standard deviation of TOA measurement in one way is chosen 150 meters.

Global coordinates are converted to the local frame by use of local conversion constant values specific to the test track in İstanbul near to $41N$ latitude and $29E$ longitude. The presented Particle Filter position estimation is a Markov process of the first order probability distribution at current time t, and it depends only on the previous state $p(X_t|X_{t-1})$. Geodetic coordinate latitude and longitude are approximately converted into the local frame by multiplying the difference in position between the two consecutive time indices with a specific constant such as $\Delta x = x_t - x_{t-1}$ is multiplied by 82.000 meters and $\Delta y = y_t - y_{t-1}$ by 111.000 meters for applying sensors fusion. Particular to test track, the conversion error to local frame in meters is bounded by 0.05% when compared to an accurate calculation that is done with the use of a spatial software at a central server.

Multiple TOA measurements with respect to different vehicular nodes can enhance the accuracy and availability of position estimation. Mutual positioning is incorporated as a result of multilateration based on TOA measurements. Each node adds in the TOA reply packet its GNSS position with a UTC timestamp. A screenshot of the simulation is given in Figure 5.7, mutual positioning is assured by applying multilateration to the TOA-distance measurement and it is an estimation problem. For simplicity, we assume we have one measurement to three neighbor nodes and the ranging or TOA-distance measurement, r_i for $i = 1, 2, 3$:

$$r_1 = \sqrt{(x-x_1)^2+(y-y_1)^2} + v_1 \tag{5.8}$$

$$r_2 = \sqrt{(x-x_2)^2+(y-y_2)^2} + v_2 \tag{5.9}$$

$$r_3 = \sqrt{(x-x_3)^2+(y-y_3)^2} + v_3 \tag{5.10}$$

where the i^{th} collaborative neighbor vehicle position $(x_i,\ y_i)$ is in the TOA protocol reply packet, $v(i)$ denotes the unknown measurement noise and (x, y) is the unknown coordinate to be estimated. Estimation problem is fit into Batch Least Squares [84] (BLS) problem by linearizing Equations 5.8, 5.9, 5.10 about their approximated known initial coordinates, i.e., $(\bar{x}, \bar{y})$

$$\left.\frac{\partial r_i}{\partial y}\right|_{(x,y)=(\bar{x},\bar{y})} = \left.\frac{(y-y_i)}{\sqrt{(x-x_i)^2+(y-y_i)^2}}\right|_{(x,y)=(\bar{x},\bar{y})} \tag{5.11}$$

$$\left.\frac{\partial r_i}{\partial x}\right|_{(x,y)=(\bar{x},\bar{y})} = \left.\frac{(x-x(i))}{\sqrt{(x-x_i)^2+(y-y_i)^2}}\right|_{(x,y)=(\bar{x},\bar{y})} \tag{5.12}$$

$$\mathbf{r_k} = H_k\mathbf{x} + v_k \tag{5.13}$$

where $\mathbf{x} = [x\ y]^T$ is the position of the ego vehicle and needs to be estimated in terms of positioning with respect to k neighbor vehicles $\mathbf{r_k} = [r_1\ r_2\ r_3 \ldots r_k]^T$.

A screenshot of mutual positioning update around the ego vehicular node is plotted in Figure 5.7. Neighbor vehicular nodes collaborate by replying the TOA request of the ego vehicular node, and they are presented by gray balls denoting their GNSS position measurements subject to a measurement variance of 10 meters. The yellow ball denotes the ego node's GNSS measurement subject to a variance of 10 meters as well. TOA measurement based multilateration or mutual positioning result is displayed with a blue ball whose position is subject to the estimation error. Particles are spread

around the ego vehicle, their colors are varied dependent on their weights, for instance, if the particle's weight is high, i.e., particle is on the road, its color is red, and if the particle is outside of the road, it has a reduced weight and it is colored in blue. The average of particle's weights determines the particle filter result.

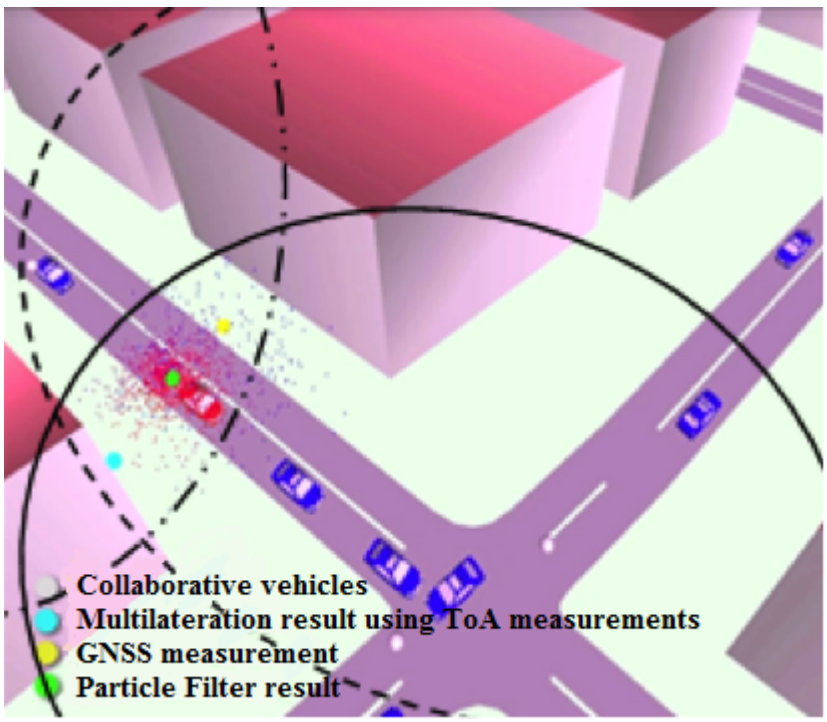

Figure 5.7. Illustration of Mutual Positioning and Map Matching.

Reliability of positioning is expected to be dependent on the number of collaborating vehicular nodes and their distribution on the road. Closely positioned collaborating vehicular nodes will cause redundant TOA measurements. In VANET, each vehicular node broadcasts its presence via CAM messages on a periodical basis. CAM frequency is 10 Hz and each CAM message includes GNSS position, speed, UTC time and road ID of the vehicular node, [82]. In our method, received CAM messages are stored in the table of the ego vehicular node with a lifetime of one second. To assure probabilistic selection, a randomly generated number is used to select a neighbor vehicular node. This randomly selected line and its corresponding neighbor vehicular node is a candidate to exchange TOA packets. If the line does not exist or previously selected, a new number is randomly generated.

At each sampling period, i.e., at each second, the ego vehicular node selects randomly the given number of the vehicular node (i.e., 3,5,7 or 9 vehicular nodes in our study) whose CAM messages have been received and written to the table. Then, TOA request is sent to the first vehicular node in an unicast scheme with a timeout of 6 ms. If 6 ms is expired, TOA request is renewed with a new packet ID and the previous request is omitted. To have a rich set of measurements and compute the mean value, 10 TOA requests are sent to the same vehicular node in a row with a timeout of 6 ms. At the end of sending 10 TOA requests, the request packet is not generated for the duration of 20 ms in order to clear the channel. Then, the same procedure of unicasting 10 TOA request packets to the second randomly selected vehicular node with a timeout of 6 ms is repeated, and this loop continues until reaching the given number of vehicular nodes.

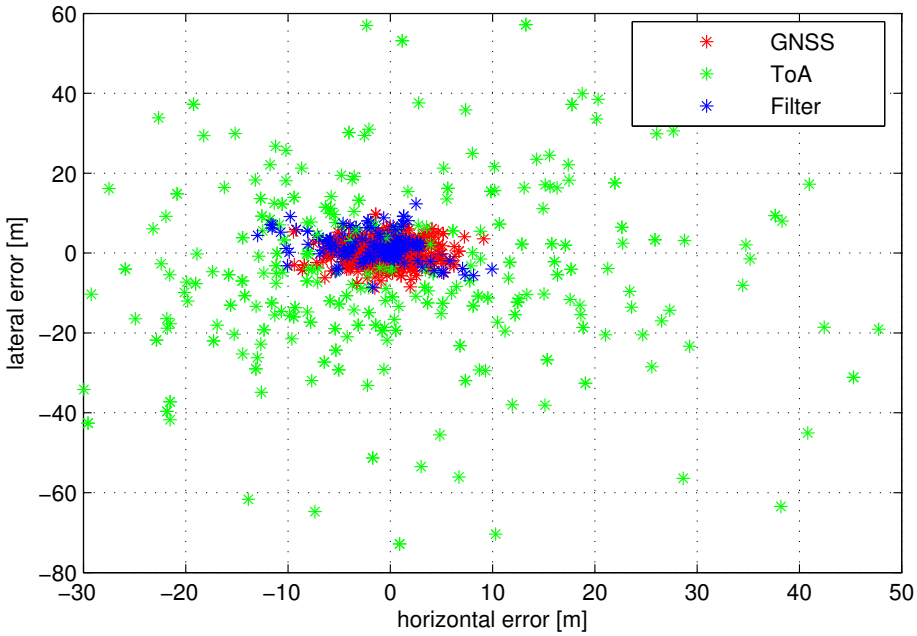

Figure 5.8. Scatter plot of GNSS positioning error, TOA based positioning error, and the results of fusion by particle filer.

The simulation scenarios are tested to validate the effectiveness of the particle filter algorithm. In Figure 5.8, the error responses of GNSS position measurement and TOA-based mutual position are plotted versus particle filter positioning error in

both of the longitudinal and lateral direction for the whole simulation scenario of 100 seconds.

The time responses of measurement errors versus Particle Filter position error are plotted in Figure 5.9.

Positioning error is calculated as follows:

$$d_e = \sqrt{(x_{true} - \hat{x})^2 + (y_{true} - \hat{y})^2} \tag{5.14}$$

where d_e is the positioning error and x_{true}, y_{true} denotes the correct position measurement in the longitudinal and lateral axis, $\hat{x}$,$\hat{y}$ denotes its estimation.

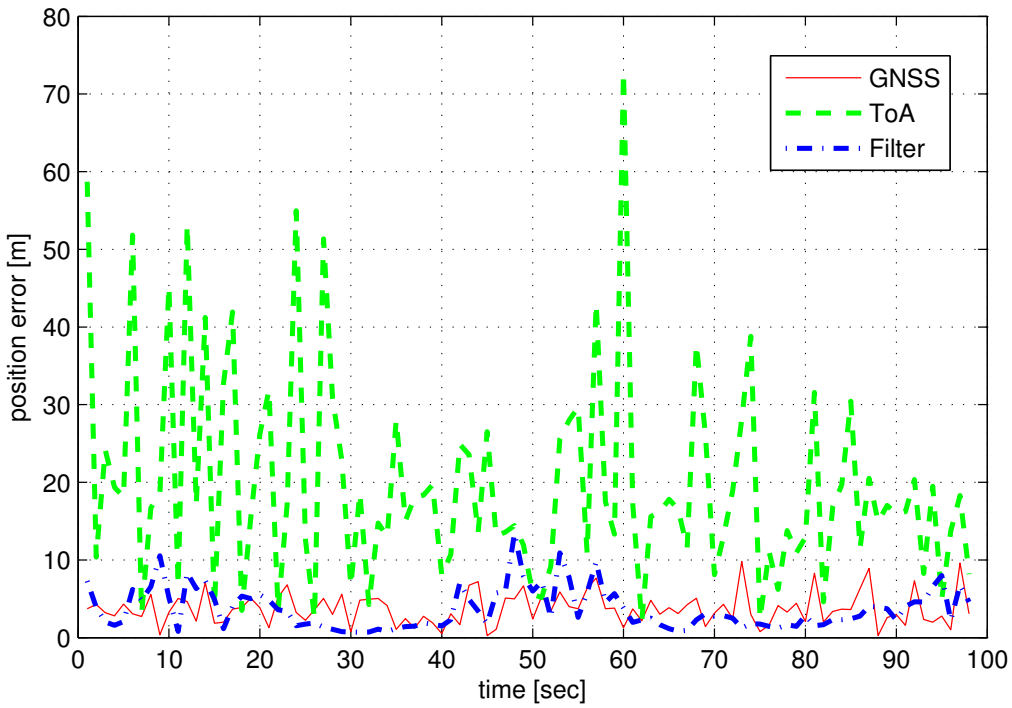

Figure 5.9. The error responses of GNSS and TOA measurements in comparison to the Particle filter error result.

The following metrics are used for comparison purposes: Circular Error Probability (CEP) refers to the radius of a circle in which 50% of the values occur, Distance

Root Mean Squared (DRMS) is related to 2D accuracy, and R95 is defined as the radius of circle centered at the true position, containing the position estimate with probability of 95%, [85].

Table 5.4. Comparison of positioning error for different number of nodes.

3 nodes		CEP	DRMS	R95	2DRMS
	GNSS	3.89	4.67	9.35	8.09
	TOA Mutual	34.35	41.80	83.59	71.45
	Particle Filter	3.83	4.64	9.28	7.97
5 nodes	GNSS	3.85	4.62	9.23	8.00
	TOA Mutual	23.12	27.76	55.52	48.08
	Particle Filter	**3.30**	4.01	8.02	6.88
7 nodes	GNSS	3.70	4.44	8.88	7.69
	TOA Mutual	19.03	23.47	46.94	39.59
	Particle Filter	**2.76**	3.34	6.67	5.74
9 nodes	GNSS	3.76	4.51	9.02	7.81
	TOA Mutual	15.86	19.30	38.61	32.89
	Particle Filter	**2.28**	2.75	5.51	4.65

When the number of vehicular nodes contributing to TOA-based mutual positioning is increased, both CEP and DRMS decrease. Table 5.4 gives results of GNSS positioning, and mutual positioning error calculated subject to a different number of collaborating vehicular nodes. In each distinct scenario, the output of the particle filter algorithm using both of GNSS receiver's position measurement model and the result of TOA-based mutual positioning result is compared. By following the results in Table 5.4, lane-level accuracy less than 3.50 meters can be achieved when the number of collaborating vehicular nodes is more than 5. For instance, when 5, 7 and 9 vehicular nodes are chosen for mutual positioning, the particle filter generates positioning errors of 3.30, 2.76 and 2.28 meters, respectively. The second scenario is repeated without using GNSS position measurement. GNSS outage is enforced for the whole duration of simulation scenario, and particle filter relies on TOA measurement based mutual

positioning and odometer readings. During GNSS outage, the particle filter generates bounded positioning error less than 10 meters for the case of five collaborating vehicular nodes, the error is reduced when the number of nodes is increased.

Table 5.5. Comparison of positioning error during GNSS outage.

		CEP	DRMS	R95	2DRMS
3 nodes	TOA Mutual	34.50	42.06	84.12	71.76
	Particle Filter	13.04	15.65	31.30	27.12
5 nodes	TOA Mutual	22.50	27.16	54.32	46.81
	Particle Filter	**9.68**	11.72	23.44	20.13
7 nodes	TOA Mutual	19.12	23.60	47.21	39.78
	Particle Filter	**9.21**	11.28	22.56	19.16
9 nodes	TOA Mutual	16.72	20.14	40.28	34.78
	Particle Filter	**7.41**	9.13	18.26	15.42

VANET performance plays an important role in transmitting the reply-request TOA packets. Lossless and fast data exchange are necessary to obtain a comprehensive set of the TOA measurements. Unicast communication scheme is preferred to avoid severe packet collision. The other option is the broadcast scheme, in which the vehicular node sends TOA requests to the vehicular nodes located in its radio transmission range, and these neighbor nodes reply to these TOA requests upon their receipts, that can cause instantaneous reply packet collision. The ns-3 simulator generates all possible causes of transmission failure: TOA packet can be dropped due to a possible collision, low signal energy level or due to high noise ratio. Other TOA reply delivery failure is caused by timeout expiration and being discarded. TOA reply-request delivery success is evaluated versus the overall number of the generated packets and it is higher than 80% in Table 5.6.

Table 5.6. Performance of TOA Packet Delivery in VANET.

	Collision	RSSI	SNR	Timeout	Total	Success
3 nodes	3.87	2.36	5.54	5.77	17.54	82.46
5 nodes	3.88	2.43	5.63	6.31	18.25	81.75
7 nodes	3.99	2.93	5.74	6.34	19.00	81
9 nodes	4	2.53	5.35	6.55	18.42	81.58

All collaborating vehicular nodes must share one common communication medium (e.g. control channel G5A-CC of 10 MHz bandwidth) with each other, and the number of vehicular nodes replying to the TOA protocol request in a unicast scheme needs to be increased for a better positioning accuracy. This is the fundamental issue in vehicular communications and similar to the so-called scalability problem [86, 87]. The Channel Busy Time (CBT) is a typical metric for measuring the current congestion on the channel, [88]. It measures the amount of time, for which the channel was sensed to be busy, and calculates the ratio with respect to a certain time interval. The channel congestion is measured by the CBT metric, which provides the ratio, for which the channel is detected as busy with respect to a certain amount of time. For evaluation, 10 CBT measuring stations are placed at the center of intersections in the simulated city area. The CBT ratio measurements are conducted by disseminating CAM messages with 10 Hz frequency and varying the different number of vehicular nodes collaborating with TOA measurement requests. When TOA protocol is not initiated, i.e., any vehicular node makes TOA measurements, CBT ratio is around 31.48%. This ratio without TOA traffic can be justified by calculating the CAM data traffic rate. For example, CAM data size is 88 Byte, 10 Hz dissemination frequency, the average number of vehicular nodes listened by CBT measuring stations is around 130 and data rate of 3 Mbps: $E(CBTratio) = (88 \times 8 \times 10 \times 130)\ /3 \times 10^6 = 0.3$. When the collaborative vehicular nodes are 9, CBT ratio is 39.28%, which states that TOA measurement traffic occupies less than 8% of the channel, results are given in Table 5.7.

Table 5.7. CBT ratio versus the TOA protocol collaborating nodes.

nodes	0 node	3 nodes	5 nodes	7 nodes	9 nodes
CBT ratio	31.48%	33.97%	36.90%	37.94%	39.28%

In our tests, the number of vehicular nodes does not exceed 9. The main reason lies in the TOA protocol implementation: when the number of collaborating vehicular nodes is chosen higher than 9, the overall TOA measurement process takes more than half seconds to complete reply-request iterations including 20 ms vacation. Although TOA measurement load does not degrade network performance, the positioning error can be increased due to outdated position information of the vehicular nodes that are chosen for mutual positioning.

Figure 5.10. Road Test with Five Collaborating Vehicles.

5.7. Road Test

TOA protocol is implemented, and the IEEE 802.11p driver is compiled in the automotive grade mini-PCs. A road experiment was conducted with 5 vehicular nodes. A screenshot is plotted in Figure 5.10. Since only four neighbor vehicles are available for replying to TOA requests, among these four vehicular nodes, 3 of them are selected randomly at each sampling period, i.e., at each second. The highway road had open sky

and open view of satellites. uBlox EVK-6 [62] is used as the mass production GNSS receiver and it has an excellent filtering capability for the automotive applications. It eliminates bias value from the GNSS absolute position measurement, and average bias value of GNSS measurement for this experiment was 5.67 meters. The GNSS measurement error versus particle filter result is compared in Table 5.8. GNSS (a) gives the error subject to bias value, and GNSS (b) is the error metrics without a bias value of 5.67 meters. Since GNSS measurement error with respect to the center of the road map is accurate, particle filter does not improve the stand-alone GNSS receiver performance. But by following the simulation results, a high penetration rate of V2V modem equipped vehicular nodes may help to improve accuracy along the increased number of collaborative vehicular nodes. stand-alone mutual positioning accuracy is also tested on the same road track. The ego vehicular node is positioning itself with respect to its neighbor vehicular nodes during GNSS outage. Mutual positioning in collaboration with three vehicular nodes assures bounded positioning error, which is consistent with the simulation study results (compare, for instance, road test results in Table 5.9, and simulation results for three nodes in Table 5.5). The packet delivery success ratio during the experiment was reached at 80%, which was calculated by taking the ratio of logged and successfully received TOA packet IDs and periodical CAM messages.

Table 5.8. Road experiment results: GNSS (a) is with a bias value of 5.67 meters, GNSS (b) is when bias is removed.

3 nodes		CEP	DRMS	R95	2DRMS
	GNSS (a)	7.38	8.32	10.98	9.23
	GNSS (b)	1.71	2.65	5.31	3.56
	TOA Mutual	34.00	52.72	105.45	70.73
	Particle Filter	5.18	6.32	12.64	10.78

Table 5.9. Road experiment results during GNSS Outage.

3 nodes		CEP	DRMS	R95	2DRMS
	TOA Mutual	35.73	55.39	110.79	74.32
	Particle Filter	11.67	18.10	36.20	24.28

The experimental setup includes: an L1 GNSS antenna and a 6 GHz ITS antenna mounted on the top of the vehicles. In detail, the current setup includes (see Figure 5.11):

- Five units of mass-market GNSS receivers (uBlox EVK-6T), capable of outputting the absolute position in the standard NMEA protocol, and an L1 GNSS antenna,
- Five units of Alix D2 embedded miniPCs (500 MHz AMD Geode LX800 CPU, 256 MB DDR DRAM, Compact Flash socket for storage, 3 Ethernet channels, DB9 serial port, dual USB port, 142.4x152.4 mm board size), suitable to be connected via miniPCI slot to a micro-router modem with AR8514 chipset and 802.11p driver, and 6 GHz ITS antennas,
- Five units of mobile antennas designed for dedicated short range communication (DSRC) 5.9 GHz, with 5 dBi gain, a 66 mm base with a magnetic mount.

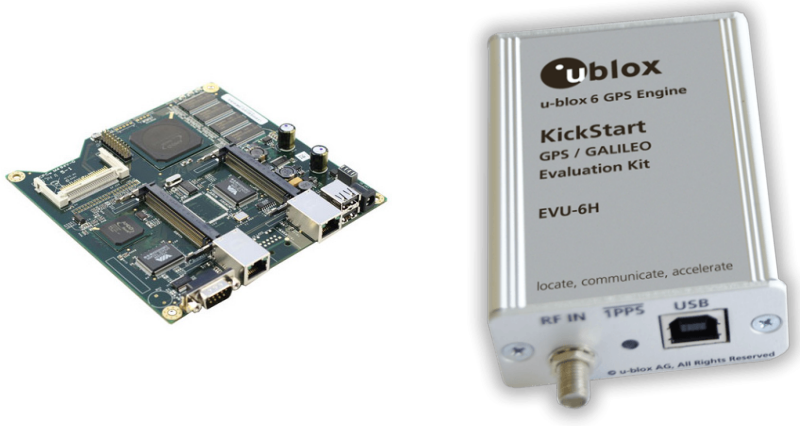

(a) (b)

Figure 5.11. Images of the Equipment Used in the Field Tests: (a) Alix Mini PC board (b) Ublox GPS Kit

The performance of the GNSS receiver is enhanced by closing the loop between the onboard integrated GNSS receiver and the V2V radio modem. V2V based relative position measurements along the digital road map improve the performance of the stand-alone GNSS receiver, which may be subject to a bad orbital configuration of visible satellites and causes poor or unavailable absolute position information.

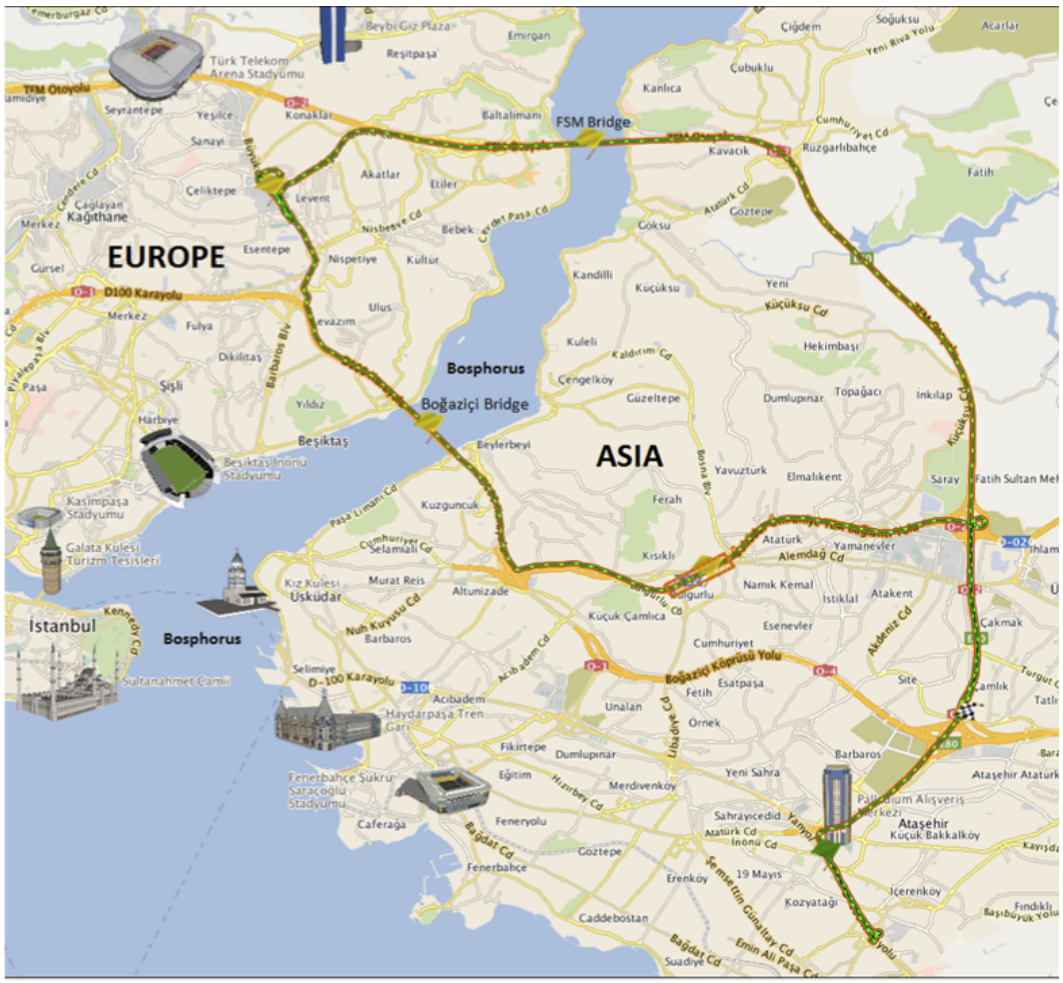

Figure 5.12. Test Route.

Error modeling and a road scenario with five cars have experimented. Figure 5.12 shows the testing route for our implementation. When the number of collaborative vehicular nodes is increased, the accuracy of the position estimation is improved without causing congestion to the channel and making the bandwidth available for other vehicular network safety messages. Simulation results and road test results illustrate the feasibility of the presented procedure.

6. CONCLUSION

In this thesis, we targeted a better and high integrity localization needed by ADAS and autonomous driving. We investigated available localization technologies, ADAS applications, and state-of-the-art in digital maps. We have seen that localization is a major component for autonomous vehicles and ADAS applications. We furthermore concluded that V2V communication provides more reliable information compared to sensory data local to the vehicle and this is important for safety critical applications. Another fact is that there is a penetration problem for VANETs at the current stage, but it is becoming a mandate soon with regulative actions. As a result, most of the modern vehicles will be equipped with a GNSS receiver, digital map and a communication modem in the near future. We take note that these relatively new technologies are yet to be exploited and take place in the literature. We also made a detailed survey of applications of these sensors in other areas and various fusion strategies.

As a result of the literature survey, state-of-art is determined, and a generic framework for better localization is decided to be very innovative, and real life implementation of such a system is possible. For creating a basic framework incorporating sensor fusion for better positioning we used a Bayesian fusion framework. With this framework, we fused conventional sensors like GNSS and odometer together with novel usage of digital maps and inter-vehicle communications. Digital maps classically are more for infotainment and VANETs are mostly for safety applications. Cross-domain usage of these sensors, introduced in this work brings additional advantage without an extra cost to the existing infrastructure of an intelligent vehicle. They also bring more long range sensing to the vehicle. When compared with traditional sensors like camera, lidar, radar they are not affected by the ambient conditions such as low light, fog, direct sunlight. Also, communication and maps are the only sensors which can bring information about nonvisible objects behind the buildings.

While establishing the Bayesian framework we had difficulty in modeling the error characteristic of the GNSS receiver. This is a known problem in the literature but with-

out an applicable solution. Most of the solutions provided are far from practical usage. We tried to solve this issue by using the 3D information available in digital maps. We also introduced novel local integrity methodology and urban canyon detection measure by local integrity heat maps.

The implementation of the Bayesian fusion framework targeted vehicle localization firstly covered map subsystem, particle filter, and integration for visualization of the results. The mapping subsystem included map compilation, routing, and location-based queries. Real life tests were accomplished in representative areas of the city to understand the behavior of the algorithm where GNSS quality is varying. There are many map matching methods, but most of the time the performance of the algorithms for correct link selection and position accuracy is not reported. We have compared our algorithm with a previous survey [10]. To make an equal comparison we have analyzed the underlying hardware structure, type of area where the algorithm tested, details of the map if used. Our algorithm performs much better with the same hardware platform without using highly detailed maps. Position accuracy of our algorithm and correct link selection performance does not degrade more than 3% in urban areas where satellite visibility is limited. We have reached correct link identification performance of 97%.

HDOP parameter is used to understand the accuracy of the position information provided by the GNSS receiver. There is no direct mapping of the HDOP to the GNSS error in meters. In the particle filter implementation, empirical values used for HDOP to meter conversion which may degrade the performance of the fusion process, since the involvement of a specific sensor is defined by its error characteristics. To be able to understand error characteristic of the GNSS receiver conditions which affect the GNSS performance is explored. As explained earlier, this leads to the local integrity. Local integrity is discussed both for the local conditions which degrade signal quality and also in the security domain for spoofing. We have focused on a more common problem of urban canyons in this context. We have proposed local integrity heat map as a suitable solution with practical implementation possibility.

The heat map can be computed and stored as an attribute of the digital map because it does not require extra hardware and has a running time of $O(n)$. When compared to other integrity models, being as a cost effective and ready to deploy mechanism, local integrity heat map becomes a feasible solution. According to the test results of the local integrity heat map relation between average distance errors, average OVF and hour of the day are revealed. As a result, local integrity heat maps can help on detection of urban canyons and can produce an augmentation depending on local conditions.

In the third phase of our research, we have focused on the integration of localization with the help of VANETs. Our Bayesian framework proved to be an easy way of integrating more than one sensor with different characteristics. However, the real challenge was how to implement relative distance as a function of TOA in such a network without affecting network performance too much and with a bounded error so that the resulting information improves overall positioning quality and reliability. Even though VANET extends vehicles sensor range, distances between vehicular nodes are not high, and a small difference in timing can cause a significant error on the calculated distance. Since we are trying to understand inter-vehicle distance from the signal propagation, the time consumed by data processing in the V2V modem should be known. We have successfully modeled and eliminated most of the error caused by modems. In real life tests, we have reached 35.73 meter error for CEP with just TOA measurements (without GNSS). It is further reduced to 11.67 with the particle filter implementation. In general, we observed 40% accuracy improvement compared to standalone GNSS receiver. This also proves the power of our Bayesian fusion framework with digital maps.

Possible hardware architectures for implementation ADAS algorithms are discussed in the literature. Even though we have done our implementation targeting embedded platforms, particle filter fusion is still computationally intense. Increasing the number of particles improves the solution quality but linearly degrades the performance. Considering this kind of problems hardware platforms made available for computationally intense algorithms [89]. To overcome possible performance issues in

the real world implementation some of the algorithms are implemented in such highly parallel platforms. [90, 91]

The framework is expandable for the inclusion of other sensors and vehicle subsystems in the future. For example, an inertial sensor would improve the performance. Speed information from the controller area network (CAN bus) of the vehicle can also be integrated into the system. A generic enhanced GNSS platform with the developed framework is possible.

Even though highly detailed maps are not a reality yet, it is possible to work on their integration to the current proposed system. Lane level map matching is a must for the autonomous cars. Highly detailed maps can be integrated into the system for lane-level matching. Currently, most of the work on lane detection is based on a camera. On camera based systems without a clear lane marking, it is not possible to make lane detection. With the fusion of highly detailed maps, it is possible to continue lane following without clear lane markings.

In the future, digital map fusion may be used for indoor mobile phone localization. It is proven that use of the digital map as a priori information may enhance localization quality. In places like shopping malls, the same concept that we used in the outdoor environment can be utilized.

We have introduced local integrity heat map in this thesis. It has a huge potential for a worldwide augmentation service. To be able to implement such a global service GNSS data collected from the public may be used. Best potential to collect such data is mobile phones. Normally, raw GNSS data are not available in phones but very recently it is announced that GNSS pseudo-ranges will be available to developers. As a future work, it is possible to use this data to generate higher coverage local integrity heat map and further tune the idea for local augmentation [92].

We have used VANETs for localization and we tested the algorithm with a limited number of vehicles. To better understand the localization improvement and communi-

cation issues with a larger number of vehicles will be needed. This is a tough task for a planned test. There are V2V pilots in many places in the world with thousands of vehicles [93]. Our methodology can be further developed in such an environment.

REFERENCES

1. Janssen, H. and W. Niehsen, "Vehicle Surround Sensing based on Information Fusion of Monocular Video and Digital Map", *IEEE 2004 Intelligent Vehicles Symposium*, pp. 244–249, June 2004.

2. Bahlmann, C., M. Pellkofer, J. Giebel and G. Baratoff, "Multi-modal Speed Limit Assistants: Combining Camera and GPS Maps", *IEEE 2008 Intelligent Vehicles Symposium*, pp. 132 – 137, June 2008.

3. Lauffenburger, J., B. Bradai, M. Basset and F. Nashashibi, "Navigation and Speed Signs Recognition Fusion for Enhanced Vehicle Location", *IFAC Proceedings Volumes*, Vol. 41, No. 2, pp. 2069 – 2074, 2008.

4. Nienhuser, D., T. Gumpp and J. M. Zollner, "A Situation context aware Dempster-Shafer fusion of digital maps and a road sign recognition system", *2009 IEEE Intelligent Vehicles Symposium*, pp. 1401–1406, June 2009.

5. Peker, A. U., O. Tosun, H. L. Akın and T. Acarman, "Fusion of map matching and traffic sign recognition", *2014 IEEE Intelligent Vehicles Symposium Proceedings*, pp. 867–872, June 2014.

6. Bishop, R., "A survey of intelligent vehicle applications worldwide", *Proceedings of the IEEE Intelligent Vehicles Symposium 2000*, pp. 25–30, 2000.

7. Shaout, A., D. Colella and S. Awad, "Advanced Driver Assistance Systems - Past, present and future", *Computer Engineering Conference (ICENCO), 2011 Seventh International*, pp. 72–82, December 2011.

8. Yannis, G. and C. Antoniou, "State-of-the-art on Advanced Driving Assistance Systems", *Workshop on the Role of Advanced Driver Assistance Systems on Traffic Safety and Efficiency*, Athens, October 2000.

9. Labaziewicz, P., *Cars are Becoming Rolling Sensor Platforms*, September 2014, https://e2e.ti.com/blogs_/b/behind_the_wheel/archive/2014/09/25/cars-are-becoming-rolling-sensor-platforms, accessed at December 2016.

10. Quddus, M. A., W. Y. Ochieng and R. B. Noland, "Current map-matching algorithms for transport applications: State-of-the-art and future research directions", *Transportation Research, Part C, Emerging Technologies*, Vol. 15, No. 5, pp. 312–328, October 2007.

11. *EGNOS Service Definition Document Open Service*, 2016, https://egnos-portal.eu/sites/default/files/EGNOS-open-service-sdd.PDF, accessed at October 2016.

12. Catalin, D. and A. Marinescu, *Improving the Position Accuracy with DGPS and EGNOS*, Master's Thesis, University Of Aalborg, 2010.

13. Ozguner, U., T. Acarman and K. Redmill, *Autonomous Ground Vehicles*, Artech House, 2012.

14. *ESA web site What is Galileo?*, 2016, http://www.esa.int/Our_Activities/Navigation/Galileo/What_is_Galileo, accessed at November 2016.

15. *GLONASS History*, 2016, https://www.glonass-iac.ru/en/guide/, accessed at November 2016.

16. *BeiDou Navigation Satellite System Home*, 2016, http://en.beidou.gov.cn, accessed at November 2016.

17. Lehtinen, M., A. Happonen and J. Ikonen, "Accuracy and time to first fix using consumer-grade GPS receivers", *16th International Conference on Software, Telecommunications and Computer Networks*, pp. 334–340, September 2008.

18. *University of Venice web site, A-GPS communication diagram*, 2016,

http://www.ricercasit.it/LabMicrodispositivi/Content.aspx?page=52, accessed at November 2016.

19. *EGNOS portal, Programme Information: Status*, 2016, https://www.egnos-portal.eu/discover-egnos/programme-information/status, accessed at November 2016.

20. *EGNOS Data Access Service (EDAS) Service Definition Document*, 2016, https://www.gsa.europa.eu/sites/default/files/EGNOS-data-access-service-sdd_0.PDF, accessed at September 2016.

21. Traveset J., V. and D. Flament, "EGNOS:The EuropeanGeostationary Navigation Overlay System. A cornerstone of Galileo", *ESA Publications Division*, 2006.

22. *VANET Communication Diagram, NHTU Computer Science Department Web Site*, 2016, http://www.cs.nthu.edu.tw/ jungchuk/research.html, accessed at October 2016.

23. Hartenstein, H. and K. Laberteaux, *ANET Vehicular Applications and Inter-Networking Technologies*, Wiley, 2010.

24. Robinson, C. L., D. Caveney, L. Caminiti, G. Baliga, K. Laberteaux and P. R. Kumar, "Efficient Message Composition and Coding for Cooperative Vehicular Safety Applications", *IEEE Transactions on Vehicular Technology*, Vol. 56, No. 6, pp. 3244–3255, November 2007.

25. *Highly Detailed Map, Tomtom web site*, 2016, http://automotive.tomtom.com/highly-automated-driving/highly-detailed-map, accessed at November 2016.

26. Tsogas, M., A. Polychronopoulos and A. Amditis, "Using digital maps to enhance lane keeping support systems", *IEEE Intelligent Vehicles Symposium*, pp. 148–153, 2007.

27. Zhang, X., Q. Wang and D. Wan, "The relationship among vehicle positioning performance, map quality, and sensitivities and feasibilities of map-matching algorithms", *IEEE Intelligent Vehicles Symposium, 2003 Proceedings*, pp. 468 – 473, June 2003.

28. Quddus, M. A., *Architectures for Efficient Implementation of Particle Filters*, Ph.D. Thesis, Imperial College London, 2006.

29. Jabbour, P. B., M. and V. Cherfaoui, "Map-Matching Integrity Using Multihypothesis Road Tracking", *Journal of Intelligent Transportation Systems*, Vol. 12, No. 4, pp. 189–201, 2008.

30. Keith A., R., K. Takeshi and U. Özguner, "DGPS/INS Integrated positioning for Control of Automated Vehicle", *IEEE Intelligent Transportation Systems Conference Proceedings*, pp. 172–178, August 2001.

31. Rezaei, S. and R. Sengupta, "Kalman filter based integration of DGPS and vehicle sensors for localization", *Mechatronics and Automation, 2005 IEEE International Conference*, pp. 455–460, July - August 2005.

32. Chausse, F., J. Laneurit and R. Chapuis, "Vehicle localization on a digital map using particles filtering", *IEEE Intelligent Vehicles Symposium 2005 Proceedings*, pp. 243 – 248, June 2005.

33. Miller, I. and M. Campbell, "Particle Filtering for Map-Aided Localization in Sparse GPS Environments", *IEEE International Conference on Robotics and Automation*, pp. 1836 – 1841, May 2008.

34. Peker, A. U., O. Tosun and T. Acarman, "Particle filter vehicle localization and map-matching using map topology", *2011 IEEE Intelligent Vehicles Symposium (IV)*, pp. 248–253, June 2011.

35. Gustafsson, F., F. Gunnarsson, N. Bergman, U. Forssell, J. Jansson, R. Karlsson

and P. J. Nordlund, "Particle filters for positioning, navigation, and tracking", *IEEE Transactions on Signal Processing*, Vol. 50, No. 2, pp. 425–437, February 2002.

36. Gustafsson, F. and F. Gunnarson, "Mobile positioning using wireless networks: possibilities and fundamental limitations based on available wireless network measurements", *IEEE Signal Processing magazine*, Vol. 22, No. 4, pp. 41 – 53, July 2005.

37. Sturza, A., M., "GPS navigation using three satellites and a precise clock", *Navigation: Journal of the Institute of Navigation*, Vol. 30, No. 2, pp. 122–132, 1983.

38. Kanchanavally, S., R. Ordonez and J. Layne, "Mobile Target Tracking by Networked Uninhabited Autonomous Vehicles via Hospitability Maps", *Proceeding of the 2004 American Control Conference*, pp. 5570 – 5575, June 30 - July 2 2004.

39. Kassas, M., Z. and U. Özguner, "A nonlinear filter coupled with hospitability and synthetic inclination maps for in-surveillance and out-of-surveillance tracking", *IEEE Transactions on Systems, Man And Cybernetics*, Vol. 40, pp. 87 – 97, 2010.

40. Oh, S. M., S. Tariq, B. N. Walker and F. Dellaert, "Map-based priors for localization", *2004 IEEE/RSJ International Conference on Intelligent Robots and Systems (IROS)*, Vol. 3, pp. 2179–2184, September 2004.

41. Bonnifait, P., J. Laneurit, C. Fouque and G. Dherbomez, "Multi-hypothesis Map-Matching using Particle Filtering", *16th World Congress for ITS Systems and Services*, pp. 1–8, Stockholm, Sweden, September 2009.

42. Kim, G. J., W. and J. Lee, "Efficient use of digital road map in various positioning for ITS", *IEEE Symposium on Position Location and Navigation*, 2000.

43. Kim, S. and J. Kim, "Adaptive fuzzy-network based C-measure map-matching algorithm for car navigation system", *IEEE Transactions on industrial electronics*,

Vol. 48, pp. 432 – 440, 2001.

44. E., W. C., D. Bernstein and A. Kornhauser, "Some map-matching algorithms for personal navigation assistants", *Transportation Research Part C*, Vol. 8, pp. 432 – 440, 2001.

45. Pyo, J.-S., D.-H. Shin and T.-K. Sung, "Development of a map matching method using the multiple hypothesis technique", *ITSC 2001. 2001 IEEE Intelligent Transportation Systems. Proceedings*, pp. 23–27, 2001.

46. Taylor, G., G. Blewitt, D. Steup, S. Corbett and A. Car, "Road Reduction Filtering for GPS-GIS Navigation", *Transactions in GIS*, Vol. 5, No. 3, pp. 193–207, 2001.

47. Bouju, A., A. Stockus, R. Bertrand and P. Boursier, "Location-based spatial data management in navigation systems", *Intelligent Vehicle Symposium, 2002. IEEE*, Vol. 1, pp. 172–177 vol.1, June 2002.

48. Yang, D., B. Cai and Y. Yuan, "An improved map-matching algorithm used in vehicle navigation system", *IEEE Proceedings on Intelligent Transportation Systems*, pp. 1246–1250, 2003.

49. Quddus, M. A., W. Y. Ochieng, L. Zhao and R. B. Noland, "A general map matching algorithm for transport telematics applications", *GPS Solutions*, Vol. 7, No. 3, pp. 157–167, 2003.

50. Syed, S. and M. E. Cannon, "Fuzzy logic-based map-matching algorithm for vehicle navigation system in urban canyons", *Proceedings of the 2004 National Technical Meeting of The Institute of Navigation*, pp. 982–993, January 2004.

51. Ochieng, W. Y., M. Quddus and R. Noland, "Map-matching in complex urban road networks", *Brazilian Journal of Cartography (Revista Brasileira de Cartografia)*, Vol. 55, pp. 1–18, 2004.

52. Quddus, M. A., R. B. Noland and W. Y. Ochieng, "A High Accuracy Fuzzy Logic Based Map Matching Algorithm for Road Transport", *Journal of Intelligent Transportation Systems: Technology, Planning, and Operations*, Vol. 10, No. 3, pp. 103–115, 2006.

53. *Space Weather Effects on GPS Systems, Official U.S. Government information about the Global Positioning System (GPS) and related topics*, 2012, `http://www.gps.gov/cgsic/meetings/2012/comberiate.pdf`, accessed at September 2016.

54. Kaplan, D., E. and C. Hegarty, *Understanding GPS: Principles and Applications*, Artech House, Norwood, MA, 2006.

55. Margaria, D. and E. Falletti, "A novel local integrity concept for GNSS receivers in urban vehicular contexts", *2014 IEEE/ION Position, Location and Navigation Symposium - PLANS 2014*, pp. 413–425, May 2014.

56. Kaplan, E., A. U. Peker, K. Par and T. Acarman, "Definition of local integrity heat map", *2014 IEEE Intelligent Vehicles Symposium Proceedings*, pp. 1441–1444, June 2014.

57. Even-Tzur, G., "Comparison of pseudo-range multipath effects in a variety of GPS antenna types", *Survey Review*, Vol. 39, No. 306, pp. 338–348, October 2007.

58. Watson, I. D. and G. Johnson, "Graphical estimation of sky view-factors in urban environments", *International Journal of Climatology*, Vol. 7, No. 2, pp. 193–197, March 1987.

59. Ratti, C., S. Di Sabatino and R. Britter, "Urban texture analysis with image processing techniques: winds and dispersion", *Theoretical and Applied Climatology*, Vol. 84, No. 1, pp. 77–90, 2006.

60. Chen, L. and E. Ng, "Sky View Factor Analysis of Street Canyons and Its Impli-

cation for Urban Heat Island Intensity. A GIS-based methodology applied in Hong Kong", *26th Conference on Passive and Low Energy Architecture*, June 2009.

61. Bradley, A. V., J. Thornes and L. Chapman, "A method to assess the variation of urban canyon geometry from sky view factor transects", *Atmospheric Science Letters*, Vol. 2, No. 1-4, pp. 155–165, June 2001.

62. *uBlox website,EVK-6 evaluation kits*, 2016, `https://www.u-blox.com/en/product/evk-6`, accessed at September 2016.

63. *Ashtech ProMark 800 datasheet*, 2016, `http://www.navtechgps.com/assets/1/7/ProMark_800_DS.pdf`, accessed at September 2016.

64. *Bulk Scan LMS 511 product information*, 2016, `https://www.sick.com/us/en/product-portfolio/fluid-sensors/flow-sensors/bulkscan-lms511/c/g253553`, accessed at October 2016.

65. *Infomobil Vehicle Tracking System*, 2016, `www.infomobil.net`, accessed at September 2016.

66. Peker, A. U., T. Acarman, C. Yaman and E. Yüksel, "Vehicle localization enhancement with VANETs", *2014 IEEE Intelligent Vehicles Symposium Proceedings*, pp. 867–872, 2014.

67. Peker, A. U. and T. Acarman, "VANET-assisted Cooperative Vehicle Mutual Positioning: Feasibility Study", *IEICE Transactions on Fundamentals of Electronics, Communications and Computer Sciences. Special Issue on ITS*, Vol. E100-A, No. 02, 2017.

68. Garello, R., L. Presti, E. Corazza and J. Samson, "Peer-to-Peer cooperative positioning, part I: GNSS-aided acquisition", *Inside GNSS*, pp. 55–63, March-April 2012.

69. Garello, R., J. Samson, M. A. Spirito and H. Wymeersch, "Peer-to-Peer cooperative positioning, part II: hybrid devices with GNSS & terrestrial ranging capability", *Inside GNSS*, pp. 20–29, July-August 2012.

70. Liu, K., H. B. Lim, E. Frazzoli, H. Ji and V. C. S. Lee, "Improving Positioning Accuracy Using GPS Pseudorange Measurements for Cooperative Vehicular Localization", *IEEE Transactions on Vehicular Technology*, Vol. 63, No. 6, pp. 2544–2556, July 2014.

71. Alam, N., A. T. Balaei and A. G. Dempster, "Relative Positioning Enhancement in VANETs: A Tight Integration Approach", *IEEE Transactions on Intelligent Transportation Systems*, Vol. 14, No. 1, pp. 47–55, March 2013.

72. Alam, N., A. Kealy and A. G. Dempster, "An INS-Aided Tight Integration Approach for Relative Positioning Enhancement in VANETs", *IEEE Transactions on Intelligent Transportation Systems*, Vol. 14, No. 4, pp. 1992–1996, December 2013.

73. Parker, R. and S. Valee, "Vehicular node localization using received-signal-strength indicator", *IEEE Transactions on Vehicular Technology*, Vol. 56, No. 6, pp. 3371–3380, November 2007.

74. Yao, J., A. T. Balaei, M. Hassan, N. Alam and A. G. Dempster, "Improving Cooperative Positioning for Vehicular Networks", *IEEE Transactions on Vehicular Technology*, Vol. 60, No. 6, pp. 2810–2823, July 2011.

75. Rohani, M., D. Gingras and D. Gruyer, "A Novel Approach for Improved Vehicular Positioning Using Cooperative Map Matching and Dynamic Base Station DGPS Concept", *IEEE Transactions on Intelligent Transportation Systems*, Vol. 17, No. 1, pp. 230–239, January 2016.

76. Pekşen, Y., Ç. Yaman, T. Acarman and A. U. Peker, "Multi-channel operation and GNSS correction issues", *2013 13th International Conference on ITS Telecommunications (ITST)*, pp. 468–473, November 2013.

77. *The MathWorks, Chi-square goodness-of-fit test*, 2015, http://www.math-works.com/help/stats/chi2gof.html, accessed at November 2015.

78. *EEE Std 802.11p-2010 Draft Standard for Information Technology Telecommunications and Information Exchange Between Systems, Local and Metropolitan Area Networks,Specific Requirements, Part 11: Wireless LAN Medium Access Control (MAC) and Physical Layer (PHY) Specifications; Amendment 7: Wireless Access in Vehicular Environments*, 2009, http://standards.ieee.org/getieee802/download/802.11p-2010.pdf, accessed at February 2015.

79. *ETSI ES 202 663 (V1.1.1) Intelligent Transport System (ITS); European Profile Standard for the Physical and Medium Access Control Layer of Intelligent Transport Systems Operating in the 5 GHz Frequency Band*, 2009, http://www.etsi.org/deliver/etsi_es/202600_202699/202663/01.01.00_50/es_202663v010100m.pdf, accessed at September 2016.

80. *SUMO Simulation of Urban MObility, DLR Institute of Transportation Systems*, 2016, http://www.dlr.de/ts/en/desktopdefault.aspx/tabid-9883/16931_read-41000/, accessed at September 2016.

81. *ns-3 idiscrete-event network simulator website*, 2016, https://www.nsnam.org/overview/what-is-ns-3/, accessed at September 2016.

82. *ETSI EN 302 637-2 V1.3.2 Intelligent Transport Systems (ITS), Vehicular Communications, Basic Set of Applications, Part 2: Specifications of Cooperative Awareness Basic Service*, 2016, http://www.etsi.org/deliver/etsi_en/302600_302699/30263702/01.03.02_60/en_30263702v010302p.pdf, accessed at September 2016.

83. Nakagami, M., "The m-distribution – A general formula of intensity distribution

of rapid fading", W. C. Hoffmann (Editor), *Statistical Methods in Radio Wave Propagation*, Pergamon Press, Elmsford, NY, 1960.

84. Simon, D., *Optimal State Estimation: Kalman, H Infinity, and Nonlinear Approaches*, Wiley-Interscience, 2006.

85. *Statistics and its relationship to accuracy measure in GPS; Novatel white paper*, 2016, `http://www.novatel.com/assets/Documents/Bulletins/apn029.pdf`, accessed at September 2016.

86. Alexander, P., D. Haley and A. Grant, "Outdoor Mobile Broadband Access with 802.11", *IEEE Communications Magazine*, Vol. 45, No. 11, pp. 108–114, November 2007.

87. Alexander, P., D. Haley and A. Grant, "Cooperative Intelligent Transport Systems: 5.9-GHz Field Trials", *Proceedings of the IEEE*, Vol. 99, No. 7, pp. 1213–1235, July 2011.

88. *ETSI TS 102 687 v1.1.1 Intelligent Transport Systems (ITS); Decentralized Congestion Control Mechanisms for Intelligent Transport Systems operating in the 5 GHz range; Access layer par*, 2016, `http://www.etsi.org/deliver/etsi_ts/102600_102699/102687/-01.01.01_60/ts_102687v010101p.pdf`, accessed at September 2016.

89. *The AI Car Computer for Self-Driving Vehicles; NVIDIA DRIVE PX 2*, 2016, `http://www.nvidia.com/object/drive-px.html`, accessed at November 2016.

90. Par, K. and O. Tosun, "Parallelization of particle filter based localization and map matching algorithms on multicore/manycore architectures", *2011 IEEE Intelligent Vehicles Symposium (IV)*, pp. 820–826, June 2011.

91. Par, K. and O. Tosun, "Real-time Traffic Sign Recognition with Map Fusipon on Multicore/Many-core Architectures", *Acta Polytechnica Hungarica*, Vol. 9, No. 2,

pp. 231–250, 2012.

92. *Google opens up GNSS pseudoranges; GPSWORLD*, 2015, `http://gpsworld.com/google-opens-up-gnss-pseudoranges/`, accessed at November 2016.

93. *Connected Vehicle Pilot Deployment Program; U.S. Department of Transportation (US DOT)*, 2015, `http://www.its.dot.gov/pilots/`, accessed at September 2016.